The Study of the Standard Model Electroweak Precision Physics at Future

Electron-Positron Colliders

by

Lisong Chen

Bachelor of Science,University at Buffalo, 2017

Submitted to the Graduate Faculty of

the Dietrich School of Arts and Sciences in partial fulfillment

of the requirements for the degree of

Doctor of Philosophy

University of Pittsburgh

2022

UNIVERSITY OF PITTSBURGH

DIETRICH SCHOOL OF ARTS AND SCIENCES

This dissertation was presented

by

Lisong Chen

It was defended on

May 5, 2022

and approved by

Prof. Dr. Ayres Freitas, Department of Physics and Astronomy

Prof. Dr. Joseph Boudreau, Department of Physics and Astronomy

Prof. Dr. Tao Han, Department of Physics and Astronomy

Prof. Dr. Arthur Kosowsky, Department of Physics and Astronomy

Prof. Dr. Doreen Wackeroth, Department of Physics, University at Buffalo

The Study of the Standard Model Electroweak Precision Physics at Future Electron-Positron Colliders

Lisong Chen, PhD

University of Pittsburgh, 2022

Future electron-positron colliders, such as the CEPC, FCC-ee, and ILC, usher in a new precision frontier where the electroweak (EW) sector of the Standard Model (SM) of particle physics can be scrutinized unprecedentedly, thereby unraveling the potential new physics beyond the Standard Model. For this purpose, one needs a deeper understanding of the SM, which is led by calculating radiative corrections to various well-defined observables, namely the electroweak precision observables (EWPOs) in the EW sector. However, to compare the EWPOs predicted by the theory with what was measured in experiments, other ingredients contributing to the relevant cross-section, such as the initial and final-state QED and QCD radiation effects, background contributions, acceptance of the detector, also need to be taken into account. This thesis will first report the recently accomplished three-loop EW corrections to some important EWPOs. Secondly, a new software package GRIFFIN (Gauge-invariant Resonance In Four-Fermion Interactions), aiming to study the gauge resonance, such as the Z-boson resonance, up to arbitrary higher order, in a manifestly gauge-invariant way, will be introduced.

<div align="center">

Table of Contents

</div>

vii

List of Tables

ix

List of Figures

Preface

First and foremost, I would like to express my deepest gratitude to my supervisor, Dr. Ayres Freitas, for his dedicated support, encouragement, and meticulous guidance throughout the journey. I am profoundly influenced by his insights and approaches to physics. It is truly unimaginable to me having a supervisor better than him.

I am also deeply indebted to Dr. Daniel Boyanovsky for his willingness to pass on knowledge and insights through discussions and collaborations, having me broaden my horizon in theoretical physics.

Without the support and nurturing given by my committee, Dr. Joseph Boudreau, Dr. Tao Han, Dr. Arthur Kosowsky, and Dr. Doreen Wackeroth, this thesis would be impossible to accomplish. I, thereby, express my gratitude to them.

My sincere thanks extend to my colleagues, including but by no means limited to Han Qin, Qian Song, Yang Ma, Leung Sze-ching (Iris), Yilun Guan, Hongbo Cai, Mudit Rai, Shu Liu, Pok Man Tam, Keping Xie, for their generous supports, sparkling discussions, constructive advice, and the resonance to those ups and downs of the life in the grad school.

Lastly, I deeply appreciate my parents and friends, Pengshan Pan, Matthew Schiavi, Yuichi Okugawa, Mahsa Habibzadeh, Muqian, Yusi Gao, and Kevin Gu, Sam Li, and Karma Su, for their love and support.

my rights, my wrongs, I'll write til I'm right with God.

—Kendrick Lamar

1.0   Introduction

1.1   the Standard Model of particle physics

The Standard Model (SM) of particle physics is a theory that describes three out of four fundamental interactions in our universe. It can be divided into two parts: Quantum Chromodynamics (QCD)[10, 11, 12, 13], which describes the strong interaction, and the Glashow-Salam-Weinberg model, namely the Electroweak Standard Model (EWSM)[14, 15, 16], which unifies the weak interaction and the electromagnetic interaction. The SM theory features a non-Abelian gauge group structure, referred to as $SU(3)_C \times SU(2)_L \times U(1)_Y$, where the $SU(3)_C$ corresponds to the QCD part, and the rest is the EWSM. The $SU(3)_C$ has gauge coupling g_s and eight generators called gluons as gauge bosons. It is a non-chiral interaction such that the gluon acts on equal footing on the L and R-chiral quark. On the contrary, the EWSM $SU(2)_L \times U(1)_Y$ is chiral. The $SU(2)_L$ has a gauge coupling g_2 and the gauge bosons W^i, $i = 1, 2, 3$, which only interact with left-handed fermions. The Abelian gauge group $U(1)_Y$ has a gauge coupling g_1 and the gauge bosons B, which interacts with both left-handed and right-handed fermions but with different hypercharge Y. Although without introducing any extra degree of freedom, the non-Abelian EWSM do not predict the masses of its gauge bosons per se, [1] three out four gauge bosons in EWSM are massive according to experiments. The EWSB, namely Brout-Englert-Higgs mechanism (or shortly, Higgs mechanism) [17, 18, 19, 20, 21], that spontaneously breaks the gauge symmetry $SU(2)_L \times U(1)_Y$ down to $U(1)_{EM}$–the gauge group that describes electromagnetic interaction, was then introduced to overcome this issue. The Higgs mechanism is implemented by employing a fundamental complex scalar doublet with a non-vanishing vacuum expectation value (VEV) that breaks the EW symmetry so that three gauge bosons $W^\pm, Z$ gain mass while the photon remains massless. Consequently, it gives rise to the masses of fermions through the

---

[1] The chiral symmetry is spontaneously broken at low energy QCD, consequently leading to eletroweak symmetry breaking, albeit by a much smaller amount that can't be used to interpret the masses of weak gauge bosons.

Yukawa couplings that describe interactions between fermions and the fundamental scalar field. For the lepton sector, taking neutrinos massless, the Yukawa couplings can be easily diagonalized, whereas, in the quark sector, the diagonalization introduces the quark-mixing, which is well-described by the Cabibbo-Kobayashi-Masakawa (CKM) matrix [22, 23].

It has been shown that the SM is a renormalizable theory [24, 25, 26, 27, 28, 29, 30, 31] and free of gauge anomaly. Hence, it is a mathematically well-constructed quantum field theory that allows us to test it at various experiments precisely. In this chapter, we introduce the SM Lagrangian, and then we briefly introduce the EW precision tests conducted by collider experiments.

1.1.1 The Standard Model Lagrangian

We begin with the classical Lagrangian of the SM, which can be divided into three individually gauge-invariant parts;

$$\mathcal{L}_{\text{SM}} = \mathcal{L}_{Gauge} + \mathcal{L}_S + \mathcal{L}_F, \tag{1}$$

where the Lagrangian of gauge fields are

$$\mathcal{L}_{Gauge} = -\frac{1}{4} G^i_{\mu\nu} G^{\mu\nu i} - \frac{1}{4} W^a_{\mu\nu} W^{\mu\nu a} - \frac{1}{4} B_{\mu\nu} B^{\mu\nu}, \tag{2}$$

where

$$G^{\mu\nu i} = \partial_\mu G^i_\nu - \partial_\nu G^i_\mu + g_s f^{ijk} G^j_\mu G^k_\nu \tag{3}$$

$$W^{\mu\nu a} = \partial_\mu W^a_\nu - \partial_\nu W^a_\mu + g_2 \epsilon^{abc} W^b_\mu W^c_\nu \tag{4}$$

$$B_{\mu\nu} = \partial_\mu B_\nu - \partial_\nu B_\mu, \tag{5}$$

where f^{ijk} and ϵ^{abc} are the structure constants of $SU(3)$ and $SU(2)$ groups, respectively. The first term in 2 solely represents the QCD part of the SM, which could be an individual subject to study. From now on, we set the QCD part aside for the moment and focus on the

EW part. The covariant derivative given by the EW gauge group is

$$D_\mu = \partial_\mu i - ig_2 I_W^a W_\mu^a + ig_1 \frac{Y_W}{2} B_\mu. \tag{6}$$

To make sure the $U(1)_{\text{EM}}$ stays unbroken after EWSB, the relation between weak hyper-charge and the third generator of $SU(2)_L$ is fixed as follows:

$$Q = I_W^3 + \frac{Y_W}{2}, \tag{7}$$

where Q is the electric charge operator, $I_W^3 = \frac{\tau_3}{2}$, and τ_i is the Pauli matrix.

The second part of Eq. (1) represents the so-called Higgs sector, where the complex scalar-doublet with non-vanishing VEV is introduced. To make sure it's electrically neutral, its hypercharge Y_W is set to be 1. The complex scalar doublet looks like

$$\Phi(x) = \frac{1}{\sqrt{2}} \begin{pmatrix} \phi_3 + i\phi_4 \\ \phi_1 + i\phi_2 \end{pmatrix} \equiv \begin{pmatrix} \phi^+(x) \\ \phi^0(x) \end{pmatrix}. \tag{8}$$

The reason of writing the first component as a linear combination is because

$$Q\Phi(x) = (I_W^3 + \frac{Y_W}{2})\Phi(x) = \begin{pmatrix} 1 & 0 \\ 0 & 0 \end{pmatrix} \Phi(x), \tag{9}$$

indicating that ϕ^+ has a charge, whereas the second component is neutral. The complex scalar doublet interacts with gauge fields through covariant derivative (6); And the Lagrangian reads

$$\mathcal{L}_S = (D_\mu \Phi)^\dagger (D^\mu \Phi) - V(\Phi, \Phi^\dagger) \tag{10}$$

where the potential term is constructed as

$$V(\Phi, \Phi^\dagger) = -\mu^2 \Phi^\dagger \Phi + \frac{\lambda^2}{4}(\Phi^\dagger \Phi)^2, \tag{11}$$

so that the new minimum of the vacuum after EWSB is non-zero.

The parity-violating interaction between gauge fields and matter fields are constructed

3

by requiring the left-handed fermions to form into $SU(2)_L$ doublet, and the right-handed fermions form into singlets.

$$L_j^L = \omega_- L_j = \begin{pmatrix} l_j^L \\ \nu_j^L \end{pmatrix}, \quad Q_j^L = \omega_- Q_j = \begin{pmatrix} u_j^L \\ d_j^L \end{pmatrix} \tag{12}$$

$$l_j^R = \omega_+ l_j, \quad u_j^R = \omega_+ u_j, \quad d_j^R = \omega_+ d_j, \tag{13}$$

where $\omega_\pm = \frac{1 \pm \gamma^5}{2}$ acting as projectors, and the j is the index of generations of the quark and lepton family. We suppress the color index here since we are not interested in QCD now. One can also easily add the $SU(2)$ singlet right-handed neutrinos in Eq. (13). However, given by the current experiments' searching, it remains uncertain whether they exist. And the SM retains consistent by discarding ν_j^R tentatively. We can write down the last part of the Lagrangian on the EW basis:

$$
\begin{aligned}
\mathcal{L}_F = & \sum_i (i\overline{L}_i^L \slashed{D} L_i^L + i\overline{L}_i^L \slashed{D} L_i^L) \\
& + \sum_i (i\overline{l}_i^R D l_i^R + \overline{u}_i^R \slashed{D} u_i^R + i\overline{d}_i^R \slashed{D} d_i^R) \\
& - \sum_i (\overline{L}_i^L Y_{ij}^l l_j^R \Phi + \overline{Q}_i^L Y_{ij}^u u_j^R \tilde{\Phi} + \overline{Q}_i^L Y_{ij}^d d_j^R \Phi + h.c.),
\end{aligned}
\tag{14}
$$

where the $G_{ij}^{l,u,d}$ are the Yukawa coupling matrices that corresponds to the fermion masses, $\tilde{\Phi}$ is the charge conjugated scalar field so that

$$\tilde{\Phi} = i\tau^2 \Phi^* = (\phi^{0*}(x), -\phi^-)^T. \tag{15}$$

1.1.2 Transferring the Electroweak Standard Model Lagrangian to physical basis

The Lagrangian written down in the last section is constructed by fields defined as the eigenstates of the EW gauge interaction, i.e., the covariant derivatives are diagonal, and all fields are not necessarily representing physical states, i.e., the eigenstates of the charge and the mass. To make use of this Lagrangian for making theoretical predictions, we need to recast the Lagrangian so that all degrees of freedom that shows up in the classical Lagrangian have physical content. We start by looking at the complex scalar sector, where we first find the new ground state of the field by taking the derivative of the potential:

$$\frac{\partial V(\Phi)}{\partial \Phi} = 0, \tag{16}$$

thereby finding the new minimum of the vacuum as

$$|\langle \Phi \rangle|^2 = \frac{2\mu^2}{\lambda} = \frac{v^2}{2} \neq 0 \quad \Rightarrow \quad \Phi_0 = \frac{1}{\sqrt{2}} \begin{pmatrix} 0 \\ v \end{pmatrix} \tag{17}$$

Note that only the non-zero VEV will lead to the breaking of $SU(2)_L \times U(1)_Y$, otherwise the EW gauge group will remain unbroken. Using the polar reparametrization and having the scalar field expand around the VEV we get

$$\Phi(x) = \begin{pmatrix} \phi^+(x) \\ \frac{1}{\sqrt{2}}[v + H(x) + i\chi(x)] \end{pmatrix}, \tag{18}$$

where $H(x)$ is the only physical degree of freedom that represents the transverse fluctuation in the vicinity of the ground state, while the others are would-be Goldstone bosons that feature no physical content in gauge theory whatsoever. Hence, to get the gist of the physical content of the Lagrangian of the EWSM, one can find a suitable gauge transformation, namely the unitary gauge, in which all Goldstone modes are eliminated. Inserting Eq. (18) into $\mathcal{L}_F$ and $\mathcal{L}_S$ while diagonalizing gauge fields and fermion fields in physical eigenstates, we would

obtain the masses for both gauge bosons and fermions as follows:

$$M_H = \sqrt{2}\mu \;, \quad M_{\phi^\pm,\chi} = 0 \;, \quad M_\gamma = 0 \;, \tag{19}$$

$$M_{\mathrm{W}^\pm} = \frac{1}{2}g_2 v \;, \quad M_{\mathrm{Z}} = \frac{1}{2}\sqrt{g_1^2 + g_2^2}\,v \;, \quad m_{\psi,i} = \frac{v}{\sqrt{2}}\sum_{k,m} U_{ik}^{f,L} Y_{km}^f U_{mi}^{f,R\dagger} \;, \tag{20}$$

where all physical fields are defined as

$$W_\mu^\pm = \frac{1}{\sqrt{2}}(W_\mu^1 \mp W_\mu^2), \quad \begin{pmatrix} Z_\mu \\ A_\mu \end{pmatrix} = \begin{pmatrix} c_{\mathrm{W}} & s_{\mathrm{W}} \\ -s_{\mathrm{W}} & c_{\mathrm{W}} \end{pmatrix} \begin{pmatrix} W_\mu^3 \\ B_\mu \end{pmatrix}, \tag{21}$$

$$\psi_i^L = \sum_k U_{ik}^{f,L} f_k^L \;, \quad \psi_i^R = \sum_k U_{ik}^{f,R} f_k^R \;, \tag{22}$$

with weak mixing angles defined as follows:

$$c_{\mathrm{W}} = \cos\theta_{\mathrm{W}} = \frac{g_2}{\sqrt{g_2^2 + g_1^2}} \cdot \quad s_{\mathrm{W}} = \sin\theta_{\mathrm{W}}, \tag{23}$$

alternatively, one can also reparametrize the weak mixing angle as $c_{\mathrm{W}} = \frac{M_{\mathrm{W}}}{M_{\mathrm{Z}}}$. The masses of gauge bosons can be acquired by diagonalizing the kinetic term of $\mathcal{L}_S$ in a straightforward way, where one has to write W-boson fields in their charge eigenstates first. Then it is natural combining W^3 and B together as they are both electrically neutral. By diagonalizing the mixing of W^3 and B, one can get the physical states of neutral gauge bosons: Z_μ and A_μ.

The diagonalization of fermions requires bi-unitary transformation as shown in Eq. (20). Due to the unitarity, the bi-unitary-transform matrices in Eq. (20) drop out in neutral currents, i.e., the interaction between fermions and neutral gauge bosons, thereby leading to a simple flavor diagonal representation of the physical states, which is not the case for the charged current–for the interaction between W bosons and quarks, due to the non-degenerate quark masses measured in experiments, the quark-mixing matrix in interacting with W boson is elucidated by CKM matrix such that

$$V_{ij} = U_{i,k}^{u,L} U_{kj}^{d,L\dagger}. \tag{24}$$

However, in the lepton sector, since we do not include the neutrino masses, one can choose

6

a suitable $U^{\nu,L}$ to eliminate the mixing, leading to a flavor-diagonal interaction between leptons and W bosons. Lastly, there are terms linearly depending on the Higgs field $H(x)$. One can group them all into a parameter t written as

$$\mathcal{L}_{tadpole} = tH(x), \quad t = \upsilon(\mu^2 - \frac{\lambda^2}{4}\upsilon^2). \tag{25}$$

Note that t vanishes at tree-level, and as we will discuss in the next chapter, choosing the redefinition of t carefully one can safely discard most quantum effects stemming from this term.

1.1.3 Quantizing the Lagrangian of the EWSM

Needless to say that the success of the SM is deeply rooted in its power of making predictions with high precision, which requires taking the quantum effects beyond the classical level of the SM Lagrangian into account.

Quantizing the Eq. (1) requires the parametrization of the gauge. Although the unitary gauge mentioned earlier is useful to identify the physical content, it becomes highly singular in higher-order calculations. One commonly used class of gauge in quantizing the SM is called R_ξ gauge, where ξ is a real parameter that runs from 0 to ∞ to specify the gauge. In R_ξ gauge class, we can write down the gauge-fixing terms according to the Faddeev Popov method[32] as follows:

$$C^\pm = \partial^\mu W_\mu^\pm \mp iM_{\mathrm{W}}\zeta'_{\mathrm{W}}\phi^\pm \quad C^Z = \partial^\mu Z_\mu - M_{\mathrm{Z}}\zeta'_{\mathrm{Z}}\chi, \quad C^A = \partial^\mu A_\mu. \tag{26}$$

$$\mathcal{L}_{GF} = -\frac{1}{2\xi_A}(C^A)^2 - \frac{1}{2\xi_{\mathrm{Z}}}(C^Z)^2 - \frac{1}{\xi_{\mathrm{W}}}C^+C^-. \tag{27}$$

By choosing 't Hooft gauge where $\zeta_{\mathrm{W,Z}} = \xi_{\mathrm{W,Z}}$, one can eliminate the mixing between gauge bosons and Goldstone modes up to irrelevant total derivative. In the meanwhile, the Goldstone modes acquire masses from Eq. (27) as $M^2_{\phi^\pm,\chi} = \xi_{\mathrm{W}^\pm,\mathrm{Z}}M_{\mathrm{W}^\pm,\mathrm{Z}}$.

To preserve the unitarity and compensate the unphysical effects introduced by Eq. (27), one needs to introduce Faddeev Popov ghosts $u^\alpha(x)$, $\bar{u}^\alpha$, where $\alpha = \gamma, Z, \pm$, along with their

Lagrangian

$$\mathcal{L}_{FP} = \bar{u}^\alpha \frac{\delta \mathcal{L}_{GF}^\alpha}{\delta \theta^\beta(x)} u^\beta, \tag{28}$$

where the $\frac{\delta \mathcal{L}_{GF}^\alpha}{\delta \theta^\beta(x)}$ is the variation with respect to infinitesimal gauge transformation. All unphysical poles stemming from the quantization in R_ξ are cancelled in the final expression for physical on-shell amplitudes, thereby resulting in gauge invariance of physical S-matrix. One common choice of the gauge used in higher-order calculation is $\xi_\alpha = 1$, namely 't Hooft-Feynman gauge, at which all the unphysical poles of the ghost fields, Goldstone fields, and longditudinal components of the gauge fields coincide with the poles of the transverse components of the gauge fields. Finally, the quantized Lagrangian of EWSM is given by

$$\mathcal{L}_{EWSM} = \mathcal{L}_{\text{EW-Gauge}} + \mathcal{L}_S + \mathcal{L}_F + \mathcal{L}_{GF} + \mathcal{L}_{FP}. \tag{29}$$

It has been proven to be gauge-invariant under a generalized gauge transformation, as known as Becchi-Rouet-Stora Transformation (BRST) [33], consequently leading to relations between Green's functions of gauge bosons and Goldstone bosons, which is known as Slavnov-Taylor identities that render the gauge invariance and renormalizability of the EWSM.

1.2 Precision Tests of the Standard Model

Owing to its renormalizability, the Standard Model has successfully and precisely predicted various phenomena spanning a wide range of energies in subatomic physics. However, its congenital deficiencies, such as the lack of a mechanism for generating neutrino masses, the absence of dark matter, and the reluctance of explaining the underlying dynamics of the electroweak spontaneous symmetry breaking, are not to be overlooked. All the puzzles mentioned above have been known for decades yet cannot be resolved by any experimental observations thus far, thereby anticipating that the new fundamental particles are out of reach of the current operating experiments due to their weak couplings or heavy masses. Not only does this anticipation require experimental machines with unprecedented precision, but it also challenges the higher-order calculation of radiative corrections to the observables that will be measured.

Historically, the precision tests of the SM have a long successful history dating back even before the discovery of the W and Z bosons [34, 35, 36] by the UA1, and UA2 collaborations [37, 38, 39, 40]. Then the Z-boson factories, LEP and SLC [41] scrutinized a set of observables such as $M_{\mathrm{Z}}, \sin^2\theta_{\mathrm{eff}}^l, \Gamma_{\mathrm{Z}}, A_{\mathrm{FB}}, etc$ defined at the Z-pole. With the help of such precision measurements of the EW sector, theorists at the time had successfully predicted that the mass of the top quark should be in the range 140 GeV $< m_t <$ 190 GeV [41, 42, 43, 44] before its discovery by the collaborations CDF[45] and DØ[46] at the Tevatron collider in 1995. Following closely, having LEP 2 run at the W^+W^- threshold and beyond, precision study groups were able to put constraints on the Higgs boson mass internally via radiative corrections [47, 48, 49, 50] , shedding light on the discovery of the Higgs boson later in 2012 [51, 52]. All the success of indirect search or constraint of new physics relied on higher-order calculations, thus guiding us to push the precision frontier further.

1.2.1 Definitions of electroweak precision observables

To scrutinize the SM, especially the EW sector, via experimental data, we usually define a set of electroweak precision observables (EWPOs) that can be measured with high pre-

cision. There is no definitive way of defining EWPOs, but one can observe their heuristic commonness in the course of study as follows:

- the EWPOs defined should be measurable by experiments and with desiring precision guaranteed.
- the EWPOs should be theoretically well-defined with respect to gauge-invariance, Lorentz invariance, etc.
- the EWPOs should be able to encapsulate all relevant short-distance physics while being insensitive to or detachable from the long-distance effects such as QED and QCD effects.
- the EWPOs should capture the sensitivity to new physics beyond the SM.
- etc.

To carry out the higher-order calculation of EWPOs, one needs to choose a set of parameters as theoretical input, which can also be determined according to the items listed above. For detailed discussion of the input parameters one can refer to sec. 2.4 or [53]. In the following, we list a set of EWPOs that are commonly used for checking the inner consistency of the EW sector in the SM and testing the potential new physics beyond the SM:

1.2.1.1 W-boson mass

The W-boson mass can be determined either by direct measurements via either W^+W^- pair production at lepton colliders such as LEP 2 or an s-channel W-boson (a Drell-Yan process with charged current) at hadron colliders. It can also be indirectly determined from muon decay. Owing to the precise measurement of the muon lifetime, we have known the Fermi constant to an unprecedented level of precision.

$$\Gamma_\mu = \frac{G_\mu^2 m_\mu^5}{192\pi^3} F(\frac{m_e^2}{m_\mu^2})(1 + \Delta q) \tag{30}$$

$$F(r) = 1 - 8r + 8r^3 - r^4 - 12r^2 \log r, \tag{31}$$

	D⊘	CDF1	ATLAS	LHCb	LEP	CDF2
$M_{\rm W}$ MeV	80375±23	80387±19	80370±19	80354±32	80376±33	80433.5 ± 9.4

Table 1: Precise determination of the W-boson mass given by several collaborations, noticing that the W-mass given by LEP is a combined result, and the latest measurement given by CDF has a significant discrepancy compared with others. In fact, it deviates from the SM prediction by 7.0 sigma.

where Δq has capture QED effects up to NNLO [54, 55, 56]. Then one can seal all less known radiative correction stemming from the EW sector into a gauge-invariant quantity Δr as

$$G_\mu = \frac{\pi\alpha}{\sqrt{2}s_{\rm w}^2 M_{\rm W}^2}(1 + \Delta r).$$

(32)

Then the W-boson mass can be solved iteratively as

$$M_{\rm W}^2 = M_{\rm Z}^2\Big[\frac{1}{2} + \sqrt{\frac{1}{4} - \frac{\alpha\pi}{\sqrt{2}G_\mu M_{\rm Z}^2}(1 + \Delta r)}\Big]$$

(33)

Experimentally, the W-mass has been determined from various collaborations from lepton and hadron colliders, followed by the methods mentioned above. Here we list the most recent measurements of $M_{\rm W}$ given by [57, 58, 59, 60, 47, 61].

1.2.1.2 EWPOs at Z-pole

The process $e^+e^- \to f\bar{f}$ running near the Z-pole, i.e. $\sqrt{s} \approx M_{\rm Z}^2$ is considered as one of the most critical testbeds of the EWSM. The observables defined at the Z-pole can be measured precisely, constraining various types of new physics thereby. They can be divided into various sets which can be individually determined hence offering the window for consistency scrutiny: (i) the cross section of $e^+e^- \to f\bar{f}$ at the Z-pole, $\sigma_f^0 = \sigma_f(s = M_{\rm Z}^2)$; (ii) The total width of the Z boson, extracted from the σ_f in the vicinity of the Z-pole dubbed as Z-lineshape ; (iii)

The branch ratio R_f of different decay channels.

$$\sigma_{had}^0 = \sigma[e^+e^- \to hadrons]_{s=M_Z^2}; \tag{34}$$

$$\Gamma_Z = \sum_f \Gamma[Z \to f\bar{f}], \tag{35}$$

$$R_l = \Gamma[Z \to hadrons]/\Gamma[Z \to l^+l^-], \qquad (l = e, \mu, \tau); \tag{36}$$

$$R_q = \Gamma[Z \to q\bar{q}]/\Gamma[Z \to hadrons], \qquad (q = b, c, s, d, u); \tag{37}$$

It can be seen that by assuming the cross section for each fermion final state features the same uncertainties given by the detector's acceptance and the integrated luminosity, it is thus better to use the ratios of σ_f/σ_f' to reduce the error.

To retrieve the EWPOs from the experiment, one also needs to extract the theoretical contributions given by QCD and QED, which are actually numerically important (due to the large logarithm stemming from soft/collinear photons) while physically less interesting. Radiator functions can sketch the contribution given by the QED as

$$\sigma_f^{\text{full}} = \int_0^{1-4m_f^2/s} dx H(x)\sigma_f^{\text{deconv}}(s'), \tag{38}$$

where $s' = s(1-x)$ and $H(x)$ contains both resummed soft photon and fixed order QED contributions, apart from the real corrections, the s-channel photon exchange, γZ interference, and box diagrams also need to be extract so that the

$$\sigma_f(s') = \sigma_f^{\text{deconv}}(s') - \sigma_f^{\gamma}(s') - \sigma_f^{\gamma Z}(s') - \sigma_f^{\text{box}}(s') \tag{39}$$

corresponds to the observables defined in Eq. (37). Theoretically, these observables are constructed by the effective vector and axial-vector form factors that encapsulate the radiative corrections of the SM and physics beyond the SM.

$$\Gamma_Z \sim \sum_f (|v_f|^2 + |a_f|^2) \tag{40}$$

$$\sigma_f \sim (|v_e|^2 + |a_e|^2)(|v_f|^2 + |a_f|^2). \tag{41}$$

12

1.2.1.3 Asymmetries and effective weak-mixing angle

It would be nice to define an observable that depends on the ratio between the effective vector and axial-vector form factors, $v_f(s)$ and $a_f(s)$ near the resonance of the Z-peak, besides the quadratic dependence given by the cross section and decay widths. For this purpose, one can define objects so-called asymmetries, at which the systematical uncertainties are also minimized by the ratio between cross sections. With polarized incoming electron (positron) beams, one can measure the left-right asymmetry

$$A_{\mathrm{LR}} = \frac{\sigma_L - \sigma_R}{\sigma_L + \sigma_R} = \frac{2\mathrm{Re}\, v_e/a_e}{1 + |v_e/a_e|^2} \equiv \mathcal{A}_e \tag{42}$$

The differential σ_f given by unpolarized beams is sketched as

$$\frac{d\sigma_f}{d\cos\theta} \sim (|v_e|^2 + |a_e|^2)(|v_f|^2 + |a_f|^2)(1 + \cos^2\theta) + 2v_e a_e v_f a_f \cos\theta \tag{43}$$

By defining forward and backward scattering as follows:

$$\sigma_F = \int_0^1 \frac{d\sigma}{d\cos\theta} d\cos\theta, \quad \sigma_B = \int_{-1}^0 \frac{d\sigma}{d\cos\theta} d\cos\theta, \tag{44}$$

we can then write down the forward-backward asymmetry as

$$A_{\mathrm{FB}} \equiv \frac{\sigma_F - \sigma_B}{\sigma_F + \sigma_B} = \frac{3\mathrm{Re}\, v_e/a_e}{1 + (v_e/a_e)^2} \frac{\mathrm{Re}\, v_f/a_f}{1 + (v_f/a_f)^2} \tag{45}$$

$$= \frac{3(1 - 4|Q_e|\sin^2\theta_{\mathrm{eff}}^e)}{1 + (1 - 4|Q_e|\sin^2\theta_{\mathrm{eff}}^e)^2} \frac{(1 - 4|Q_f|\sin^2\theta_{\mathrm{eff}}^f)}{1 + (1 - 4|Q_f|\sin^2\theta_{\mathrm{eff}}^f)^2}, \tag{46}$$

where the $\sin^2\theta_{\mathrm{eff}}^f$ is defined as

$$\sin^2\theta_{\mathrm{eff}}^f = \frac{1}{4|Q_f|}\left(1 - \mathrm{Re}\,\frac{v_f}{a_f}\right). \tag{47}$$

The measurement of A_{FB} can thus be used to determine the value of $\sin^2\theta_{\mathrm{eff}}^f$. It has been measured at both lepton colliders, such as the LEP and SLD, and hadron colliders, including the TeVatron and the LHC, yielding corresponding $\sin^2\theta_{\mathrm{eff}}^l$ with relative precisions below 0.1% and 0.2%, respectively. One can refer to Table 3.8 in Ref. [62] for more thorough details.

1.2.2 Precision tests in the future e^+e^- colliders

From a theoretical point of view, the SM higher-order corrections to the effective vector and axial-vector form factors, along with the Δr defined in muon decay, is essential when comparing with the measurements provided by experiments. Over a span of several decades, the complete one-loop[63, 64], complete two-loop EW [65, 66, 67, 68, 69, 70, 71, 72, 73, 74, 75], mixed EW-QCD two-loop[76, 77, 78, 79, 80, 81, 82, 83, 84, 85] corrections to the $\sin^2\theta_{\text{eff}}^f$ and $\Gamma[Z \to f\bar{f}]$, along with partial numerically significant contributions given at higher-loop orders, such as the top-Yukawa enhanced contributions at three and four-loop level [86, 87, 88, 89, 90, 91, 92] have been carried out, altogether yielding the theoretical uncertainties due to missing higher orders shown as in the Tab. 2.

	Exp	Current theo. error	CEPC	FCC-ee	ILC/GigaZ
M_{W}[MeV]	12	$4(\alpha^3, \alpha^2\alpha_{\text{s}})$	1	$0.5 \sim 1$	2.5
Γ_Z[MeV]	2.3	$0.4(\alpha^3, \alpha^2\alpha_{\text{s}}, \alpha\alpha_{\text{s}}^2)$	0.5	0.1	1.0
$\sin^2\theta_{\text{eff}}^f$ $[10^{-5}]$	16	$4.5(\alpha^3, \alpha^2\alpha_{\text{s}})$	< 1	0.6	1

Table 2: *This table demonstrates the current experimental uncertainties given by the global fits of measurements taken from the LEP, SLD, and LHC vs. future experimental accuracies projected for CEPC, FCC-ee, and ILC for three EWPOs [2, 3, 4, 5, 6]. For ILC, the GigaZ option is considered, which is a Z-pole run with 100 fb^{-1}.*

One can easily see that the current theoretical uncertainties are well-below the uncertainties given by experiments. However, several future e^+e^- colliders, such as FCC-ee [93], CEPC [2], ILC [94, 95], and CLIC [96, 97] have laid out a new precision frontier, that one can test the EW sector to an unprecedented level. The experimental uncertainties given by these colliders are listed in the Tab. 2. One can see that they can improve the precision by

at least one order of magnitude. Hence should one of these colliders be built, the three-loop and leading-four loop EW and mix EW-QCD corrections are required for testing the SM.

2.0 Radiative Corrections in Electroweak theory

2.1 Renormalization

2.1.1 Renormalization in perturbative QFT

The Lagrangian of the SM contains several free parameters. Defining these parameters and relating them to physical observables are the essence of the renormalization procedure. A peculiar feature given by higher-order perturbation of QFT is that the loop integrals that account for quantum effects diverge, which impedes the renormalization procedure from being straightforward, both physically and mathematically. There are two classes of divergences: integrating over the loop momentum k of a massless propagator when $|k|$ tends to 0 or having one massless propagator in the loop become collinear with one neighbor external light-like momentum in the neighbor, which give rise to the so-called soft divergence and collinear divergence, respectively. Usually, they are also commonly referred to as infrared (IR) singularities. When integrating over k as $|k| \to \infty$, another type of divergence may occur, which is so-called ultra-violet (UV) divergence. From a math point of view, it is crucial to regularize these divergences before commenting on the physics of their corresponding quantum effects. There are many systematic ways of regularizing the divergences arising from loops. All regularization schemes inevitably introduce an extra degree of freedom, which characterizes the energy or distance scales. Here we set the dimensional regularization scheme (DR) as default. Although being subject to technical difficulties in practice, the IR divergences have long been conceptually well-understood and can be safely removed by combining virtual loop corrections and real emissions. However, the UV divergences articulate that all observables defined locally in relativistic QFT only approximately represent the underlying physics. Accordingly, in EFT language, the UV divergences are seen as the measure of sensitivity to the underlying new physics at a shorter distance and higher energy scale. Hence one can remove those UV divergences systematically from higher-order calculations where the scale of the physical process described by a theory is insensitive to the underlying physics. The removal of UV divergences can henceforth be embedded in redefining the Lagrangian parameters. Different ways of relating redefined Lagrangian parameters to observables correspond to various renormalization schemes. Should observables be physically well-defined, they are independent of the choice of regularization schemes, i.e., they all should be cut-off independent.

Care must be taken when re-defining the parameters in Lagrangian so that all symmetries

shall remain unspoiled. Hence, one should first choose an independent set of parameters from tree-level Lagrangian (namely "bare" Lagrangian) that respects all symmetries, then introduce a multiplicative renormalization constant to each independent parameter and each bare field. In the spirit of perturbation theory, one can thus perform series expansion solely on renormalization constants. By imposing a set of *renormalization conditions*, one fixes the renormalization constants and defines the relation between renormalized parameters and physical observables unequivocally. The bare Lagrangian can split into *renormalized* and *counterterm* Lagrangian as follows

$$
\begin{aligned}
g_0 &= Z_g g = g(g, m, \mu) + \delta^{(1)} Z_g(g, m, \mu) + \ldots \\
m_0^2 &= Z_m m^2 = m^2(g, m, \mu) + \delta^{(1)} m^2(g, m, \mu) + \ldots \\
\phi_0 &= Z_\phi^{1/2} \phi = 1 + \frac{1}{2} \delta^{(1)} Z_\phi \phi + \ldots \\
\mathcal{L}(\phi_0, g_0, m_0) &= \mathcal{L}(\phi, g, m, \mu) + \delta\mathcal{L}(\phi, g, m, \delta Z_\phi, \delta g, \delta m^2, \mu),
\end{aligned}
\tag{48}
$$

where μ is the renormalization scale introduced by DR. The UV divergences stemming from the bare Lagrangian will then cancel against those in the counterterm Lagrangian, rendering the renormalized Lagrangian finite.

2.1.2   Renormalization in the SM

2.1.2.1   *Reparametrization of the bare Lagrangian*

Upon the spirit introduced above, we reparameterize the bare Lagrangian of the SM (in physical basis) as in the Table. 3 below. By choosing the t' Hooft gauges($\xi_b = \zeta_b$, $b = W, Z$), one can see that the poles given by the unphysical degree of freedom coincide with the poles of the transverse component of physical degree of freedom. Several caveats should be stressed hereï¼ that we have set the CKM matrix to be unitary matrix and ignored the neutrino and light quark (except the top) masses due to their irrelevant impact on the EW physics, we have also set the counterterm of the vacuum expectation value v as a non-free parameter such that all tadpole contributions of 1-point Higgs vertex function are absorbed into the counterterm δt. For more thorough discussion please see Ref. [98] and references therein.

Figure 1: $\hat{\Gamma}_R^H = \Gamma^H + \delta t = 0$

2.1.2.2 Renormalization condition

As mentioned above, all renormalization constants can be fixed by imposing renormaliza-tion conditions. One of the most common sets of renormalization conditions is the so-called on-shell scheme, in which all renormalized masses of massive particles are defined as the physical masses , i.e. the real part of the pole of corresponding propagators. For couplings, they are usually defined at a three-point function under a certain limit. Therefore, masses and couplings can be determined from radiative corrections within one-particle irreducible (1-PI) two-point functions and three-point functions, respectively. Firstly, let us define the Green's function of gauge bosons with self-energy Σ as

$$
\begin{aligned}
\hat{G}_{\mu\nu}(k^2) &= iD_{\mu\nu}(k^2) + iD_{\mu\rho}(k^2)\hat{\Sigma}^{\rho\sigma}(k^2)D_{\sigma\nu}(k^2) + \dots \\
&= iD_{\mu\rho}D^{-1\rho\sigma}D_{\sigma\nu} + iD_{\mu\rho}\hat{\Sigma}^{\rho\sigma}D_{\sigma\nu} + \dots \\
&= iD_{\mu\rho}(-i\tilde{D}^{-1}{}^{\rho\sigma} - i\hat{\Sigma}^{\rho\sigma})D_{\sigma\nu} + \dots \\
&\equiv iD_{\mu\rho}\hat{\Gamma}^{\rho\sigma}D_{\sigma\nu} + \dots ,
\end{aligned}
\tag{49}
$$

where $D_{\mu\nu}(k^2)$ is the gauge-boson propagator in momentum space, and $\hat{\Gamma}^{\rho\sigma}$ is named as two-point function. In Feynman -'t Hooft gauge, the electroweak gauge bosons' 1-PI two-point functions can be written as the follow

Couplings	$e_0 = (1 + \delta Z_e)e, \quad g_{s,0} = (1 + \delta g_s)g_s$	
Gauge Bosons	$G_0^a = \sqrt{1 + \delta Z_G}\, G^a \quad [a = 1, ...8]$ $W_0^\pm = \sqrt{1 + \delta Z_W}\, W^\pm$ $\begin{pmatrix} Z_0 \\ A_0 \end{pmatrix} = \begin{pmatrix} \sqrt{1 + \delta Z_{ZZ}} & \frac{1}{2}\delta Z_{ZA} \\ \frac{1}{2}\delta Z_{AZ} & \sqrt{1 + \delta Z_{AA}} \end{pmatrix} \begin{pmatrix} Z \\ A \end{pmatrix}$	$M_{0,W}^2 = M_W^2 + \delta M_W^2$ $M_{0,Z}^2 = M_Z^2 + \delta M_Z^2$
Higgs Boson	$H_0 = \sqrt{1 + \delta Z_H}\, H$	$M_{0,H}^2 = M_H^2 + \delta M_H^2$
Fermions	$\psi_{f,0}^L = \sqrt{1 + \delta Z_f^L}\, \psi_f^L$ $\psi_{f,0}^R = \sqrt{1 + \delta Z_f^R}\, \psi_f^R$	$M_{0,f}^2 = M_f^2 + \delta M_f^2$
Unphysical Sector	$\chi_0 = (1 + \frac{1}{2}\delta Z_\chi)\chi, \quad \phi_0^\pm = (1 + \frac{1}{2}\delta Z_\phi)\phi^\pm$ $u_0^\pm = (1 + \delta\tilde{Z}_\pm)u^\pm$ $\begin{pmatrix} u_0^Z \\ u_0^A \end{pmatrix} = \begin{pmatrix} 1 + \delta\tilde{Z}_{ZZ} & \delta\tilde{Z}_{ZA} \\ \delta\tilde{Z}_{AZ} & 1 + \delta\tilde{Z}_{AA} \end{pmatrix} \begin{pmatrix} Z \\ A \end{pmatrix}$ $\zeta_{0,b} = Z_{\zeta_b}\zeta_b \quad \xi_{0,A} = Z_{\xi_A}\xi_A, \qquad b = W, Z$	

Table 3: Reparametrization of the SM Lagrangian in physical basis.

$$\hat{\Gamma}_{\mu\nu}^W(k^2) = -ig_{\mu\nu}(k^2 - M_W^2) - i(g_{\mu\nu} - \frac{k_\mu k_\nu}{k^2})\hat{\Sigma}_T^W(k^2) - i\frac{k_\mu k_\nu}{k^2}\hat{\Sigma}_L^W(k^2) \tag{50}$$

$$\hat{\Gamma}_{\mu\nu}^Z(k^2) = -ig_{\mu\nu}(k^2 - M_Z^2) - i(g_{\mu\nu} - \frac{k_\mu k_\nu}{k^2})\hat{\Sigma}_T^Z(k^2) - i\frac{k_\mu k_\nu}{k^2}\hat{\Sigma}_L^Z(k^2) \tag{51}$$

$$\hat{\Gamma}_{\mu\nu}^\gamma(k^2) = -ig_{\mu\nu}k^2 - i(g_{\mu\nu} - \frac{k_\mu k_\nu}{k^2})\hat{\Sigma}_T^\gamma(k^2) - i\frac{k_\mu k_\nu}{k^2}\hat{\Sigma}_L^\gamma(k^2), \tag{52}$$

$$\hat{\Gamma}^H(k^2) = i(k^2 - M_H^2) + i\hat{\Sigma}^H(k^2) \tag{53}$$

where

$$\hat{\Sigma}_T^{\mathrm{W}}(k^2) = \Sigma_T^{\mathrm{W}}(k^2) + (k^2 - M_W^2)\delta Z_{\mathrm{W}} - \delta M_W^2 \tag{54}$$

$$\hat{\Sigma}_T^{\mathrm{Z}}(k^2) = \hat{\Sigma}_T^{\mathrm{ZZ}}(k^2) - \frac{[\hat{\Sigma}_T^{\gamma Z}(k^2)]^2}{k^2 + \hat{\Sigma}_T^{\gamma\gamma}(k^2)} \tag{55}$$

$$\hat{\Sigma}_T^{\mathrm{ZZ}}(k^2) = \Sigma_T^{\mathrm{Z}}(k^2) + (k^2 - M_Z^2)\delta Z_{\mathrm{Z}} - \delta M_Z^2 \tag{56}$$

$$\hat{\Sigma}_T^{\gamma Z}(k^2) = \Sigma_T^{\gamma Z}(k^2) + \tfrac{1}{2}\delta Z^{Z\gamma}(k^2 - M_Z^2 - \delta M_Z^2) + \tfrac{1}{2}\delta Z^{\gamma Z}k^2, \tag{57}$$

$$\hat{\Sigma}_T^{\gamma\gamma}(k^2) = \Sigma_T^{\gamma\gamma}(k^2) + \tfrac{1}{4}(\delta Z^{Z\gamma})^2(k^2 - M_Z^2 - \delta M_Z^2) + \delta Z^{\gamma\gamma}k^2. \tag{58}$$

$$\hat{\Sigma}^{H}(k^2) = (k^2 - M_H^2)\delta Z_H + \Sigma^H(k^2) - \delta M_H^2 \tag{59}$$

Similarly for the fermion:

$$\hat{\Gamma}_f(\slashed{k}) = i(\slashed{k} - m_f) + i[\,\slashed{k}\omega_-\hat{\Sigma}_f^L(k^2) + \slashed{k}\omega_+\hat{\Sigma}_f^R(k^2) + m_f\hat{\Sigma}_f^S(k^2)\,] \tag{60}$$

where

$$\hat{\Sigma}_f^L(k^2) = \Sigma_f^L(k^2) + \delta Z_f^L \tag{61}$$

$$\hat{\Sigma}_f^R(k^2) = \Sigma_f^R(k^2) + \delta Z_f^R \tag{62}$$

$$\hat{\Sigma}_f^S(k^2) = \Sigma_f^S(k^2) - \frac{1}{2}(\delta Z_f^L + \delta Z_f^R) - \frac{\delta m_f}{m_f}, \tag{63}$$

and $\omega_\pm = \frac{1\pm\gamma_5}{2}$. One can get the corresponding propagator of each renormalized 1-PI two-point vector-boson function by taking an inverse. That is to say, locating propagators at poles is equivalent to setting renormalized 1-PI two-point functions to zero while projecting to physical states (such as $\varepsilon^\mu(k)$, $u(k)$, and $\overline{u}(k)$). By normalizing the residue of the renormalized propagator to be 1 in the on-shell limit, one determines the renormalization constant of the field. For $\gamma - Z$ mixing, we determine the off-diagonal field strength counterterms by requiring matrices of renormalized 1-PI two-point functions are diagonal at photon-pole
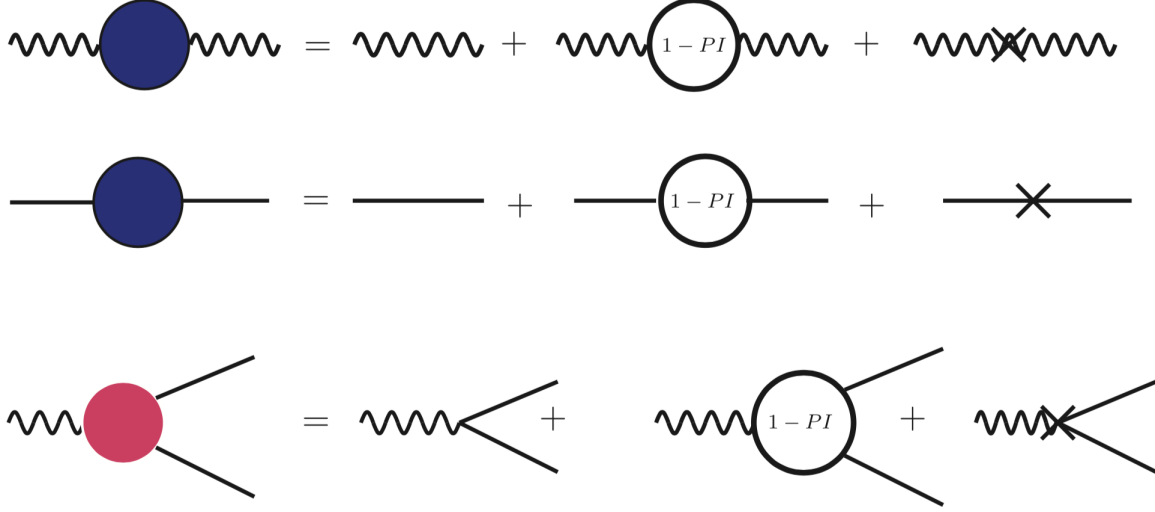
Figure 2: Feynman diagrams for 1-PI renormalized two and three-point functions.

$k^2 = 0$ and Z-pole $k^2 = M_Z^2$. All conditions can be expressed as

$$\text{Re}\,\hat{\Gamma}_{\mu\nu}^W(k^2)\varepsilon^\nu(k)\Big|_{k^2=M_W^2} = 0 \qquad\qquad \text{Re}\,\hat{\Gamma}_{\mu\nu}^{AZ}(k^2)\varepsilon^\nu(k)\Big|_{k^2=M_Z^2} = 0 \tag{64}$$

$$\text{Re}\,\hat{\Gamma}_{\mu\nu}^{AZ}(k^2)\varepsilon^\nu(k)\Big|_{k^2=0} = 0 \qquad\qquad \text{Re}\,\hat{\Gamma}_{\mu\nu}^{ZZ}(k^2)\varepsilon^\nu(k)\Big|_{k^2=M_Z^2} = 0 \tag{65}$$

$$\lim_{k^2\to M_W^2} \frac{1}{k^2 - M_W^2}\text{Re}\,\hat{\Gamma}_{\mu\nu}^W(k^2)\varepsilon^\nu(k) = -i\varepsilon_\mu(k) \qquad\qquad \lim_{k^2\to 0} \frac{1}{k^2}\text{Re}\,\hat{\Gamma}_{\mu\nu}^{AA}(k^2)\varepsilon^\nu(k) = -i\varepsilon_\mu(k) \tag{66}$$

$$\lim_{k^2\to M_Z^2} \frac{1}{k^2 - M_Z^2}\text{Re}\,\hat{\Gamma}_{\mu\nu}^Z(k^2)\varepsilon^\nu(k) = -i\varepsilon_\mu(k) \qquad\qquad \lim_{k^2\to M_H^2} \frac{1}{k^2 - M_H^2}\text{Re}\,\hat{\Gamma}^H(k^2) = i \tag{67}$$

$$\lim_{\slashed{k}=m_f} \text{Re}\,\hat{\Gamma}^f(k)u(k) = 0 \qquad\qquad \lim_{\slashed{k}=m_f} \frac{\text{Re}\,\hat{\Gamma}^f(k)}{\slashed{k} - m_f}u(k) = iu(k) \tag{68}$$

While solving for counterterms order-by-order in gauge boson sector from Eq. (64)- (68), one sees that only the transverse components of renormalized 1-PI two-point vector-boson functions in Eqs. (54)- (59) contribute. At the same time, the longitudinal part of the 1-PI self-energy function cancels the self-energy given by physical-unphysical field mixing if one chooses gauge-fixing counterterms appropriately. Since the renormalization of all unphysical parameters is irrelevant to the S-matrix, we can choose a convenient way of renormalizing the whole unphysical sector while having the Slavnov-Taylor identity manifested at the same time.(see Ref. [99] for more detail.) Restricting our discussion at one-loop level, we can thus

write down the one-loop EW renormalization counterterms based on Eq. (68)

$$\delta^{(1)}M_{\mathrm{W}}^2 = \operatorname{Re}\Sigma_T^{W\,(1)}(M_{\mathrm{W}}^2) \qquad\qquad \delta^{(1)}M_{\mathrm{Z}}^2 = \operatorname{Re}\Sigma_T^{ZZ\,(1)}(M_{\mathrm{Z}}^2) \tag{69}$$

$$\delta^{(1)}Z_{\mathrm{W}} = -\operatorname{Re}\left.\frac{\partial\Sigma_T^W(k^2)}{\partial k^2}\right|_{k^2=M_{\mathrm{W}}^2} \qquad\qquad \delta^{(1)}Z_{ZZ} = -\operatorname{Re}\left.\frac{\partial\Sigma_T^{(1)ZZ}(k^2)}{\partial k^2}\right|_{k^2=M_{\mathrm{Z}}^2} \tag{70}$$

$$\delta^{(1)}Z_{\gamma\mathrm{Z}} = -2\operatorname{Re}\frac{\Sigma_T^{\gamma Z\,(1)}(M_{\mathrm{Z}}^2)}{M_{\mathrm{Z}}^2} \qquad\qquad \delta^{(1)}Z_{\mathrm{Z}\gamma} = 2\operatorname{Re}\frac{\Sigma_T^{Z\gamma\,(1)}(0)}{M_{\mathrm{Z}}^2} \tag{71}$$

$$\delta^{(1)}Z_{\gamma\gamma} = -\operatorname{Re}\left.\frac{\partial\Sigma_T^{\gamma Z\,(1)}(k^2)}{\partial k^2}\right|_{k^2=0}, \tag{72}$$

$$\delta^{(1)}M_H^2 = \operatorname{Re}\Sigma_T^{H\,(1)}(M_H^2) \qquad\qquad \delta^{(1)}Z_H = -\operatorname{Re}\left.\frac{\partial\Sigma_T^{(1)H}(k^2)}{\partial k^2}\right|_{k^2=M_H^2} \tag{73}$$

Similarly for fermions:

$$\delta^{(1)}m_f = \frac{1}{2}m_f[\operatorname{Re}\Sigma_f^L(m_f^2) + \operatorname{Re}\Sigma_f^R(m_f^2) + 2\operatorname{Re}\Sigma_f^S(m_f^2)], \tag{74}$$

$$\delta^{(1)}Z_f^L = -\operatorname{Re}\Sigma_f^L(m_f^2) - m_f^2\frac{\partial^2}{\partial p^2}\operatorname{Re}\left[\Sigma_f^L(m_f^2) + \Sigma_f^R(m_f^2) + 2\Sigma_f^S(m_f^2)\right]\Big|_{p^2=m_f^2}, \tag{75}$$

$$\delta^{(1)}Z_f^R = -\operatorname{Re}\Sigma_f^R(m_f^2) - m_f^2\frac{\partial^2}{\partial p^2}\operatorname{Re}\left[\Sigma_f^L(m_f^2) + \Sigma_f^R(m_f^2) + 2\Sigma_f^S(m_f^2)\right]\Big|_{p^2=m_f^2}. \tag{76}$$

To determine the renormalization constant for the charge, we inspect the renormalized three-point function (at one-loop level)

$$\hat{\Gamma}_\mu^{\gamma ff}(p', p) = ieQ_f\gamma_\mu + ieQ_f\Lambda_\mu^{\gamma ff}(p', p) - Q_f\gamma_\mu(\delta Z_e + \frac{1}{2}\delta Z_{\gamma\gamma} + \delta Z_L^f\omega_- + \delta Z_R^f\omega_+) \tag{77}$$

$$+ \gamma_\mu(v_f - a_f\gamma_5)\frac{1}{2}\delta Z_{Z\gamma}, \tag{78}$$

in which the physical charge e is defined through Thompson scattering so that

$$\overline{u}(p)\hat{\Gamma}_\mu^{\gamma ff}(p, p)\overline{u}(p) \equiv \overline{u}(p)\gamma_\mu\overline{u}(p). \tag{79}$$

By imposing Ward identity and some other useful relations

$$\overline{u}(p)\Lambda_\mu^{\gamma ff}(p, p)u(p) = -eQ_f\overline{u}(p)\left[\frac{\partial}{\partial p^\mu}\Sigma^{\bar{f}f(1)}(p)\right]u(p) - a_f\overline{u}(p)\gamma_\mu(1-\gamma_5)u(p)\Sigma_T^{\gamma Z(1)}(0)/M_{\mathrm{Z}}^2, \tag{80}$$

$$\overline{u}(p)[\frac{\partial}{\partial p^\mu}\Sigma^{\bar{f}f(1)}(p)]u(p) = -\overline{u}(p)\gamma_\mu(\delta Z_L^f\omega_- + \delta Z_R^f\omega_+)u(p), \tag{81}$$

$$\Sigma_T^{\gamma Z(1)}(0) = \frac{M_{\mathrm{Z}}^2}{2}\delta^{(1)}Z_{Z\gamma}, \tag{82}$$

$$v_f - a_f = -Q_f\frac{s_{\mathrm{W}}}{c_{\mathrm{W}}}. \tag{83}$$

22

We can eventually obtain

$$\delta^{(1)}Z_e = -\frac{1}{2}\delta^{(1)}Z_{\gamma\gamma} - \frac{1}{2}\frac{s_{\mathrm{W}}}{c_{\mathrm{W}}}\delta^{(1)}Z_{\mathrm{Z}\gamma} = \frac{1}{2}\frac{\partial\Sigma_T^{\gamma\gamma(1)}(k^2)}{\partial k^2}\bigg|_{k^2=0} - \frac{s_{\mathrm{W}}}{c_{\mathrm{W}}}\Sigma_T^{\gamma Z(1)}(0) \tag{84}$$

As a consequence, the renormalization of the charge coupling is fermion-flavor independent after all. The reparametrization of weak-mixing angle from bare Lagrangian reads

$$s_{0,\mathrm{W}}^2 = 1 - c_{0,\mathrm{W}}^2 = 1 - \frac{M_{0,\mathrm{W}}^2}{M_{0,\mathrm{Z}}^2}. \tag{85}$$

In the OS scheme, it is derived from requiring such a relation hold at arbitrary higher order[100]. So that at one-loop level, one can write

$$\frac{\delta^{(1)}s_{\mathrm{W}}^2}{s_{\mathrm{W}}^2} = \frac{c_{\mathrm{W}}^2}{s_{\mathrm{W}}^2}\left(\frac{\delta^{(1)}M_{\mathrm{Z}}^2}{M_{\mathrm{Z}}^2} - \frac{\delta^{(1)}M_{\mathrm{W}}^2}{M_{\mathrm{W}}^2}\right), \tag{86}$$

where the renormalization constant of weak-mixing angle is determined by gauge-boson masses' counterterms. Therefore, the weak-mixing angle in the OS scheme is a process-independent quantity. There are many other schemes for imposing renormalization conditions. For instance, in $\overline{\mathrm{MS}}$ scheme, all counterterms only absorb the UV divergences, i.e., no finite constants in counterterms whatsoever. The parameters renormalized under $\overline{\mathrm{MS}}$ scheme are not physical, and depend on a temporarily introduced renormalization scale μ. It is thus formally easy but physically not so straightforward comparing to the OS scheme. We will revisit this scheme in chapter 4 where we use $\overline{\mathrm{MS}}$ prescription for the top-quark mass in mixed EW-QCD corrections.

2.2 Techniques of calculating loop integrals

We have studied the way of determining renormalization constants by imposing a set of renormalization condition. Yet the radiative corrections captured in the self-energy function $\Sigma_T(k^2)$ and vertex function $\Lambda_\mu(p', p)$ remain to be computed[1]. A Feynman loop integral corresponds to a Feynman diagram that contains one or multiple closed loops. Given by the nature of quantum field theory, the momentum flowing inside of each loop must be integrated over, which potentially gives rise to the UV and IR divergences that are ought to be regularized in prior to the renormalization procedure. The evaluation of the Feynman loop integral forms a vast topic per se. One can find thorough reviews on analytical approaches in [101] and numerical approaches in [102]. In this section, we will be focusing on methods adopted in our research. And they can be split into two steps: (i) the algebraic reduction, (ii) the evaluation of loop integrals.

2.2.1 Loop integral reduction

For a given process laid out as Feynman amplitudes containing one or multi-loop integrals at given order, one can break it further down to a linear combination of scalar integral family known as "master integrals" (MIs). There are many methods tackling this issue. We discuss two methods in the following.

2.2.1.1 Tensor reduction and Passarino-Veltman approach

For one-loop and partially two-loop cases, one uses the so-called Passarino-Veltmann method. To illustrate this method, we firstly write down a generic one-loop N-point integral in d-dimension as

$$T^N_{\mu_1\dots\mu_M}(p_1, ..., p_{N-1}, m_0, ..., m_{N-1}) = \frac{(2\pi\mu)^{4-D}}{i\pi^2} \int d^D q$$

$$\times \frac{q_{\mu_1} \cdots q_{\mu_M}}{(q^2 - m_0^2 + i\epsilon)([(q + p_1)^2 - m_1^2 + i\epsilon] \cdots [(q + p_{N-1})^2 - m_{N-1}^2 + i\epsilon]}, \tag{87}$$

where the convention $T^1 \equiv A$, $T^2 \equiv B$, $T^3 \equiv C$, *etc* is used. When $M = 0$, we obtain the scalar integral family A_0, B_0, C_0, *etc*, which is also recognized as the master integral basis of all one-loop integrals. It so turns out that these Lorentz covariant tensor-integrals can be decomposed into tensors constructed from external momenta and metric tensor with

---

[1] out of the scope of the renormalization of the SM, there are also other possible multi-point functions that need to be computed, such as box diagrams, etc.

symmetric coefficients. This can be explicitly shown as the follow:

$$B_\mu = p_1^\mu B_1 \,,$$

$$B_{\mu\nu} = g_{\mu\nu} B_{00} + p_{1\mu} p_{2\nu} B_{11} \,,$$

$$C_\mu = p_{1\mu} C_1 + p_{2\mu} C_2 \,,$$

$$C_{\mu\nu} = g_{\mu\nu} C_{00} + \sum_{i,j=1}^{2} p_{i\mu} p_{j\nu} C_{ij} \,,$$

$$C_{\mu\nu\rho} = \sum_{i=1}^{2} (g_{\mu\nu} p_{i\rho} + g_{\nu\rho} p_{i\mu} + g_{\mu\rho} p_{i\nu}) C_{00i} + \sum_{i,j,k=1}^{2} p_{i\mu} p_{j\nu} p_{k\rho} C_{ijk} \,,$$

$$D_\mu = \sum_{i=1}^{3} p_{i\mu} D_i \,,$$

$$\ldots . \tag{88}$$

All these tensor coefficients can be solved as linear combinations of one-loop MIs A_0, B_0, C_0, D_0, etc
by applying the following contractions

- contracting Eq. (88) with external momenta $p^{i\mu}$

$$p_i^{\mu_1} q_{\mu_1} = \frac{1}{2}[(q + p_i)^2 - m_i^2] - \frac{1}{2}(q^2 - m_0^2) - \frac{1}{2}(p_i^2 - m_i^2 + m_0^2)$$

- contracting with metric tensor $g^{\mu\nu}$

$$g^{\mu\nu} q_\mu q_\nu = (q^2 - m_0^2) + m_0^2$$

recursively and simultaneously solve the set of linear equations of tensor coefficients. Since each time of applying one of those contractions will bring the tensor integral one rank down and/or one propagator less. In circumstances where such a linear equation system is singular, the Passarino-Veltman approach breaks down and one has to find alternative way to circumvent it. However, sometimes it is better dealing just with scalar quantities at the beginning rather than going through this recurisve algorithm. Hence one can in principle construct relevant projection operators to decompose the tensor structure of two, three, and four-point functions. Such a method is extremely helpful for dealing with polarized amplitudes beyond tree-level. See appendix 6.1.

2.2.1.2 Integration-by-parts (IBP) approach[1]

When moving from one-loop to two-loop and cases beyond, the number of loop integrals at a given order of the correction becomes enormous. Therefore, it is important to reduce

thousands of loop integrals to a small set of MIs. Given that the surface integral vanishes in DR, one can apply the following identity to an L-loop integral

$$\int \prod_{i=1}^{L} \frac{d^d k_i}{i\pi^{d/2}} \frac{\partial}{\partial k_i} \left(\frac{\{k_j, p_j\}}{D_1^{\alpha_1} \dots D_N^{\alpha_N}} \right) = 0 \,, \tag{89}$$

with

$$D_a = (k_i + p_i)^2 - m_a^2 + i\epsilon \tag{90}$$

recursively until it finally reaches a minimal linear combination of MIs. It has been shown that such finite MI basis always exists[103]. The essential idea of IBP approach is that instead of evaluating hundreds or thousands of integrals, one can just carry out a smaller set of MIs by recursively using Eq.(89) along with some other Lorentz identities[104] and symmetries. Several cutting-edge public codes such as AIR, FIRE, REDUZE, LITERED, MINCER[105, 106, 107, 108, 109], have been developed to tackle the IBP reduction of general multi-loop integrals. Besides, there are many other mordern techniques developed recently, one can refer to [98] for a thorough discussion.

2.2.2 The calculation of master integrals

Multifarious techniques of calculating MIs have been developed. Analytically, evaluating MIs is essentially writing MIs in terms of a set of well-defined functions of invariants of external momenta, propagator masses. However, the variation of masses and external momenta give rise to the difficulties of solving MIs by elementary functions, which motivates people to search for numerical methods. Here, we give introductions to two methods employed in this thesis.

2.2.2.1   Feynman parameters approach

A scalar L-loop integral in d-dimension with N propagators to the power ν_j

$$I = \int \prod_{i=1}^{L} \frac{d^d k_i}{i\pi^{d/2}} \prod_{j=1}^{N} \frac{1}{D_j^{\nu_j}} \tag{91}$$

can be parametrized as

$$I = \Gamma(N_\nu) \int \prod_{j=1}^{N} dx_j x_j^{\nu_j - 1} \delta(1 - \sum_{i=1}^{N} x_i) \int \prod_{i=1}^{L} \frac{d^d k_i}{i\pi^{d/2}} \frac{1}{\left[x_1 D_1 + \dots + x_j D_j \right]^{N_\nu}} \,, \tag{92}$$

26

where the denominator can be re-parametrized as

$$x_1 D_1 + \ldots + x_j D_j = \sum_{j,l=1}^{L} k_j \cdot k_l M_{jl} - 2 \sum_{j=1}^{L} k_j \cdot Q_j + J \, , \tag{93}$$

where the $L \times L$ matrix M_{jl}, the L-column vector Q_j, and the scalar function J are functions of Feynman parameters x_j. By shifting the momenta to eliminate the linearly k-dependent terms in the square bracket, the integral becomes

$$I = (-1)^{N_\nu} \frac{\Gamma(N_\nu - Ld/2)}{\prod_{j=1}^{N} \Gamma(\nu_j)} \int_0^\infty \prod_{j=1}^{N} dx_j x_j^{\nu_j - 1} \delta(1 - \sum_{i=1}^{N} x_i) \frac{\mathcal{U}^{N_\nu - (L+1)d/2}}{\mathcal{F}^{N_\nu - Ld/2}} \tag{94}$$

where

$$\mathcal{U} = det(\text{M}) \, , \; N_\nu = \sum_{j=1}^{N} \nu_j \, , \tag{95}$$

$$\mathcal{F} = det(\text{M}) \Big[\sum_{i,j=1}^{L} Q_i M_{ij} Q_j - J - i\delta \Big]. \tag{96}$$

This is in fact the most straightforward way of evaluating simple MIs, such as one-loop integral family, $A_0, B_0, C_0, D_0 etc$ [110]. More complicated multi-loop MIs requires additional techniques or some totally different approaches. Feynman parametrization has not only been used analytically in Ref. [111, 112, 113, 114, 115, 116], but also to carry out two-loop radiative corrections numerically [117, 118, 119, 120, 121]. However, the numerical Feynman parametrization technique cannot handle IR singularities straightforwardly, which makes it less applicable in higher-loop QCD calculations. Besides, the determination of the integration contour depends on the topology of the Feymann diagrams, hence whittling down the extendibility of such technique.

2.2.2.2   *Dispersion relation*

Let us consider a complex-valued function, $F(s)$, where s can be in general complex, with the following features: (i) a branch-cut on real axis as $s > M^2$, (ii) is analytical everywhere but along the branch-cut, (iii) real as real $s < M^2$. If the discontinuity is defined as

$$F(s \pm i\epsilon) = \text{Re}\, F(s) \pm i\text{Im}\, F(s), \tag{97}$$

by Schwartz' reflection principle and Cauchy's theorem we derive[2]

$$F(q^2) = \frac{1}{\pi} \int_{M^2}^{\infty} ds \frac{\operatorname{Im} F(s)}{s - q^2 - i\epsilon}.$$ (98)

Eq. (98) shows that if a loop integral shares the same features as $F(s)$, then it can be reconstructed from its discontinuity, which is determined from the Cutkosky rules. It especially reveals its power for sub-loop diagrams where one can use dispersion relation to write a multi-loop integral as a series of one-loop integral multiply by the right hand side of Eq. (98).For non-trivial topologies, one can combine dispersion relation with Feynman parametrization, converting complicated sub-loop structure into self-energy sub-loop, and use the discontinuity of B_0 function. Many EW and mixed EW-QCD two-loop corrections have been carried out by using dispersion relation[66, 122, 123, 124, 125, 126, 127, 67, 128, 129, 130, 131, 132]. A public package TVID has been developed for three-loop planar self-energy with arbitrary masses [133, 9]. The dispersion relation provides excellent numerical stability and convergence but the removal of UV and IR divergences needs to be studied case-by-case, which makes it difficult for automation.

2.3 Theoretical profiling of the unstable particle

Most particles in the SM are unstable. They don't exist long enough in the lab frame to be captured by tracks in detectors, but rather appear as resonance in the decay products. The lifetime of each unstable particle is the inverse of the width of corresponding resonance. From a theoretical point of view, the in and out-states of S-matrix must be asymptotic, hence all unstable particles can only appear as intermediate states in the S-matrix, making an amplitude features a pole as $\mathcal{A} \sim \frac{1}{p^2 - M^2}$, where M^2 is the square of the physical mass. This leads to a singularity if $p^2 \sim M^2$. This issue is alleviated by having both the real and imaginary part of the 1-PI self-energy properly resummed. It can be shown diagramatically as Fig. 3. The inverse of the renormalized dressed propagator G_R, can be written as

$$G_R(p) = \frac{1}{Z} G(p), \quad G_R^{-1}(p) = Z((p^2 - M^2) + \Sigma(p^2)), \qquad M^2 = M_{\mathrm{p}}^2 + \delta M^2 \quad (99)$$

where M_{p} is the renormalized mass. Now, defining the pole of this propagator as s_0, we get

$$Z(s_0 - M^2) + \Sigma(s_0) = 0. \quad (100)$$

---

[2]it has assumed that $\lim_{\Lambda^2 \to \infty} \oint_{|s|=\Lambda^2} ds \frac{F(s)}{s-q^2} = 0$, otherwise, further subtraction will be needed.

Figure 3: Dyson-resummation of 1-PI of a scalar propagator, where $\Sigma(p^2)$ is a complex self-energy function at certain order.

Combining Eq. (99) (100) to eliminate the bare mass M, we acquire the renormalized Green's function that looks like

$$G_R(p) = \frac{iZ^{-1}}{p^2 - s_0 + \Sigma(p^2) - \Sigma(s_0)} = \frac{iZ^{-1}}{p^2 - s_0}\left(1 - \frac{\Sigma(p^2) - \Sigma(s_0)}{p^2 - s_0} + \ldots\right) \equiv \frac{i}{p^2 - s_0} \quad (101)$$

as $p^2 \to s_0$, featuring a pole exactly at $p^2 = s_0$ and a residue i, leading to the field strength renormalization constant $Z^{-1} = \lim_{p^2 \to s_0} 1 - \frac{\Sigma(p^2) - \Sigma(s_0)}{p^2 - s_0} + \ldots$. Eq.(101) has been rigorously shown that the pole of the resummed propagator is gauge-invariant[134]. One can also argue that since the position of the pole can be determined from cross section using dispersion relation and analytical continuation, it has to be also gauge-invariant[135]. The part facotorized out in the parenthesis is equivalent to the renormalization constant Z of the field. If it is a stable particle, then $\Sigma(s_0)$ is real and s_0 locates on the real axis. If the particle is unstable, then $\Sigma(s_0)$ is a complex value, and we can derive the imaginary part of the pole s_0 as

$$\operatorname{Im} s_0 = -\operatorname{Im} \Sigma(s_0), \quad (102)$$

where $\operatorname{Im} \Sigma(s_0) > 0$ due to optical theorem. Hence the imaginary part of the pole should be negative. The forward time evolution of the propagator is obtained by the inverse Fourier transform in frequency:

$$\tilde{G}(t) = \int \frac{dp_0}{2\pi} e^{-ip_0 t} G(p_0), \quad t > 0 \quad (103)$$

Using the residue theorem and squaring the $\tilde{G}(t)$, we get

$$|\tilde{G}(t)|^2 \sim e^{2\mathrm{Im}\sqrt{s_0}t}, \tag{104}$$

which corresponds to the exponential decay $\sim e^{-\Gamma t}$. It has been argued[136, 137] that only having the pole of unstable particle defined at

$$\sqrt{s_0} = M_p - \frac{i}{2}\Gamma, \tag{105}$$

do we obtain the quantum mechanical definition of the mass and width of the unstable particle. In the limit where $\Gamma \ll M_p$ we can write

$$s_0 = (M_p - \frac{i}{2}\Gamma)^2 \approx M_p^2 - iM_p\Gamma, \tag{106}$$

which is widely used for the massive gauge bosons in the SM.

2.3.1 Gauge-invariance issue

As we have mentioned, the complex pole of the propagator, both the real part and the imaginary part of which has physical meaning, has been rigorously proved to be gauge-invariant. This gives rise to a several gauge-dependence concerns. The first one is about the renormalization prescription. Historically, people used

$$m^2 - M^2 + \mathrm{Re}\,\Sigma_T(m^2) \equiv 0 \tag{107}$$

instead of Eq. (100) for the W and Z-boson mass prescription, where m is the real physical mass, the M is the bare mass, and the Σ_T is the transverse component of the self-energy. [3] Such discrepancy on defining pole location results in the difference of renormalized mass at two-loop order shown as[126]

$$m - M_p = \frac{1}{2}\Gamma\mathrm{Im}\,\Sigma'(M_p^2) + \mathcal{O}(\alpha^3) \tag{108}$$

One can then argue that since M_p, Γ are gauge-invariant, and the bosonic part of $\mathrm{Im}\,\Sigma'(M_p^2)$ contains gauge-parameter-dependent Heaviside functions due to the gauge-dependent mass of relevant unphysical Goldstone fields, the m must be gauge-dependent. This leads to the conclusion that the renormalization counterterm given by Eq. (107) is gauge-dependent, and such gauge-dependency enters at two-loop level. Hence for the renormalization of unstable particle, we define the location of the pole followed by Eq. (100), thereby obtaining the

---

[3]This also originated the running width scheme used in Eq. (112), see [136]

gauge-independent counterterms as follows:

$$\delta M^2 = \frac{1}{Z}\mathrm{Re}\,\Sigma(s_0)\,, \quad Z = \Big(1 + \mathrm{Re}\,\Sigma'(s_0)\Big)^{-1} \tag{109}$$

Consequently, one can also obtain the width:

$$\Gamma = \frac{\mathrm{Im}\,\Sigma(s_0)}{ZM_p}. \tag{110}$$

The renormalization counterterms defined above can be found compatible with Sec. (2.1.2.2) at one-loop if one expands the terms depending on s_0 in $\Gamma/M \sim \alpha$. It has been explicitly shown that Eq. (100) lead to gauge-independent mass and field counterterms at two-loop level in the SM [138, 139, 140].

Another concern of gauge invariance, stemming from the study of unstable particles, especially the Z-pole at the LEP, is the gauge dependence of the scattering amplitude in the vicinity of resonance. It has been argued that the use of Dyson-resummed propagator performed in Fig. 3 in the Z-resonant amplitude spoils the delicate gauge cancellation among different Feynman diagrams which are separately gauge-dependent [141, 142, 143]. And we will explore the details of the resolutions in the following subsections. We will be focusing on the Pole scheme in the upcoming subsection 2.3.2 since it relates to the work of this thesis, and we give some brief introduction to other schemes in Sec. 2.3.3.

2.3.2 Pole scheme

Guided by the construction principle of the S-matrix, the amplitude derived from a massive gauge theory, containing one unstable particle can be written as a Laurent series as follows:

$$\mathcal{A} = \frac{R}{s - s_0} + B(s), \tag{111}$$

where $B(s)$ is the non-resonant background, R is the resonant residue, and the s_0 is the pole. We have argued that the s_0 is defined to be gauge-invariant in the last section, and the residue R and the background $B(s)$ feature different pole structure, thereby having no gauge cancellation between R and $B(s)$. Hence R and $B(s)$ are separately gauge-invariant as well.[141, 142, 143, 144]. Several subtleties worth a mention here:

- Practically, the Laurent series needs the power counting $\mathcal{O}(\Gamma/M) \ll 1$ to avoid the complex kinematical arguments in matrix elements and to incoporate with the OS renormalization scheme.
- For a non-factorizable higher-order loop diagram, especially when dealing with a charged

31

resonating propagator, the separation between resonant part and non-resonant part, and the corresponding Dyson-resummation of the resonant part are highly non-trivial[145, 146]. This can be seem later in Chapter 4.

Due to the well-defined separation between resonance and background in the pole scheme, it provides a well-suited framework for resonant processes in which signals dominate over the background. This scheme is widely used in the 4-fermion process with a gauge resonance such as the W and Z-boson [146, 147, 148]. In this thesis, we follow the same practice in computing the NNLO Z-resnoance in e^+e^- colliders in Chapter 4.

2.3.3 Other schemes

2.3.3.1 Complex-mass scheme (CMS)

Another way to circumvent the singularity issue in the resonant amplitude is to have the masses of propagating particles complex at the beginning. Such a scheme is the so-called Complex Mass Scheme, where all internal unstable particles are identified with complex value as in Eq. (106). Thus the perturbation series of bare parameters in the Lagrangian need a rearrangement such that not only are renormalization constants becoming complex, both couplings and weak-mixing angle are also complex. We stress several aspects of the CMS in the follow (for a detailed review, one can refer to [98]):

- Since all gauge-boson masses are replaced by complex values via analytical continuation, the relevant Ward or Slavnov-Taylor identities are retained exactly. However, the complex weak-mixing angle and the coupling do introduce spurious terms that spoil the Cutkosky cutting rules, thereby violating the unitarity. However, all these spurious terms stemming from the imaginary part of the weak-mixing angle and the coupling are at least an order higher than the wanted order of calculations.

- The complex counterterm lead to further complications on evaluating loop integrals with complex kinematical variables. Although it is feasible in one-loop cases through analytical continuations[149], it is challenging dealing with complex kinematics in calculations beyond one loop. A simplified version of the complex renormalization, where one will have to expand around the real part of the complex mass as $\Gamma \ll M$ in the SM, is thus developed to circumvent such challenge. However, such expansion fails at the charged unstable particles' self-energy contributions given by logarithmic branch points that linearly vanish at the mass shell[4] as shown in Fig. 4. Therefore, one needs to determine

---

[4]It also has been shown that this infrared behavior might alter the decay law algebraically in real time (non-asymptotically), thereby leading to an alternative production mechanism, of which the efficiency of populating ultralight particles in the long-time limit could be as much as exponential decay in the early
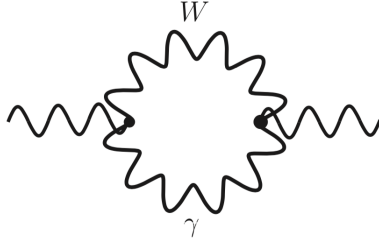
Figure 4: the emission and re-absorption of the massless gauge quanta, featuring a branch point that linearly vanished near the pole as $\Sigma(p^2) \sim \alpha(p^2 - s_0) \log(p^2 - s_0)$

the add-back value that amounts to the failure of the expansion in such renormalization procedure.

2.3.3.2 Fermion-loop scheme

Stemming from the fact that closed fermion loops always provide a subset of gauge-invariant radiative corrections, one can thus Dyson-resum the close fermion loops solely while maintaining the delicate gauge-dependence cancellation among other contributions. However, as an approximate approach that cannot deliver arbitrary accuracy, the legitiamcy of the customized Dyson-resummation needs to be checked process-by-process. And it breaks down if the bosonic contribution dominates to the width in a certain BSM model. Hence it is less likely to be a general method. One can refer to [153, 154, 155] for more details.

2.3.3.3 Effective Field Theories

An EFT of the SM based on the power counting $\mathcal{O}(\Gamma/M) \ll 1$ can be used to describe the resonance of the unstable particle[156, 157, 158]. It is theoretically well set-up and can be systematically extended to off-resonance region, such as pair production, by imposing further expansion such as $\frac{s - 4M_V^2}{4M_V^2} \sim \upsilon^2 \ll 1$ [159, 160] . However, the natural deficiency of using EFT is that it requires more complications on linking EFT degree of freedom to experiments when differential properties of observables are needed.

---

universe. See [150, 151, 152] for more discussion.

33

2.4 Input parameters of the Electroweak Standard Model

Albeit all couplings and masses can be traced back to the original set of couplings from $SU_W(2) \times U_Y(1)$ as $\{g_1, g_2, \lambda, \mu, Y_{ij}^f\}$, we replace them by masses and charges that have direct physical meaning and can be determined through measurements. To make a sensible precision test of the SM, one has to choose an appropriate set of input parameters, which depends not only on specific processes but also the renormalization scheme. Here we address some aspects regarding to input parameters under OS scheme:

- **Light fermion masses**: the masses of fundamental particles are defined as the real part of the pole in each corresponding propagator rendered as a resonance peak phenomenologically. However, in low-energy QCD, light quarks are not propagating degree of freedom, making the pole mass definition of quarks problematic. One way to circumvent this is to use alternative prescription of quark masses, such as the running mass at appropriate scale. Nevertheless, the properly defined EWPOs should be insensitive to the light-fermion masses effect suppressed by m_f^2/Λ_{EW}, where Λ_{EW} is around masses of EW gauge bosons.

- **the CKM matrix**: parametrizing renormalization constants for the CKM matrix at higher order in perturbation theory is difficult as it is subject to gauge-dependent issue [161]. But for most high-energy scattering processes, the CKM matrix can be safely approximated as a unitary matrix due to its negligble effect.

- **Gauge-boson masses**: the boson masses $M_{W,Z,H}$ are defined as the real part of the pole according to OS scheme, in which the widths in propagators are constants. However, for historical reason, one alternative resonance formula, rather than the original Breit-Wigner approximation, was used for experimental fitting. For instance, the resonant part of the cross section for $e^+e^- \to f\bar{f}$ uses the form

$$\sigma_{res} = \sigma_0 \frac{s\Gamma_Z^2}{(s - M_Z^2)^2 + \frac{s^2\Gamma_Z^2}{M_Z^2}} , \quad \sigma = \frac{12\pi}{M_Z^2} \cdot \frac{\Gamma_e\Gamma_f}{\Gamma_Z} \tag{112}$$

Hence the actual pole masses and widths are different from the measured values by

$$\overline{M}_Z = M_Z(1 + \gamma^2)^{-1/2}, \ \overline{\Gamma}_Z = \Gamma_Z(1 + \gamma^2)^{-1/2} , \gamma = \Gamma_Z/M_Z. \tag{113}$$

where the $\overline{M}_Z$ and $\overline{\Gamma}_Z$ are defined as pole-mass quantities. It has been found that such discrepancy results in numerical impact as

$$\overline{M}_Z \approx M_Z - 34 \text{ MeV}, \qquad \overline{\Gamma}_Z \approx \Gamma_Z - 0.9 \text{ MeV} \tag{114}$$

Since $\overline{M}_Z, \overline{\Gamma}_Z, \overline{M}_W, \overline{\Gamma}_W$ can both be used as input parameters due to their precise mea-

surement. One has to take care of such translation while computing higher order corrections.

- **Running of the couplings**: the renormalization of the electromagnetic charge e is defined through Eq. (84) that it receives corrections from vacuum polarization. For light quarks u, d, s, c, b running in the loop, it results in spoiler of perturbation calculation since the QCD at the light-quark mass scale is inherently non-perturbative.

$$\frac{\partial \Sigma_T^{\gamma\gamma(1)}(k^2)}{\partial k^2}\bigg|_{k^2=0} \equiv \Pi(0) = \Pi_{\text{lep}}(0) + \Pi_{\text{had}}(0) + \Pi_{\text{top}}(0) \tag{115}$$

Writing

$$\Pi(0) - \text{Re}\,\Pi(M_Z^2) = \Pi_{\text{lep}}(0) - \text{Re}\,\Pi_{\text{lep}}(M_Z^2) + \Pi_{\text{had}}(0) - \text{Re}\,\Pi_{\text{had}}(M_Z^2) + \Pi_{\text{top}}(0) - \text{Re}\,\Pi_{\text{top}}(M_Z^2), \tag{116}$$

and $\Pi(0)$ can be recast into

$$\Pi(0) = \Delta\alpha + \Pi_{\text{top}}(0) + \text{Re}\,\Pi_{\text{lf}}(M_Z^2), \tag{117}$$

hence the charge renormalization one-loop counterterm can be written as

$$\delta^{(1)}Z_e = \frac{1}{2}(\Delta\alpha + \Pi_{\text{top}}(0) + \text{Re}\,\Pi_{\text{lf}}(M_Z^2)) \tag{118}$$

where the last two terms can be evaluated perturbatively while the first term $\Delta\alpha$ features contributions from two parts, one comes from the leptonic part, another one comes from the hadronic part. The leptonic part is purely QED, where perturbation theory still holds accountable and has been carried out up to four-loop [162, 163], whereas the $\text{Re}\,\hat{\Pi}_{\text{had}}(s)$ can be determined from experimental data by using dispersion relation and optical theorem.

$$\text{Re}\,\hat{\Pi}_{\text{had}}(s) = \frac{\alpha}{3\pi}s\text{Re}\int_{4m_\pi^2}^{\infty} ds' \frac{R^{\gamma\gamma}(s')}{s'(s'-s-i\epsilon)}, \tag{119}$$

where

$$R^{\gamma\gamma}(s') = \frac{\sigma(e^+e^- \to \gamma^* \to hadrons)}{\sigma(e^+e^- \to \gamma^* \to \mu^+\mu^-)}. \tag{120}$$

For more details and recent updates on $\Delta\alpha_{\text{had}}^{(5)}$ from $R^{\gamma\gamma}$ measurement, one can refer to [164, 165, 166]. It is worth mentioning that there are many other ways of determining $\Delta\alpha_{\text{had}}^{(5)}$, such as using lattice QCD [167, 168, 169], and from measurements of Bhabha scattering[170, 171, 172]. Nevertheless, it is inevitable introducing $\Delta\alpha$ as an extra input

for α coupling in EW radiative correction and it amounts to the running of α from $q^2 = 0$ to $q^2 = M_Z^2$. According to the renormalization group equation

$$\mu \frac{d\alpha}{d\mu} = -\frac{\beta_0}{2\pi} \alpha^2, \quad \beta_0 = \frac{-4}{3} \sum_{f \neq t} Q_f^2, \tag{121}$$

we can turn the coupling $\alpha(0)$ into $\alpha(\overline{M}_Z^2)$ as resumming the leading large logarithm from light fermion loops.

$$\alpha(\overline{M}_Z^2) = \frac{\alpha(0)}{1 - \Delta\alpha(\overline{M}_Z^2)} \tag{122}$$

Alternatively, one can also use the four-Fermi coupling constant G_μ instead of QED coupling α, with the translation

$$\frac{G_\mu}{\sqrt{2}} = \frac{\pi\alpha}{2 s_W^2 c_W^2 \overline{M}_Z^2} (1 + \Delta r), \tag{123}$$

where Δr is the gauge-invariant QED-excluded radiative correction to muon-decay. For strong coupling α_s, due to the asymptotic freedom, one can simply employ running $\alpha_s(\overline{M}_Z^2)$ for the EW relevant processes in high-energy colliders.

Redundancy among $\alpha, G_\mu, \overline{M}_Z, \overline{M}_W$ leads to various choices for the input. According to the discussion above, we can propose a several input schemes for computing the EW radiative corrections:

- $\alpha(0), \overline{M}_W, \overline{M}_Z$: This is the most "natural" scheme based on OS renormalization scheme in which the QED coupling is defined at Thompson limit. This sets the α coupling on an equal footing everywhere including real photon radiation. However, it brings light-fermion masses as intrinsic input from universal large logarithms while quantifying the running from $\alpha(0)$ to $\alpha(M_Z^2)$. Fortunately, owing to the gauge invariance of the fermionic contribtuion, such large logarithms can be resummed while leaving the bosonic contribution intact. With precise measurement of the W-boson mass determined at the LEP-II and the LHC, this input scheme becomes more reliable.
- $\alpha(\overline{M}_Z^2), \overline{M}_Z, \overline{M}_W$: Using Eq. (122), we define a new α which resums the leading logarithmic corrections. Therefore, the light-fermion masses can be neglected. However, this $\alpha(\overline{M}_Z^2)$ scheme cannot be solely used when external photons existing in the process. Due to the exact cancellation of light-fermion-mass logarithms between $\delta Z_{\gamma\gamma}$ and δZ_e, the external photons couple to final states with $\alpha(0)$ effectively. Therefore, extra complications stem from using $\alpha(\overline{M}_Z^2)$ in general cases.
- $G_\mu, \overline{M}_W, \overline{M}_Z$: This is considered to be a good scheme for charged-current interac-

36

tion at high energy scale while it raises real photon couplings from $\alpha(0) \sim 1/137$ to $\alpha_{G_\mu} = G_\mu \sqrt{2} \overline{M}_W^2 (1 - \overline{M}_W^2/\overline{M}_Z^2)/\pi \sim 1/132$ at tree-level, which is considered as a large parametric shift that requires higher-order correction to be taken into account. It is thus also a bad scheme for neutral current interaction where photon couplings play significant roles in off-resonance regions.

- $\alpha(0), G_\mu, \overline{M}_Z$: The is the scheme used for LEP physics, where $\overline{M}_W$ needs to be derived. It has the minimal parametric uncertainty in predictions and these three input parameters are precisely measured.

It is worth mentioning that eventually, all input-parameter schemes shall agree on the same physics. It is the arrangement of perturbation series and the limited knowledge of our input parameters leading to one scheme being preferable to another in a specific process. Also, we have only focused on the EW input schemes in the OS renormalization scheme, whereas for $\overline{\text{MS}}$ renormalization scheme, one can refer to [98] for more discussion and reference therein.

3.0 Leading Fermionic Three-Loop corrections to EWPOs

3.1 Introduction

As aforementioned in Sec. 1.2.2, all the EWPOs predicted in the SM yield corresponding theoretical uncertainties being safely below the experimental precision. Yet the expected precision projected by future e^+e^- colliders will improve the measurement accuracy by one order of magnitude at most. Hence to test the SM and probe the possible new physics beyond at the future e^+e^- colliders, we have to carry out the three-loop EW, mixed EW-QCD, and the leading four-loop corrections of the EWPOs. In this chapter, we discuss the recently accomplished computations of leading fermionic three-loop corrections to a set of EWPOs at EW $\mathcal{O}(\alpha^3)$ and mixed EW-QCD $\mathcal{O}(\alpha^2\alpha_s)$, where "leading fermionic" means the maximal number of closed fermion loops at given orders. This subset of radiative corrections is considered to be gauge-independent and parametrically important. In sec. 3.2, we introduce the renormalization procedures for cases with and without QCD contributions. Sec. 3.4 highlights the technical aspects including the derivative and evaluation of the MIs and the computer algebra tools we used. One can find numerical results and shed light on future projections thereby in sec. 3.5. and we gave a discussion at the end in sec. 3.6.

3.2 Renormalization at three-loop level

We adopted the OS renormalization scheme for all electroweak radiative corrections. However, in the case of leading fermionic three-loop at $\mathcal{O}(\alpha^2\alpha_s)$, where the top-quark mass receives radiative corrections from gluon exchange, we use OS scheme and modified minimal subtraction scheme ($\overline{\text{MS}}$) alternately to describe the renormalized top-quark mass. The reason for using both schemes is the following: the OS top mass definition is subject to the renormalon ambiguity from which the $\overline{\text{MS}}$ top-quark mass prescription is exempt. The $\overline{\text{MS}}$ top-quark mass prescription is thus preferable in practical calculations, yet an extra step is required to relate the $\overline{\text{MS}}$ value to an observable. These two schemes are related by a finite function, which has been carried out up to four-loop level[173, 174, 116, 175]. The results carried out in both schemes after summing up all orders in perturbation theory should converge up to non-perturbative effects, and our numerical comparison between two schemes will reveal an inkling of it (see 3.5), which can also be used for interpolating the theory error due to missing higher orders.

Followed by Eq. (113), we define the pole of particles with a non-negligible decay width,

such as the W and Z bosons, to be complex:

$$s_0 = \overline{M}^2 - i\overline{M}\overline{\Gamma}. \tag{124}$$

Then one can obtain the counterterms and widths by expanding Eq. (109) (110) systematically around the real part of the pole, i.e., taking $\mathcal{O}(\overline{\Gamma}/\overline{M}) \sim \mathcal{O}(\alpha)$ as an assumption. We exclude the field or wavefunction renormalization for the gauge boson and the top quark since all of them only appears as intermediate particles in physical processes. As a matter of fact, we have checked the cancellation among field renormalization constants explicitly in our calculation.

3.2.1 Renormalization in pure EW case

By expanding Eq. (109) (110) simultaneously, and inserting the later into the former one recursively, we get the W-mass counterterms at each order as follows:

$$\delta\overline{M}^2_{\mathrm{W}(1)} = \mathrm{Re}\,\Sigma_{\mathrm{W}(1)}(\overline{M}^2_{\mathrm{W}}), \tag{125}$$

$$\delta\overline{M}^2_{\mathrm{W}(2)} = \mathrm{Re}\,\Sigma_{\mathrm{W}(2)}(\overline{M}^2_{\mathrm{W}}) + \left[\mathrm{Im}\,\Sigma_{\mathrm{W}(1)}(\overline{M}^2_{\mathrm{W}})\right]\left[\mathrm{Im}\,\Sigma'_{\mathrm{W}(1)}(\overline{M}^2_{\mathrm{W}})\right], \tag{126}$$

$$\begin{aligned}
\delta\overline{M}^2_{\mathrm{W}(3)} = {} & \mathrm{Re}\,\Sigma_{\mathrm{W}(3)}(\overline{M}^2_{\mathrm{W}}) + \left[\mathrm{Im}\,\Sigma_{\mathrm{W}(2)}(\overline{M}^2_{\mathrm{W}})\right]\left[\mathrm{Im}\,\Sigma'_{\mathrm{W}(1)}(\overline{M}^2_{\mathrm{W}})\right] \\
& + \left[\mathrm{Im}\,\Sigma_{\mathrm{W}(1)}(\overline{M}^2_{\mathrm{W}})\right]\left\{\mathrm{Im}\,\Sigma'_{\mathrm{W}(2)}(\overline{M}^2_{\mathrm{W}}) - \left[\mathrm{Im}\,\Sigma'_{\mathrm{W}(1)}(\overline{M}^2_{\mathrm{W}})\right]\left[\mathrm{Re}\,\Sigma'_{\mathrm{W}(1)}(\overline{M}^2_{\mathrm{W}})\right]\right. \\
& \left. - \tfrac{1}{2}\left[\mathrm{Im}\,\Sigma_{\mathrm{W}(1)}(\overline{M}^2_{\mathrm{W}})\right]\left[\mathrm{Re}\,\Sigma''_{\mathrm{W}(1)}(\overline{M}^2_{\mathrm{W}})\right]\right\}.
\end{aligned} \tag{127}$$

The numbers in lower parenthesis denote the EW loop order. For the Z-mass counterterm, we have to take the $\gamma - Z$ mixing effect into account. Hence we get modified equations of counterterms and widths as

$$\delta\overline{M}^2_{\mathrm{Z}} = \mathrm{Re}\,\Sigma_{\mathrm{Z}}\big(\overline{M}^2_{\mathrm{Z}} - i\overline{M}_{\mathrm{Z}}\overline{\Gamma}_{\mathrm{Z}}\big) + \tfrac{1}{4}\overline{M}^2_{\mathrm{Z}}(\delta Z^{\gamma\mathrm{Z}})^2, \tag{128}$$

$$\overline{\Gamma}_{\mathrm{Z}} = \frac{1}{\overline{M}_{\mathrm{Z}}[1 + \tfrac{1}{4}(\delta Z^{\gamma\mathrm{Z}})^2]}\,\mathrm{Im}\,\Sigma_{\mathrm{Z}}\big(\overline{M}^2_{\mathrm{Z}} - i\overline{M}_{\mathrm{Z}}\overline{\Gamma}_{\mathrm{Z}}\big), \tag{129}$$

where the self-energy is defined in Eq. (59). According to the OS scheme, the $\gamma - Z$ mixing should vanish when $s = 0\,, \overline{M}^2_{\mathrm{Z}}$, thereby leading to

$$\hat{\Sigma}_{\gamma\mathrm{Z}}(0) = 0, \qquad \mathrm{Re}\,\hat{\Sigma}_{\gamma\mathrm{Z}}\big(\overline{M}^2_{\mathrm{Z}} - i\overline{M}_{\mathrm{Z}}\overline{\Gamma}_{\mathrm{Z}}\big) = 0. \tag{130}$$

Combining Eq. (128)–Eq.(130), the relevant self-energies defined in Eq.(59), and expanding in orders of α yields

$$\delta\overline{M}^2_{\mathrm{Z}(1)} = \mathrm{Re}\,\Sigma_{\mathrm{ZZ}(1)}(\overline{M}^2_{\mathrm{Z}}) \tag{131}$$
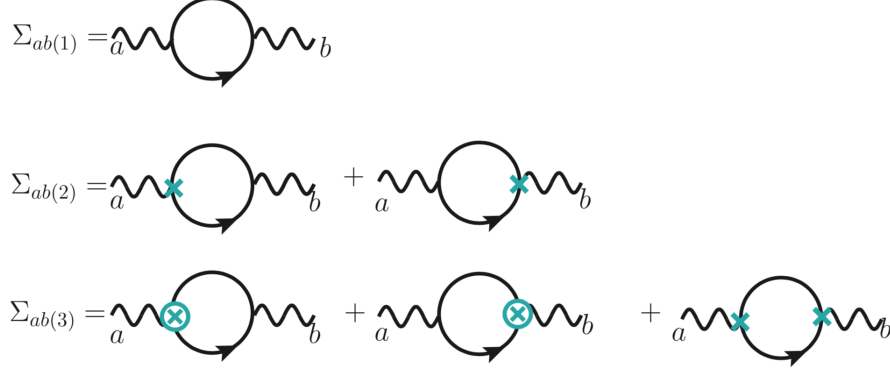
Figure 5: Diagrams with leading fermion loops of 1-PI self energies at each order. The a and b indicate possible gauge bosons. The one-loop order counterterm is denoted as "×", while the two-loop one's is "⊗".

$$
\delta \overline{M}^2_{Z(2)} = \operatorname{Re} \Sigma_{ZZ(2)}(\overline{M}^2_Z) + \left[\operatorname{Im} \Sigma_{ZZ(1)}(\overline{M}^2_Z) \right] \left[\operatorname{Im} \Sigma'_{ZZ(1)}(\overline{M}^2_Z) \right]
$$
$$
+ \frac{\left[\operatorname{Im} \Sigma_{\gamma Z(1)}(\overline{M}^2_Z) \right]^2}{M^2_Z} + \tfrac{1}{4} \overline{M}^2_Z \, (\delta Z^{\gamma Z}_{(1)})^2 \tag{132}
$$

$$
\delta \overline{M}^2_{Z(3)} = \operatorname{Re} \Sigma_{ZZ(3)}(\overline{M}^2_Z) + \left[\operatorname{Im} \Sigma_{ZZ(2)}(\overline{M}^2_Z) \right] \left[\operatorname{Im} \Sigma'_{ZZ(1)}(\overline{M}^2_Z) \right]
$$
$$
+ \left[\operatorname{Im} \Sigma_{ZZ(1)}(\overline{M}^2_Z) \right] \Big\{ \operatorname{Im} \Sigma'_{ZZ(2)}(\overline{M}^2_Z) - \left[\operatorname{Im} \Sigma'_{ZZ(1)}(\overline{M}^2_Z) \right] \left[\operatorname{Re} \Sigma'_{ZZ(1)}(\overline{M}^2_Z) \right]
$$
$$
- \tfrac{1}{2} \left[\operatorname{Im} \Sigma_{ZZ(1)}(\overline{M}^2_Z) \right] \left[\operatorname{Re} \Sigma''_{ZZ(1)}(\overline{M}^2_Z) \right]
$$
$$
- \frac{\operatorname{Im} \Sigma_{\gamma Z(1)}(\overline{M}^2_Z)}{\overline{M}^2_Z} \left[2 \operatorname{Re} \Sigma'_{\gamma Z(1)}(\overline{M}^2_Z) + \delta Z^{\gamma Z}_{(1)} + \delta Z^{Z \gamma}_{(1)} \right] \Big\}
$$
$$
+ \frac{\operatorname{Im} \Sigma_{\gamma Z(1)}(\overline{M}^2_Z)}{\overline{M}^2_Z} \Big\{ 2 \operatorname{Im} \Sigma_{\gamma Z(2)}(\overline{M}^2_Z) - \frac{\operatorname{Im} \Sigma_{\gamma Z(1)}(\overline{M}^2_Z)}{\overline{M}^2_Z} \left[\operatorname{Im} \Sigma_{\gamma \gamma(1)}(\overline{M}^2_Z) \right] \Big\}
$$
$$
+ \tfrac{1}{2} \overline{M}^2_Z \, \delta Z^{\gamma Z}_{(1)} \, \delta Z^{\gamma Z}_{(2)} . \tag{133}
$$

All self-energies here are considered as 1-PI contributions from one-loop diagrams with counterterms insertions at vertices, see Fig. 5, with relevant counterterm Feynman rules shown in Fig. 6. We can safely drop all field renormalization constants from Feynman rules

Figure 6: All-order Feynman rules of gauge-boson-fermion-fermion vertex with counterterms, where $\omega_\pm = \frac{1}{2}(1 \pm \gamma^5)$

as aforementioned. And we define some parameters as follows:

$$s_\mathrm{w} = s_\mathrm{w}^R + \delta s_\mathrm{w}\,, \qquad c_\mathrm{w} = \sqrt{1 - (s_\mathrm{w}^R + \delta s_\mathrm{w})} \tag{134}$$

$$g_A = \frac{eZ_e I_3^f}{2s_\mathrm{w} c_\mathrm{w}}\,, \qquad g_V = \frac{eZ_e[I_3^f - 2Q_f(s_\mathrm{w})^2]}{2s_\mathrm{w} c_\mathrm{w}}\,, \tag{135}$$

where s_w^R is the renormalized weak-mxing angle.Besides the W and Z-mass counterterms, other relevant counterterms specified for the leading fermionic EW corrections are listed as

follows:

$$\delta Z_{(n)}^{Z\gamma} = 0, \tag{136}$$

$$\delta Z_{e(1)} = \frac{\alpha}{9\pi}\left[\frac{12}{\epsilon} + \frac{50}{3} - 2\,L(m_{\mathrm{t}}^2) - 10\,L(M_Z^2)\right] + \frac{\Delta\alpha}{2}\,, \tag{137}$$

$$\delta Z_{e(2)} = \frac{3}{2}(\delta Z_{e(1)})^2, \tag{138}$$

$$\delta Z_{e(3)} = \frac{5}{2}(\delta Z_{e(1)})^3, \tag{139}$$

$$s_{\mathrm{w}} + \delta s_{\mathrm{w}} = \sqrt{1 - \frac{\overline{M}_{\mathrm{W}}^2 + \delta\overline{M}_{\mathrm{W}}^2}{\overline{M}_Z^2 + \delta\overline{M}_Z^2}} \tag{140}$$

and $L(m^2) \equiv \log(\frac{m^2}{4\pi\mu}) + \gamma_E$. $\Delta\alpha$ is the value mentioned in sec. 2.4. The simple results of charge renormalization counterterms are the consequences of considering leading fermion loops only. One needs to pay attention the $L(M_Z^2)$ in Eq. (146) where the running-width-scheme mass is adopted instead of pole-scheme mass $\overline{M}_Z^2$. This is due to the $\Delta\alpha_{\mathrm{had}}$ measured from experiments uses M_Z^2, thereby leading us using M_Z^2 accordingly. The counterterm of weak-mixing angle beyond one-loop order can be obtained by carefully expanding Eq. (140) and inserting results from Eq. (133) (127).

3.2.2 Renormalization in mixed EW-QCD at $\mathcal{O}(\alpha_s\alpha^2)$ case

While computing radiative corrections in QCD, the $\overline{\mathrm{MS}}$is more commonly used. In leading fermion three-loop contributions of order $\mathcal{O}(\alpha^2\alpha_s)$, only the top-quark mass needs to be renormalized. Hence we give two alternative prescriptions for the top-quark mass, OS, and $\overline{\mathrm{MS}}$. The OS top-quark mass, as we have discussed, has direct physical interpretation, and it can be determined via template fit approach[176]. The OS prescription suffers from the renormalon ambiguity and other non-perturbative QCD effects while the $\overline{\mathrm{MS}}$prescription retains intact from long-distance phenomena and thus preferable from the theory aspect. Again, expanding Eq. (109) (110) for both W and Z bosons systematically in orders α, α_s, we get

$$\delta\overline{M}_{\mathrm{W}(\alpha_s\alpha)}^2 = \mathrm{Re}\,\Sigma_{\mathrm{W}(\alpha_s\alpha)}(\overline{M}_{\mathrm{W}}^2),$$
$$\delta\overline{M}_{\mathrm{W}(\alpha_s\alpha^2)}^2 = \mathrm{Re}\,\Sigma_{\mathrm{W}(\alpha_s\alpha^2)}(\overline{M}_{\mathrm{W}}^2)$$
$$+ [\mathrm{Im}\,\Sigma_{\mathrm{W}(\alpha_s\alpha)}(\overline{M}_{\mathrm{W}}^2)]\,[\mathrm{Im}\,\Sigma_{\mathrm{W}(\alpha)}'(\overline{M}_{\mathrm{W}}^2)] + [\mathrm{Im}\,\Sigma_{\mathrm{W}(\alpha_s\alpha)}'(\overline{M}_{\mathrm{W}}^2)]\,[\mathrm{Im}\,\Sigma_{\mathrm{W}(\alpha)}(\overline{M}_{\mathrm{W}}^2)].$$
$$\tag{141}$$

$$\delta \overline{M}^2_{Z(\alpha_s\alpha)} = \mathrm{Re}\, \Sigma_{ZZ(\alpha_s\alpha)}(\overline{M}^2_Z)\,,$$

$$\delta \overline{M}^2_{Z(\alpha_s\alpha^2)} = \mathrm{Re}\, \Sigma_{ZZ(\alpha_s\alpha^2)}(\overline{M}^2_Z) + [\mathrm{Im}\, \Sigma_{ZZ(\alpha_s\alpha)}(\overline{M}^2_Z)]\, [\mathrm{Im}\, \Sigma'_{ZZ(\alpha)}(\overline{M}^2_Z)]$$

$$+ [\mathrm{Im}\, \Sigma_{ZZ(\alpha)}(\overline{M}^2_Z)]\, [\mathrm{Im}\, \Sigma'_{ZZ(\alpha_s\alpha)}(\overline{M}^2_Z)] \tag{142}$$

$$+ \frac{2}{\overline{M}^2_Z} [\mathrm{Im}\, \Sigma_{\gamma Z(\alpha_s\alpha)}(\overline{M}^2_Z)]\, [\mathrm{Im}\, \Sigma_{\gamma Z(\alpha)}(\overline{M}^2_Z)] + \frac{1}{2}\overline{M}^2_Z\, \delta Z^{\gamma Z}_{(\alpha)}\, \delta Z^{\gamma Z}_{(\alpha_s\alpha)}\,.$$

The 1-PI self-energies receives one and two-loop contributions including counterterms insertion at both fermion lines and vertices. However, only the top quark is considered massive hence only the top-mass receives radiative corrections. See Fig. 7 for diagrammatic illustration.
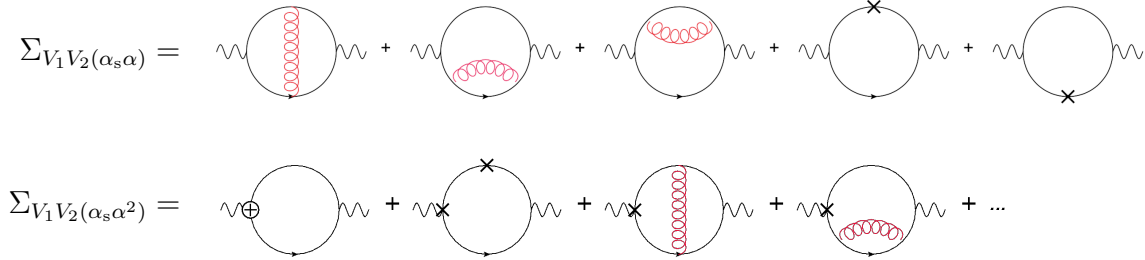
Figure 7: *Diagrams with closed fermion loops contributing to self-energies at different orders. V_1 and V_2 denote the possible different in- and outgoing gauge bosons. Vertices "$\oplus$" and "$\times$" indicate the counterterms at the loop order $\mathcal{O}(\alpha_s\alpha)$ and $\mathcal{O}(\alpha)$ or $\mathcal{O}(\alpha_s)$, respectively. Note that there are no actual three-loop diagrams with two explicit closed fermion loops at the order $\mathcal{O}(\alpha_s\alpha^2)$, but instead, all contributions stem from sub-loop counterterm insertions.*

One can obtain the on-shell top-mass counterterm by following Eq. (74). Alternatively, in the $\overline{\mathrm{MS}}$ scheme the counterterm only contains the divergent piece along with the universal $\log 4\pi$ and Euler number γ_E. At one-loop order it reads

$$\delta m_{t(\alpha_s)} = -\frac{3C_F g_s^2}{16\pi^2}\left(\frac{1}{\epsilon} + \log 4\pi - \gamma_E\right) m_t(\mu). \tag{144}$$

Here the lower case m is used to denote $\overline{\mathrm{MS}}$ quantities, and μ is the renormalization scale.

Figure 8: *The gluon self-energy correction to the top quark.*

At one-loop level, the relation between the OS and $\overline{\text{MS}}$ mass can be easily derived from these formulae, with the result

$$\frac{M_t}{m_t} = 1 + \frac{\alpha_{\text{s}} C_F}{4\pi}\left(3\log\frac{M_t^2}{\mu^2} - 4\right) + \mathcal{O}(\alpha_{\text{s}}^2).$$

(145)

For other relevant counterterms, besides $\delta Z_{\text{Z}\gamma_{(n)}}$ which are zeros, the weak-mixing angle counterterms can be carried out in the same manner as aforementioned. Finally, the charge counterterms are given by

$$\delta Z_{e(\alpha)} = \frac{1}{2}\left[\Delta\alpha + \Sigma_{\gamma\gamma(\alpha)}^{\text{top}\prime}(0) + \Pi_{\gamma\gamma(\alpha)}^{\text{lf}}(M_{\text{Z}}^2)\right],$$

(146)

$$\delta Z_{e(\alpha_{\text{s}}\alpha)} = \frac{1}{2}\left[\Sigma_{\gamma\gamma(\alpha_{\text{s}}\alpha)}^{\text{top}\prime}(0) + \Pi_{\gamma\gamma(\alpha_{\text{s}}\alpha)}^{\text{lf}}(M_{\text{Z}}^2)\right],$$

(147)

$$\delta Z_{e(\alpha_{\text{s}}\alpha^2)} = 3\,\delta Z_{e(\alpha)}\delta Z_{e(\alpha_{\text{s}}\alpha)},$$

(148)

where

$$\Pi_{\gamma\gamma}(q^2) = \frac{\Sigma_{\gamma\gamma}(q^2)}{q^2}\,.$$

(149)

3.3   Defining Observables

3.3.1   Fermi constant G_μ

EXperimentally, the Fermi constant is determined via muon decay [177] with high precision. In the SM, it's predicted through radiative corrections of the muon decay as

$$G_\mu = \frac{\pi\alpha}{\sqrt{2}s_{\text{w}}^2\overline{M}_{\text{W}}^2}(1 + \Delta r),$$

(150)

where Δr quantifies all the closed fermionic radiative corrections and can be parametrized as

$$1 + \Delta r = \left(\frac{1 + \delta Z_e}{s_{\mathrm{w}} + \delta s_{\mathrm{w}}} \right)^2 \frac{\overline{M}_{\mathrm{W}}^2 (1 - \overline{M}_{\mathrm{W}}^2/\overline{M}_{\mathrm{Z}}^2)}{\overline{M}_{\mathrm{W}}^2 + \delta \overline{M}_{\mathrm{W}} - \Sigma_W(0)}. \tag{151}$$

Because $m_\mu \ll \overline{M}_{\mathrm{W}}$, it is permissible setting the momentum transfer in the W propagator to zero. Eq. (151) can be used to systematically compute the higher order corrections to Fermi constant.

3.3.2 W-boson mass

Using Eq. (150), we can compute $\overline{M}_{\mathrm{W}}$ by

$$\overline{M}_{\mathrm{W}}^2 = \frac{\overline{M}_{\mathrm{Z}}^2}{2} \left(1 + \sqrt{1 - \frac{4\pi\alpha}{G_\mu \sqrt{2}\overline{M}_{\mathrm{Z}}^2}(1 + \Delta r)} \right). \tag{152}$$

As what we have discussed in sec. 2.4, Δr can be carried out by different set of input parameters, we should nevertheless point out that even with $\overline{M}_{\mathrm{W}}$ being as one of the inputs, Eq. (152) can be still used iteratively to determine the radiative corrections received by the W-boson mass.

3.3.3 Effective weak-mixing angle $\sin^2\theta_{\mathrm{eff}}^f$

The effective weak-mixing angle is determined by the ratio between the effective vector and axial-vector couplings to the Z-boson to a fermion pair final state as

$$\sin^2\theta_{\mathrm{eff}}^f = \frac{1}{4|Q_f|} \left(1 - \mathrm{Re}\, \frac{v_f(s)}{a_f(s)} \right)_{s = \overline{M}_{\mathrm{Z}}^2}, \tag{153}$$

where

$$a_f(s) = g_A \tag{154}$$

$$v_f(s) = g_V + eZ_e Q_f \frac{\Sigma_{\gamma Z}(s) - \frac{1}{2}\delta Z^{\gamma Z}\Sigma_{\gamma\gamma}(s)}{s + \Sigma_{\gamma\gamma}(s)}. \tag{155}$$

One should be aware of that Eq. (154),(155) only capture closed-fermion loop corrections. The effective $Zf\bar{f}$ vertex can be depicted as Fig. 9.
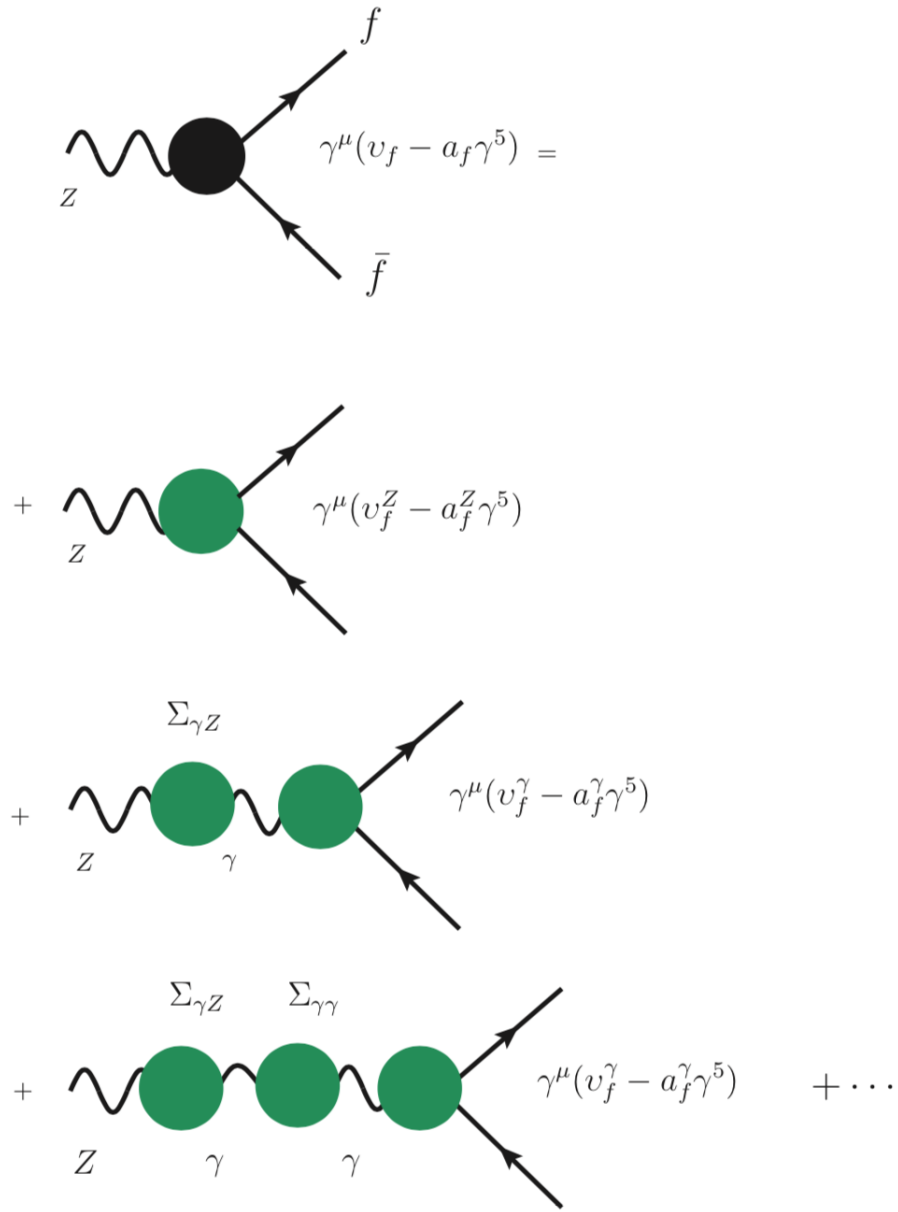
Figure 9: Decomposition of the 1-PI effective $Zf\bar{f}$ vertex into self-energies building blocks

3.3.4 Partial width $\Gamma[Z \to f\bar{f}]$

The Z width can be obtained order-by-order by expanding Eq. (129). At three-loop order, it reads

$$
\begin{aligned}
\overline{\Gamma}_{\text{Z}} = \frac{1}{\overline{M}_{\text{Z}}} \Big\{ & \text{Im}\,\Sigma_{\text{Z}(1)} + \text{Im}\,\Sigma_{\text{Z}(2)} - (\text{Im}\,\Sigma_{\text{Z}(1)})(\text{Re}\,\Sigma'_{\text{Z}(1)}) \\
& + \text{Im}\,\Sigma_{\text{Z}(3)} - (\text{Im}\,\Sigma_{\text{Z}(2)})(\text{Re}\,\Sigma'_{\text{Z}(1)}) \\
& + (\text{Im}\,\Sigma_{\text{Z}(1)})\big[(\text{Re}\,\Sigma'_{\text{Z}(1)})^2 - \text{Re}\,\Sigma'_{\text{Z}(2)} - \tfrac{1}{4}(\delta Z^{\gamma\text{Z}}_{(1)})^2 - \tfrac{1}{2}(\text{Im}\,\Sigma_{\text{Z}(1)})(\text{Im}\,\Sigma''_{\text{Z}(1)})\big] \\
& + \text{Im}\,\Sigma_{\text{Z}(4)} - (\text{Im}\,\Sigma_{\text{Z}(3)})(\text{Re}\,\Sigma'_{\text{Z}(1)}) \\
& + (\text{Im}\,\Sigma_{\text{Z}(2)})\big[(\text{Re}\,\Sigma'_{\text{Z}(1)})^2 - \text{Re}\,\Sigma'_{\text{Z}(2)} - \tfrac{1}{4}(\delta Z^{\gamma\text{Z}}_{(1)})^2 - (\text{Im}\,\Sigma_{\text{Z}(1)})(\text{Im}\,\Sigma''_{\text{Z}(1)})\big] \\
& + (\text{Im}\,\Sigma_{\text{Z}(1)})\big[-(\text{Re}\,\Sigma'_{\text{Z}(1)})^3 + 2(\text{Re}\,\Sigma'_{\text{Z}(2)})(\text{Re}\,\Sigma'_{\text{Z}(1)}) - \text{Re}\,\Sigma'_{\text{Z}(3)} \\
& - \tfrac{1}{2}\delta Z^{\gamma\text{Z}}_{(1)}\delta Z^{\gamma\text{Z}}_{(2)} + \tfrac{1}{2}(\text{Re}\,\Sigma'_{\text{Z}(1)})(\delta Z^{\gamma\text{Z}}_{(1)})^2 - \tfrac{1}{2}(\text{Im}\,\Sigma_{\text{Z}(1)})(\text{Im}\,\Sigma''_{\text{Z}(2)}) \\
& + \tfrac{3}{2}(\text{Im}\,\Sigma_{\text{Z}(1)})(\text{Re}\,\Sigma'_{\text{Z}(1)})(\text{Im}\,\Sigma''_{\text{Z}(1)}) + \tfrac{1}{6}(\text{Im}\,\Sigma_{\text{Z}(1)})^2(\text{Re}\,\Sigma'''_{\text{Z}(1)})\big] \Big\}_{s=\overline{M}_{\text{Z}}^2} . \quad (156)
\end{aligned}
$$

Note that Σ_{Z} features $\gamma - \text{Z}$ mixing effects. Then through optical theorem, one can express the imaginary part of Σ_{Z} as the decay rate for $Z \to f\bar{f}$:

$$
\text{Im}\,\Sigma_{\text{Z}} = \frac{1}{3\overline{M}_{\text{Z}}} \sum_f \sum_{spins} \int d\Phi(|v_f|^2 + |a_f|^2), \quad (157)
$$

where v_f and a_f are defined in Eq. (155) and Eq. (154), respectively. Noticing that

$$
\overline{\Gamma}_{\text{Z}} = \sum_f \overline{\Gamma}_f, \quad (158)
$$

hence by plugging Eq. (158) and Eq. (157) on both side of Eq. (156), and taking the factorizable QCD and QED final-state corrections into account, we get

$$
\overline{\Gamma}_{\text{Z}} = \sum_f \overline{\Gamma}_f, \qquad \overline{\Gamma}_f = \frac{N_c^f \overline{M}_{\text{Z}}}{12\pi} \Big[\mathcal{R}_{\text{V}}^f F_{\text{V}}^f + \mathcal{R}_{\text{A}}^f F_{\text{A}}^f\Big]_{s=\overline{M}_{\text{Z}}^2}, \quad (159)
$$

$$
\begin{aligned}
F_{\text{V}}^f = & \; v_{f(0)}^2 + 2\,\text{Re}\,(v_{f(0)} v_{f(1)}) - v_{f(0)}^2 \,\text{Re}\,\Sigma'_{\text{Z}(1)} \\
& + 2\,\text{Re}\,(v_{f(0)} v_{f(2)}) + |v_{f(1)}|^2 - 2\,\text{Re}\,(v_{f(0)} v_{f(1)})\,\text{Re}\,\Sigma'_{\text{Z}(1)} \\
& + v_{f(0)}^2\big[(\text{Re}\,\Sigma'_{\text{Z}(1)})^2 - \text{Re}\,\Sigma'_{\text{Z}(2)} - \tfrac{1}{4}(\delta Z^{\gamma\text{Z}}_{(1)})^2 - \tfrac{1}{2}(\text{Im}\,\Sigma_{\text{Z}(1)})(\text{Im}\,\Sigma''_{\text{Z}(1)})\big]
\end{aligned}
$$

47

$$
\begin{aligned}
&+ 2\,\mathrm{Re}\,(v_{f(0)}v_{f(3)} + v^*_{f(1)}v_{f(2)}) - \big[2\,\mathrm{Re}\,(v_{f(0)}v_{f(2)}) + |v_{f(1)}|^2\big]\,\mathrm{Re}\,\Sigma'_{Z(1)} \\
&+ 2\,\mathrm{Re}\,(v_{f(0)}v_{f(1)}) \big[(\mathrm{Re}\,\Sigma'_{Z(1)})^2 - \mathrm{Re}\,\Sigma'_{Z(2)} - \tfrac{1}{4}(\delta Z^{\gamma Z}_{(1)})^2 - (\mathrm{Im}\,\Sigma_{Z(1)})(\mathrm{Im}\,\Sigma''_{Z(1)})\big] \\
&+ v^2_{f(0)}\big[-(\mathrm{Re}\,\Sigma'_{Z(1)})^3 + 2(\mathrm{Re}\,\Sigma'_{Z(2)})(\mathrm{Re}\,\Sigma'_{Z(1)}) - \mathrm{Re}\,\Sigma'_{Z(3)} \\
&\qquad\quad - \tfrac{1}{2}\delta Z^{\gamma Z}_{(1)}\delta Z^{\gamma Z}_{(2)} + \tfrac{1}{2}(\mathrm{Re}\,\Sigma'_{Z(1)})(\delta Z^{\gamma Z}_{(1)})^2 - \tfrac{1}{2}(\mathrm{Im}\,\Sigma_{Z(1)})(\mathrm{Im}\,\Sigma''_{Z(2)}) \\
&\qquad\quad + \tfrac{3}{2}(\mathrm{Im}\,\Sigma_{Z(1)})(\mathrm{Re}\,\Sigma'_{Z(1)})(\mathrm{Im}\,\Sigma''_{Z(1)}) + \tfrac{1}{6}(\mathrm{Im}\,\Sigma_{Z(1)})^2(\mathrm{Re}\,\Sigma'''_{Z(1)})\big],
\end{aligned}
\tag{160}
$$

and F_A can be obtained analogously by replacing v_f with a_f. Similarly one can obtain the corrections from $\mathcal{O}(\alpha^\alpha_s)$ as

$$
\Delta\overline{\Gamma}_{f,(\alpha^2\alpha_s)} = \frac{N^f_c \overline{M}_Z}{12\pi}\Big[\Delta F^f_{V,(\alpha^2\alpha_s)} + \Delta F^f_{A,(\alpha^2\alpha_s)}\Big]_{s=\overline{M}^2_Z},
\tag{161}
$$

$$
\begin{aligned}
\delta F^f_{V(\alpha^2\alpha_s)} = {}& v^2_{f(0)}\big[2(\mathrm{Re}\,\Sigma'_{Z(\alpha)})(\mathrm{Re}\,\Sigma'_{Z(\alpha_s\alpha)}) - \mathrm{Re}\,\Sigma'_{Z(\alpha_s\alpha^2)} \\
&\quad - \tfrac{1}{2}(\mathrm{Im}\,\Sigma_{Z(\alpha)})(\mathrm{Im}\,\Sigma''_{Z(\alpha_s\alpha)}) - \tfrac{1}{2}\delta Z^{(\alpha)}_{\gamma Z}\delta Z^{(\alpha_s\alpha)}_{\gamma Z}\big] \\
&+ 2\,\mathrm{Re}\,(v_{f(0)}v_{f(\alpha)})(-\mathrm{Re}\,\Sigma'_{Z(\alpha_s\alpha)}) + 2\,\mathrm{Re}\,(v_{f(0)}v_{f(\alpha_s\alpha)})(-\mathrm{Re}\,\Sigma'_{Z(\alpha)}) \\
&+ 2\,\mathrm{Re}\,(v^*_{f(\alpha)}v_{f(\alpha_s\alpha)}) + 2\,\mathrm{Re}\,(v_{f(0)}v_{f(\alpha_s\alpha^2)}),
\end{aligned}
\tag{162}
$$

and the radiator functions $\mathcal{R}_{V,A}$ are included in general but could be set to zero as we considering closed fermion loops only in this study.

3.4 Technicalities of Computing EWPOs at leading fermionic three-loop level

In this calculations we treat the CKM matrix as an unitary matrix and we set all fermion masses to zero, except the top quark. FEYNARTS 3.3[178] and FEYNCALC 9.2.0[179] are employed for amplitudes generation and algebraic reduction. The loop-integral evaluation is carried out by using TVID 2.0 [9]. When comparing with previous results with two fermionic loops in Refs. [123, 126, 127, 72, 73], we have found exact algebraic agreement except one term which stems from the derivative of $\mathrm{Re}\,\Sigma'_Z(s)$ (see, for example, the thrid line of Eq. (160)):

$$
\mathrm{Re}\,\Sigma'_{ZZ}(s) - \frac{d}{ds}\Big(\frac{\big[\mathrm{Im}\,\Sigma_{\gamma Z(1)}(s)\big]^2}{s}\Big),
\tag{163}
$$

where the second term, which stems from $\gamma - Z$ mixing at two-loop level (see Eq. (55)) in partial Z width was missing in the previous literature [72, 73]. This error has been corrected and its numerical impact was evaluated.

For genuine two-loop amplitudes, the MIs reductions are done in two independent ways: integration-by-part (IBP) identities as implemented in FIRE6[180], and the integral reduc-
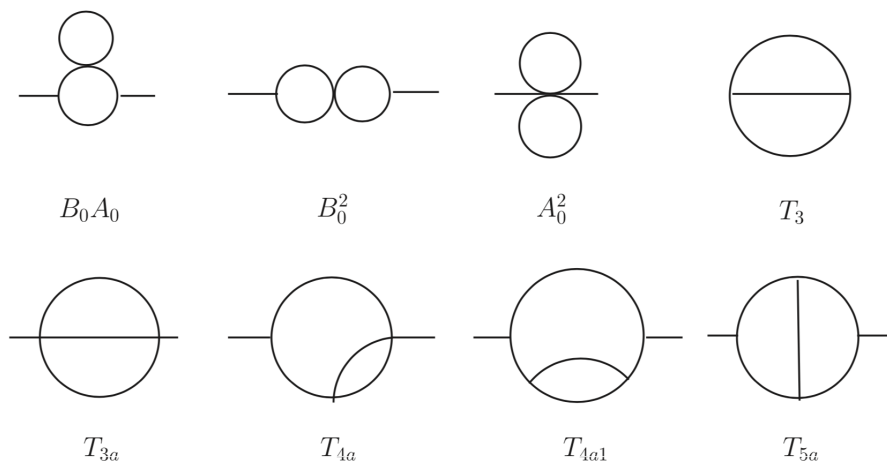
Figure 10: *The MI topologies used for genuine two-loop self-energy contributions, with notation taken from [9].*

tion techniques of Ref. [181]. We should mention that, unlike one-loop cases, the choice of a MI basis at the two-loop level is not unique and may also not be minimal. This leads two aspects considered in practice: First, it is thus difficult comparing results carried out by two individuals symbolically; Secondly, due to the arbitrariness in the choice of the MI basis, some $\mathcal{O}(D-4)$ coefficients of scalar one-loop integrals would be necessary in our case. One can carry them out by following Eq. 4.1 in Ref.[182]. One of the MI bases used in this calculation is shown in Fig 10. However, despite the different choices of the MI basis, the two independent calculations by the authors agree numerically. Furthermore, one must also compute the derivatives of one and two-loop self-energy functions to carry out the necessary renormalization counterterms. Care must be taken when deriving the derivative of the one and two-loop self-energy master integral with zero external momentum.

3.5 Numerical Results

3.5.1 Numerical results in the OS scheme

Given the benchmark inputs in Tab. 10, the numerical results for the leading fermionic

$$M_Z = 91.1876 \text{ GeV} \left.\right\} \Rightarrow \overline{M}_Z = 91.1535 \text{ GeV}$$

$$\Gamma_Z = 2.4952 \text{ GeV}$$

$$M_W = 80.358 \text{ GeV} \left.\right\} \Rightarrow \overline{M}_W = 80.331 \text{ GeV}$$

$$\Gamma_W = 2.089 \text{ GeV}$$

$$M_t = 173.0 \text{ GeV}$$

$$M_{f \neq t} = 0$$

$$\alpha_s = 0.1179$$

$$\alpha = 1/137.035999084$$

$$\Delta\alpha = 0.05900$$

$$G_\mu = 1.1663787 \times 10^{-5} \text{ GeV}^{-2}$$

Table 4: *Benchmark input parameters used in the numerical analysis, based on Ref. [7]. Input values for both top-quark mass prescriptions are listed.*

contributions to all above-mentioned EWPOs at both $\mathcal{O}(\alpha^3)$ and mixed EW-QCD $\mathcal{O}(\alpha^2\alpha_s)$ in the OS prescription are shown in Tab. 5. Δ' denotes the parametric shift from $\Delta M_{W(3)}$, of the predicted value of the W-boson mass in the SM, using eq. (152). Given that $\Delta r_{(3)}$, it is sufficient to expand eq. (152) up to linear order in $\Delta r_{(3)}$ and $\Delta M_{W(3)}$, leading to

$$\Delta\overline{M}_{W(3)} \approx \frac{\pi\alpha\overline{M}_Z^2}{2\sqrt{2}G_\mu\overline{M}_W(\overline{M}_Z^2 - 2\overline{M}_W^2)}\Delta r_{(3)} = -0.389 \text{ MeV}. \tag{164}$$

Accordingly, if we assume the W-boson mass is induced from G_μ, we can then predict the parametric shift of effective weak mixing angle and partial widths due to this input scheme

translation:

$$\Delta' \sin^2 \theta_{\text{eff},(3)}^f = \Delta \sin^2 \theta_{\text{eff},(3)}^f - \frac{\Delta \overline{M}_{\text{W}(3)}^2}{\overline{M}_Z^2} \tag{165}$$

$$\Delta' \overline{\Gamma}_{f,(3)} = \Delta \overline{\Gamma}_{f,(3)} - \frac{\Delta \overline{M}_{\text{W}(3)}^2}{\overline{M}_Z} \times \frac{\alpha N_c^f}{6 s_{\text{w}}^4 c_{\text{w}}^4} \left[(2 s_{\text{w}}^2 - 1)(I_3^f)^2 + 2 s_{\text{w}}^4 Q_f (Q_f - I_3^f) \right] \tag{166}$$

It is evident that all the corrections computed at leading fermionic three-loop level are negligible for the precision tests conducted at the LEP and LHC, see Tab. 2. However, one can also see that the experimental uncertainties laid out by future e^+e^- colliders, such as the FCC-ee, CEPC,and ILC/GigaZ, are comparable to the three-loop corrections(see Tab. 2 and references therein). Hence these corrections cannot be ignored. Combining the $\mathcal{O}(\alpha^3)$ and $\mathcal{O}(\alpha^2 \alpha_s)$ corrections, we see $\Delta \overline{M}_W$ and $\Delta' \overline{\Gamma}$ having a sizable corrections while others are subject to accidental cancellations. Such accidental cancellations can also been observed in the corrections of partial widths in Tab. 6, where the total number given by $\mathcal{O}(\alpha^3) + \mathcal{O}(\alpha^2 \alpha_s)$ of $\Delta \overline{\Gamma}_Z^f$ becomes smaller, thereby leading to the necessity of carrying out the rest part of the three-loop contributions.

	Δr	$\Delta \overline{M}_{\text{W}}$ (MeV)	$\Delta \sin^2 \theta_{\text{eff}}$	$\Delta' \sin^2 \theta_{\text{eff}}$	$\Delta \overline{\Gamma}_{\text{tot}}$ [MeV]	$\Delta' \overline{\Gamma}_{\text{tot}}$ [MeV]
$\mathcal{O}(\alpha^3)$	2.5×10^{-5}	-0.389	1.34×10^{-5}	2.09×10^{-5}	0.331	0.255
$\mathcal{O}(\alpha^2 \alpha_s)$	-0.000109	1.703	1.31×10^{-5}	-1.98×10^{-5}	-0.103	0.229
Sum	-0.000084	1.314	2.65×10^{-5}	0.11×10^{-5}	0.228	0.484

Table 5: *This table shows the numerical results of the leading fermionic three-loop corrections to EWPOs at $\mathcal{O}(\alpha^3)$ and at $\mathcal{O}(\alpha^2 \alpha_s)$ from Ref. [8]. The EWPOs denoted with a prime use M_W predicted from the Fermi constant G_μ rather than the value in Tab. 10. One can see that the two contributions have comparable size, except for $\Delta \overline{M}_W$, where the mixed EW–QCD three-loop correction is about four times larger in magnitude than the pure EW three-loop.*

	$\mathcal{O}(\alpha^3)$		$\mathcal{O}(\alpha^2\alpha_s)$	
	$\Delta\overline{\Gamma}_Z^f(\text{ MeV})$	$\Delta'\overline{\Gamma}_Z^f(\text{ MeV})$	$\Delta\overline{\Gamma}_Z^f(\text{ MeV})$	$\Delta'\overline{\Gamma}_Z^f(\text{ MeV})$
$l\bar{l}$	0.019	0.017	-0.0157	-0.0049
$\nu\bar{\nu}$	0.026	0.022	-2.0×10^{-4}	0.0166
$u\bar{u}$	0.035	0.024	-0.0203	0.0260
$d\bar{d}$	0.041	0.029	-0.0049	0.0475

Table 6: *This table demonstrates the numerical size of leading fermion three-loop corrections of partial width $\overline{\Gamma}_Z^f$ at each channel, in OS renormalization scheme.*

3.5.2 Numerical results in terms of the $\overline{\text{MS}}$ top mass

When switching the top-quark mass from OS to $\overline{\text{MS}}$ prescription, using the benchmark value given in Tab. 10, except the top mass, which gets replaced by

$$m_t(\mu = m_t) = 163.229 \text{ GeV}. \tag{167}$$

the overall magnitude of leading fermionic $\mathcal{O}(\alpha^2\alpha_s)$ corrections become noticeably smaller. This is normally expected as $\overline{\text{MS}}$ prescription converges faster than OS for QCD corrections. This matches the pattern in previous calculations of $\mathcal{O}(\alpha\alpha_s^n)$, where a better convergence behavior was observed for the $\overline{\text{MS}}$ top mass [88, 89, 90, 91, 92]. We perform the similar numerical evaluations summarized in Tab. 7. When using $\overline{\text{MS}}$ prescription for the top-quark mass at $\mathcal{O}(\alpha^2\alpha_s)$, one must also use the $\overline{\text{MS}}$ top-quark mass, Eq. (167), as input at the lower order $\mathcal{O}(\alpha^2)$, for the sake of consistency. The leading fermionic $\mathcal{O}(\alpha^2)$ contributions have previously been computed in Refs. [123, 126, 127, 122, 66, 68, 72, 73] and re-evaluated in Ref. [8]. The corresponding numbers of both perturbative orders are listed in Table 8. One can see that the numerical changes at $\mathcal{O}(\alpha^2)$ and $\mathcal{O}(\alpha^2\alpha_s)$ partially compensate each other when going from the OS to the $\overline{\text{MS}}$ scheme. This is expected since the all-order results should be identical in both schemes (up to non-perturbative effects). The difference of the sum $\mathcal{O}(\alpha^2) + \mathcal{O}(\alpha^2\alpha_s)$ between the two schemes could be used as an estimate of the size of the unknown higher-order corrections at $\mathcal{O}(\alpha^2\alpha_s^2)$. A more detailed analysis of theoretical uncertainties from missing higher-order contributions will be left for future work.

Finally, we also wish to study in the impact of the error that was found in the previous

calculation of the fermionic two-loop contribution to the partial decay widths, $\Delta\overline{\Gamma}_{f,(2)}$, as discussed in section 3.4. Using the inputs from Tab. 10, the difference amounts to

$$\Delta\overline{\Gamma}_{f,(2)}\Big|_{\text{this work}} - \Delta\overline{\Gamma}_{f,(2)}\Big|_{\text{Ref. [?, ?]}} = -N_c^f\left(v_{f(0)}^2 + a_{f(0)}^2\right)\overline{M}_Z\frac{25\alpha^2(3-8s_{\text{w}}^2)^2}{3888\pi s_{\text{w}}^2 c_{\text{w}}^2} \qquad (168)$$

$$= \begin{cases} -0.0028 \text{ MeV} & \text{for } f = \ell, \\ -0.0056 \text{ MeV} & \text{for } f = \nu, \\ -0.0126 \text{ MeV} & \text{for } f = d, \\ -0.0098 \text{ MeV} & \text{for } f = u, \\ -0.0830 \text{ MeV} & \text{for } f = \text{tot}. \end{cases} \qquad (169)$$

It turns out that the numerical impact is very small, but for the sake of consistency it is important to identify and correct this error.

$\Delta r_{(\alpha^2\alpha_s)}$ [10^{-4}]	$\Delta M_{\text{W}(\alpha^2\alpha_s)}$ [MeV]
-0.50	0.78

X	$\Delta X_{(\alpha^2\alpha_s)}$	$\Delta' X_{(\alpha^2\alpha_s)}$
$\sin^2\theta_{\text{eff}}$ [10^{-5}]	0.75	-0.76
Γ_ℓ [MeV]	-0.0003	0.0047
Γ_ν [MeV]	0.0009	0.0086
Γ_d [MeV]	-0.0018	0.0223
Γ_u [MeV]	-0.0029	0.0183
Γ_{tot} [MeV]	-0.0093	0.143

Table 7: *Leading fermionic three-loop corrections to EWPOs at $\mathcal{O}(\alpha^2\alpha_s)$ with $\overline{MS}$ prescription for the top mass.*

	on-shell M_t		$\overline{\text{MS}}$ m_t	
	$\mathcal{O}(\alpha^2)$	$\mathcal{O}(\alpha^2\alpha_\text{s})$	$\mathcal{O}(\alpha^2)$	$\mathcal{O}(\alpha^2\alpha_\text{s})$
Δr $[10^{-4}]$	7.85	-1.09	7.56	-0.50
$\Delta \sin^2 \theta_\text{eff}^f$ $[10^{-5}]$	30.98	1.31	31.18	0.75
$\Delta\overline{\Gamma}_\ell$ [MeV]	0.2412	-0.0157	0.2284	-0.0003
$\Delta\overline{\Gamma}_\nu$ [MeV]	0.4145	-0.0002	0.4152	0.0009
$\Delta\overline{\Gamma}_\text{d}$ [MeV]	0.6666	-0.0049	0.6780	-0.0018
$\Delta\overline{\Gamma}_\text{u}$ [MeV]	0.4964	-0.0203	0.4911	-0.0029
$\Delta\overline{\Gamma}_\text{tot}$ [MeV]	4.951	-0.103	4.947	-0.0093

Table 8: *Numerical comparison of leading fermionic $\mathcal{O}(\alpha^2)$ and $\mathcal{O}(\alpha^2\alpha_\text{s})$ results between the on-shell and $\overline{\text{MS}}$ top-quark mass prescriptions. See text for more details.*

3.6   Discussion

In this chapter we summarize the calculation of leading fermionic three-loop corrections at both $\mathcal{O}(\alpha^3)$ and $\mathcal{O}(\alpha^2\alpha_s)$ to several important EWPOs including the W-boson mass induced from Fermi constant G_μ, the effective weak mixing angle, and the partial and total decay widths of the Z boson. In terms of technicalities, this calculation requires solving one- and two-loop self-energy integrals and their derivative. To ensure the gauge invariance, we set the pole of massive gauge bosons as complex, and use the OS scheme. However, when considering $\mathcal{O}(\alpha^2\alpha_s)$, from which the top-quark mass receives QCD corrections, we use both the OS and $\overline{\text{MS}}$ prescription for the top-quark mass. Numerical results are presented separately. In the course of the calculation, an error was found in the previous literature, which has been corrected in this calculation and we also analyze the numerical impact given by this error.

It turns out that the numerical size of the corrections was small compared to the experimental precision for direct measurements of these observables today. However, the precision test laid out by the study of future e^+e^- colliders counts on these corrections due to the

targeting precision of those future colliders. The order of magnitude of the corrections in the OS scheme matches the theory error estimation given by [183, 184]. When switching the top-quark mass from the OS to the $\overline{\text{MS}}$ prescription, we observe a sizable numerical reduction. We believe that there exists an accidental cancellation among the $\mathcal{O}(\alpha^2\alpha_s)$. For instance, we observe that most EWPOs will increase by roughly a factor of 5 by setting $\Delta\alpha$ to zero. This means there are some substantial delicate cancellations happening between terms involving $\Delta\alpha$ and other contributions. On the other hand, experience from pure EW two-loop calculations have shown that the leading fermionic contributions and that of next-to-leading fermionic can be of comparable size. Consequently, the remainly corrections in both $\mathcal{O}(\alpha^3)$ and $\mathcal{O}(\alpha^2\alpha_s)$ might be just as important. These contributions needs to be carried out for performing precision test at future colliders. However, they meets requirements of solving genuine three-loop integrals with various scales, thereby being left as future projection.

4.0   GRIFFIN: **A program for higher order gauge invariant description of the Z-pole resonance at future electron-positron colliders**

4.1   Introduction

Study of four-fermion scattering $f\bar{f} \to f'\bar{f}'$ of which center-of-mass energies are in the vicinity of the intermediate resonance, $\sqrt{s} \sim M_X$, wher X can be either the W or Z boson, have long been considered as a standard candle in elucidating the structure of the SM and constraining the BSM physics. As aforementioned in sec. 1.2.2, the precision frontier laid out by future e^+e^- colliders, together with the HL-LHC demands further study of the four-fermion scattering $f\bar{f} \to f'\bar{f}'$. For $e^+e^- \to f\bar{f}$ running near the Z-boson resonance at future colliders, to simplify the analysis, a set of so-called electroweak pseduo-observables (EWPOs) are defined that encapsulates the dominant radiative corrections in the SM and renders prominent sensitivity to potential BSM physics. One can refer to sec. 1.2.1 and reference therein for more details about the EWPOs. However, as the name suggests, the EWPOs cannot be directly determined through measurements. One needs to extract them from the relevant background and acceptance corrections, such as initial-state and final-state QED and QCD radiative effects, and so on. It is thus crucial having a consistent and model-independent theoretical description of the scattering process. Historically, for the study of Z-boson resonance at the LEP and SLC, numerous computer packages were developed, providing complete NLO and partially NNLO corrections[185, 186, 187, 188, 189, 190, 147, 191, 192, 193, 194, 195, 196, 197, 198]. The packages ZFITTER[187, 188] and TOPAZ0 [186] also implemented the real photon radiation and certain selection cut amid all the achievements, thereby being widely used in experimental studies. Alternatively, the implementation of QED radiation can also be simulated with Monte-Carlo (MC) methods. For example, one can link an EW radiative corrections library, such as DIZET [185] to several MC programs such as KoralZ[199] and KKMC [200].

From a theory point of view, as what we have discussed in sec. 2.3, one needs to find a suitable scheme to describe a resonant process so that not only does the gauge invariance is manifested, but it can also be easily extended to higher order. For $e^+e^- \to f\bar{f}$ around Z-peak, the pole scheme seems to be the most optimal one. However, none of the existing computer programs dedicated on the Z-pole study were designed for targeting the fully NNLO precision and beyond. For instance, the treatment of the $\gamma - Z$ box diagrams in ZFITTER contradicts to what one would obtain from pole scheme[122], leading to possible gauge-violating effects at the EWPOs at NNLO. The numerical impacts of such discrepancy are indeed small

compared with the precision given by the LEP/SLC and LHC, while nevertheless give rise to the necessity of constructing a new framework that treat all radiative corrections consistently and systematically with respect to the pole scheme at NNLO level and beyond. From an experimental point of view, owing to the unprecedented precision level targeted by the future e^+e^- colliders, such as the FCC-ee, the non-factorizable QED effect makes the semi-analytical approaches of separating QED corrections from EW corrections less reliable than the MC methods such as CEEX scheme[184]. Hence, to incorporate with the future projections laid out as aforementioned, we develop a new software package GRIFFIN(Gauge-invariant Resonance In Four-Fermion INteractions) that aims to construct a framework that resolves all the concerns discussed earlier. It is written in C++ and defines a structure of classes that can be extended within or beyond the SM. And the external users can link the results from GRIFFIN to some MC or fitting programs without putting efforts on building interface.

4.2 Theoretical framework set-up

For a parity-violating $f\bar{f} \to f'\bar{f}'$ process, one can decompose it onto four chiral basis, or alternatively, vector and axial-vector basis as follows:

$$\mathcal{M} = \left[M_{\mathrm{VV}} \gamma^\mu \otimes \gamma_\mu - M_{\mathrm{VA}} \gamma^\mu \otimes \gamma_\mu \gamma^5 - M_{\mathrm{AV}} \gamma^\mu \gamma^5 \otimes \gamma_\mu + M_{\mathrm{AA}} \gamma^\mu \gamma^5 \otimes \gamma_\mu \gamma^5 \right] \tag{170}$$

Accordingly, the differential cross section can be written as

$$\frac{d\sigma}{d\cos\theta} = \frac{N_c}{32\pi s} |\mathcal{M}|^2 \tag{171}$$

$$= \frac{N_c s}{32\pi} \left[(1 + c_\theta^2)\left(|M_{\mathrm{VV}}|^2 + |M_{\mathrm{VA}}|^2 + |M_{\mathrm{AV}}|^2 + |M_{\mathrm{AA}}|^2 \right) \right. \tag{172}$$

$$+ 4c_\theta \operatorname{Re}\left\{ M_{\mathrm{VV}} M_{\mathrm{AA}}^* + M_{\mathrm{VA}} M_{\mathrm{AV}}^* \right\}$$

$$- 2P_e(1 + c_\theta^2) \operatorname{Re}\left\{ M_{\mathrm{VV}} M_{\mathrm{AV}}^* + M_{\mathrm{VA}} M_{\mathrm{AA}}^* \right\}$$

$$\left. - 4P_e c_\theta \operatorname{Re}\left\{ M_{\mathrm{VV}} M_{\mathrm{VA}}^* + M_{\mathrm{AV}} M_{\mathrm{AA}}^* \right\} \right],$$

where P_e is the degree of polarization of the incoming fermions, for instance, electrons in e^+e^- colliders. For Z-boson exchange at tree-level, these four chiral matrices are

$$M_{\mathrm{VV}}^{(0)} = \frac{v_{e(0)}^{\mathrm{Z}} v_{f(0)}^{\mathrm{Z}}}{s - s_0}, \quad M_{\mathrm{VA}}^{(0)} = \frac{v_{e(0)}^{\mathrm{Z}} a_{f(0)}^{\mathrm{Z}}}{s - s_0}, \quad M_{\mathrm{AV}}^{(0)} = \frac{a_{e(0)}^{\mathrm{Z}} v_{f(0)}^{\mathrm{Z}}}{s - s_0}, \quad M_{\mathrm{AA}}^{(0)} = \frac{a_{e(0)}^{\mathrm{Z}} a_{f(0)}^{\mathrm{Z}}}{s - s_0}, \tag{173}$$

$$v_{f(0)}^{\mathrm{Z}} = \frac{e I_f^3 (1 - 4|Q_f| s_{\mathrm{w}}^2)}{2 s_{\mathrm{w}} c_{\mathrm{w}}}, \qquad a_{f(0)}^{\mathrm{Z}} = \frac{e I_f^3}{2 s_{\mathrm{w}} c_{\mathrm{w}}}. \tag{174}$$

Followed by the pole scheme, we perform Laurent expansion near the pole for the matrix

element beyond Born-level:

$$M_{ij} = \frac{R_{ij}}{s - s_0} + S_{ij} + (s - s_0)S'_{ij} + ... \qquad (i, j = \text{V}, \text{A}). \qquad (175)$$

where $s_0 = M_\text{Z}^2 - iM_\text{Z}\Gamma_\text{Z}$.

As we have argued in sec. 2.3, the s_0 , R_{ij} , S_{ij}, and S'_{ij} should be individually gauge in-dependent at each order. Hence we can tackle each one of them separately. To minimize the notation cluttering, we denote the mass and width of Z-boson (and W boson) used in complex-pole scheme by M_Z and Γ_Z, differentiating from last chapter. And we use M^{exp} and Γ^{exp} to denote the mass and width in running-width scheme. Two definitions are related by

$$M_\text{Z} = M_\text{Z}^{exp} \left(1 + (\Gamma_\text{Z}^{\text{exp}}/M_\text{Z}^{\text{exp}})^2\right)^{-1/2}, \qquad \Gamma_\text{Z} = \Gamma_\text{Z}^{\text{exp}} [1 + (\Gamma_\text{Z}^{\text{exp}}/M_\text{Z}^{exp})^2]^{-1/2}. \qquad (176)$$

For the square of the amplitude, one can either square Eq. (175) directly, or choose a truncated version as follows:

$$|M_{ij}|^2 = \frac{|R_{ij}|^2}{|s - s_0|^2} + \frac{2\operatorname{Re}\{(s - s_0)^* R_{ij} S_{ij}^*\}}{|s - s_0|^2} + |S_{ij}|^2 + \frac{2\operatorname{Re}\{(s - s_0)^{*2} R_{ij} S'^*_{ij}\}}{|s - s_0|^2} + \mathcal{O}(s - s_0)$$

$$(177)$$

$$= \frac{|R_{ij}|^2 + 2M_\text{Z}\Gamma_\text{Z}\operatorname{Im}\{R_{ij}S_{ij}^*\} + (M_\text{Z}\Gamma_\text{Z})^2 \left[|S_{ij}|^2 - 2\operatorname{Re}\{R_{ij}S'^*_{ij}\}\right]}{|s - s_0|^2}$$

$$+ (s - M_\text{Z}^2)\frac{2\operatorname{Re}\{R_{ij}S_{ij}^*\} + 4M_\text{Z}\Gamma_\text{Z}\operatorname{Im}\{R_{ij}S'^*_{ij}\}}{|s - s_0|^2}$$

$$+ (s - M_\text{Z}^2)^2 \frac{2\operatorname{Re}\{R_{ij}S'^*_{ij}\} + |S_{ij}|^2}{|s - s_0|^2}$$

$$+ \mathcal{O}\left((s - M_\text{Z}^2)^3\right). \qquad (178)$$

The former one will bring in higher orders corrections, whereas the later get truncated at desired order in perturbation. There is no evidence of suggesting whichever is more reliable than the other. We give numerical values for both in our implementation and discuss the phenomenology therein in sec. 4.4.

4.2.1 Building blocks of the matrix elements

We break down the matrix element in terms of several building blocks that encapuslate that radiative corrections:

$$Z_{Vf}(s) = v_f^Z(s) + v_f^\gamma(s)\frac{\Sigma_{\gamma Z}(s)}{s + \Sigma_{\gamma\gamma}(s)}, \qquad\qquad G_{Vf}(s) \equiv v_f^\gamma(s) = -eQ_f, \qquad (179)$$

$$Z_{Af}(s) = a_f^Z(s) + a_f^\gamma(s)\frac{\Sigma_{\gamma Z}(s)}{s + \Sigma_{\gamma\gamma}(s)}, \qquad\qquad G_{Af}(s) \equiv a_f^\gamma(s) = 0, \qquad (180)$$

$$\Sigma_Z(s) = \Sigma_{ZZ}(s) - \frac{[\Sigma_{\gamma Z}(s)]^2}{s + \Sigma_{\gamma\gamma}(s)}. \qquad (181)$$

We should point out that this is not the unique way of grouping the radiative corrections, but it keeps the higher order corrections from double-counting consistently. For the boxes/non-
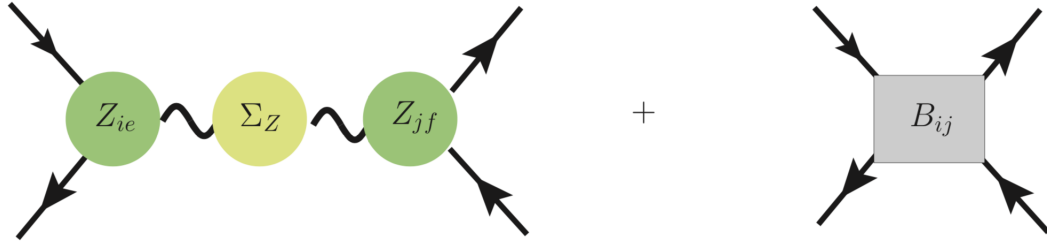
Figure 11: Diagrammatically showing the building blocks for the amplitudes. One should pay attention that the diagram on the left hand side does not really reflect the practical calculation since there is no Dyson-resummation in the propagator in the pole scheme. For the decomposition of the green blobs, one can refer to Fig. 9

.

factorizable contribution B_{ij}, it is important separating the pole contributions from the regular ones in a manifestly gauge-invariant way. There are two types of non-factorizable
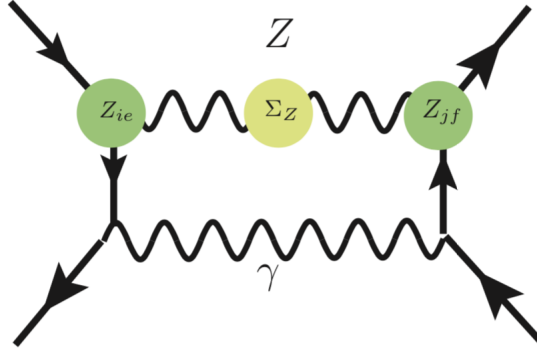
Figure 12: Diagrammatically showing the building blocks for the γZ box amplitudes.

radiative contributions:

$$B_{ij}(s,t) : \text{Contribution of } \gamma\gamma, ZZ \text{ and } WW \text{ box diagrams for initial-state} \tag{182}$$

vector/axial-vector current $(i = \mathrm{V}, \mathrm{A})$ and final-state vector/axial-vector current $(j = \mathrm{V}, \mathrm{A})$;

$$B_{\gamma\mathrm{Z},ij}(s,t) = \frac{B^R_{\gamma\mathrm{Z},ij}}{s - s_0} + B^S_{\gamma\mathrm{Z},ij} + (s - s_0)B^{S'}_{\gamma\mathrm{Z},ij} + \dots :$$

Contribution of γZ box diagrams, which can also contribute to the $\tag{183}$ leading pole term R_{ij}.

One should pay attention that in the γZ box diagrams, when naively carrying out the loop integral, one obtains a branch point at $s = M_{\mathrm{Z}}^2$ in the logarithm $\log(1 - s/M_{\mathrm{Z}}^2)$, which might blow up for $s = M_{\mathrm{Z}}^2$. A careful treatment suggested by Ref. [145] is that owing to the gauge invariance of the coefficients of scalar one-loop integrals is manifested, it is thus permissible "resumming" the propagator before carrying out the integral. We give a schematic way of showing how one can replace logarithm $\log(1 - s/M_{\mathrm{Z}}^2)$ by $\log(1 - s/s_0)$ as follows[1]:

$$B_{\gamma\mathrm{Z}} \sim \int \frac{d^4q}{(2\pi)^4} \frac{\dots}{q^2(\slashed{q} + \slashed{p}_2)(\slashed{q} + \slashed{k}_2)} \underbrace{\frac{Z_i(s', s_i)Z_f(s', s_f)}{s' - m_{\mathrm{Z}0}^2 + \Sigma_Z(s')}}_{W(s', s_i, s_f)}, \tag{184}$$

---

[1]It is worth pointing out that such an issue won't exist in the CMS scheme since all masses of unstable particles are complex in the first place

where

$$s' = (q + p_2 + p_1)^2, \quad s_i = (q + p_2)^2, \quad s_f = (q + k_2)^2. \tag{185}$$

When the Z-propagator is nearly on-shell, $q^2 \sim 0 \Rightarrow s_{i,f} \sim 0$. We hence write $W(s', s_i, s_f)$ under pole scheme as

$$
\begin{aligned}
W(s', s_i, s_f) &= \frac{Z_i(s', s_i) Z_f(s', s_f)}{s' - m_Z^2 + \Sigma_Z(s')} \\
&= \frac{Z_i(s_0, 0) Z_f(s_0, 0) + Z_i(s', s_i) Z_f(s', s_f) - Z_i(s_0, 0) Z_f(s_0, 0)}{s' - s_0 + \Sigma_Z(s') - \Sigma_Z(s_0)} \\
&= \frac{Z_i(s_0, 0) Z_f(s_0, 0)}{(s' - s_0)(1 + \Sigma_Z'(s_0))} + \frac{Z_i(s', s_i) Z_f(s', s_f) - Z_i(s_0, 0) Z_f(s_0, 0)}{s' - s_0 + \Sigma_Z(s') - \Sigma_Z(s_0)} \tag{186} \\
&\equiv \frac{P(s_0)}{s' - s_0} + N(s', s_i, s_f) \tag{187}
\end{aligned}
$$

where the $s_0 - m_{Z0}^2 + \Sigma_Z(s_0) \equiv 0$ has been applied to eliminate the bare Z-boson mass in the denominator. And it is obvious that the first term is the principle term of the pole $s' - s_0$, and the rest is regular since it vanishes as $s' \to s_0$. Hence again, by applying pole scheme before evaluating the loop integral, we successfully separate the leading pole component from the background part. And by replacing the original Z-boson propagator into Eq.(187), we can restore the coincidence between the pole and the branch point as $\log(1 - s/s_0)$. This can only apply to one-loop non-factorizable diagram in the presence of a single resonance, for cases beyond, more sophisticated techniques needs to be developed.

The coefficients of Laurent series can be then parametrized by the building blocks introduced above as follows:

$$R_{ij} = \left[\frac{Z_{if} Z_{jf'}}{1 + \Sigma_Z'} \right]_{s=s_0} + B_{\gamma Z, ij}^R, \tag{188}$$

$$S_{ij} = \left[\frac{Z_{if} Z_{jf'}' + Z_{if}' Z_{jf'}}{1 + \Sigma_Z'} - \frac{Z_{if} Z_{jf'} \Sigma_Z''}{2(1 + \Sigma_Z')^2} + \frac{G_{if} G_{jf'}}{s + \Sigma_{\gamma\gamma}} + B_{ij} \right]_{s=s_0} + B_{\gamma Z, ij}^S, \tag{189}$$

$$
\begin{aligned}
S_{ij}' = &\left[\frac{Z_{if} Z_{jf'}'' + Z_{if}'' Z_{jf'} + 2 Z_{if}' Z_{jf'}'}{2(1 + \Sigma_Z')} - \frac{(Z_{if} Z_{jf'}' + Z_{if}' Z_{jf'}) \Sigma_Z'' + \frac{1}{3} Z_{if} Z_{jf'} \Sigma_Z'''}{2(1 + \Sigma_Z')^2} + \frac{Z_{if} Z_{jf'} (\Sigma_Z'')^2}{4(1 + \Sigma_Z')^3} \right. \\
&\left. + \frac{G_{if} G_{jf'}' + G_{if}' G_{jf'}}{s + \Sigma_{\gamma\gamma}} - \frac{G_{if} G_{jf'} (1 + \Sigma_{\gamma\gamma}')}{(s + \Sigma_{\gamma\gamma})^2} + B_{ij}' \right]_{s=s_0} + B_{\gamma Z, ij}^{S'}, \tag{190}
\end{aligned}
$$

Here X' denotes the derivative of X with respect to s.

4.2.2 the Subtraction of IR divergences

The current version of GRIFFIN uses the IR subtraction scheme followed by Jadach, Ward, et al (See Ref. [201]), but other schemes for removing the IR-divergent contributions could be easily implemented as well.

The vertex form factors and box diagrams can have IR divergences from QED and/or QCD corrections, which will be handled by MC phase-space/shower generators when interfacing with MC program. Hence to avoid double counting we subtract the IR divergent terms from the "hard" matrix element accordingly in GRIFFIN.

For most ISR and FSR vertex corrections, they can be factorized into a radiator function, i.e., the form factors can really be $Z_{if}^{tot} = R_{QED/QCD}^{if} \times Z_{if}$, where R_{if} ($i = V, A$) contains the QCD/QED corrections to the fermion pairs (see *e.g.* Ref. [202]). For the non-factorizable EW/QCD effect induced from mixed QCD-EW irreducible vertex [80, 203], owing to its IR finitness, one can still incorporate it with Z_{if} order by order. Hence, all the form factors shown here are IR-subtracted. For subtracting the IR divergent parts in box diagrams, it becomes less straightforward due to its initial-final state interference nature. We restrict ourselves to a discussion at NLO, where one encounters IR-divergent IFI terms from two sources, the $\gamma\gamma$ boxes and the γZ boxes. Following the CEEX MC scheme of Ref. [201], they can be removed with the following subtraction terms:

$$\gamma\gamma \text{ box:} \qquad B_{\text{VV}(1)} = B_{\text{VV}(1)}^{\text{tot}} - S_{\text{VV}}^{(0)} \frac{\alpha}{\pi} Q_e Q_f \, f_{\text{IR}}(m_\gamma, t, u), \tag{191}$$

$$\gamma Z \text{ box:} \qquad B_{\gamma Z, ij(1)} = B_{\gamma Z, ij(1)}^{\text{tot}} - \frac{R_{ij}^{(0)}}{s - s_0} \frac{\alpha}{\pi} Q_e Q_f \left[f_{\text{IR}}(m_\gamma, t, u) + \delta_G(s, t, u) \right], \tag{192}$$

$$f_{\text{IR}}(m_\gamma, t, u) = \ln\left(\frac{1 - c_\theta}{1 + c_\theta}\right) \left[\ln\left(\frac{2m_\gamma^2}{s\sqrt{1 - c_\theta^2}}\right) + \frac{1}{2} \right],$$

$$\delta_G(s, t, u) = -2 \ln\left(\frac{1 - c_\theta}{1 + c_\theta}\right) \ln\left(\frac{s_0 - s}{s_0}\right). \tag{193}$$

Here θ is the scattering angle, m_γ is a mass regulator used for regulating the soft IR divergences, and the subscripts (n) indicate the loop order. If we wish to expand up to NNLO for the leading pole term, one would in principle also need the γZ box to two-loop order, which is currently unknown. However, it was shown in Refs. [204, 205] that at NLO the total contribution of IFI terms to R_{ij} vanishes when adding up the virtual γZ boxes and real photon radiation. In the CEEX scheme, it is practically negligible due to the narrow width suppression $\mathcal{O}(\Gamma_Z/M_Z) \sim \alpha^2$, see Refs. [207, 208]). A similar argument should apply

---

[2]this suppression will be lifted if the experimental cut on photon energy is of order of the resonance width, see Ref. [206].

to the $\gamma\gamma Z$ boxes at NNLO, although a more careful analysis of this issue would be desirable. Assuming that this argument holds, one only needs to include $B^R_{\gamma Z(m)}$, $m = 1, ..., n-1$ for the computation of $R^{(n)}_{ij}$.

4.2.3   the NNLO description of the Z-boson resonance

Near the Z resonance, when aiming for a description at N^nLO precision, it is typically sufficient to compute only the leading coefficient coefficient R to n-loop order, whereas $(n-1)$-loop and $(n-2)$-loop precision are adequate for S and S', respectively. In principle, this power counting can be extended to more terms, beyond S', in the Laurent expansion.. Furthermore, the ratio $\Gamma_Z/M_Z = \mathcal{O}(\alpha)$, where $\mathcal{O}(\alpha)$ denotes electroweak NLO corrections, which implies that one can perform expansions in the perturbative order, α, and Γ_Z/M_Z in parallel. For example, $f(s_0) = f(M_Z^2) - iM_Z\Gamma_Z f'(M_Z^2) - \frac{M_Z^2\Gamma_Z^2}{2} f''(M_Z^2) + ...$ Thus, in summary, we adopt the power counting $(s - s_0)/M_Z^2 \sim \Gamma_Z/M_Z \sim \alpha$ for the expansion of the matrix element near the Z pole.

$$R^{(0)}_{ij} = Z_{if(0)}Z_{jf'(0)}, \tag{194}$$

$$R^{(1)}_{ij} = \left[Z_{if(0)}Z_{jf'(1)} + Z_{if(1)}Z_{jf'(0)} - Z_{if(0)}Z_{jf'(0)}\Sigma'_{Z(1)}\right]_{s=M_Z^2}, \tag{195}$$

$$R^{(2)}_{ij} = \left[Z_{if(0)}Z_{jf'(2)} + Z_{if(2)}Z_{jf'(0)} + Z_{if(1)}Z_{jf'(1)} - Z_{if(0)}Z_{jf'(0)}\Sigma'_{Z(2)} - \Sigma'_{Z(1)}R^{(1)}_{ij}\right.$$
$$\left. - iM_Z\Gamma_Z(Z_{if(0)}Z'_{jf'(1)} + Z'_{if(1)}Z_{jf'(0)} - Z_{if(0)}Z_{jf'(0)}\Sigma''_{Z(1)})\right]_{s=M_Z^2} + B^R_{\gamma Z,ij(1)}, \tag{196}$$

$$S^{(0)}_{ij} = \frac{1}{M_Z^2}G_{if(0)}G_{jf'(0)}, \tag{197}$$

$$S^{(1)}_{ij} = \left[Z_{if(0)}Z'_{jf'(1)} + Z'_{if(1)}Z_{jf'(0)} - \frac{1}{2}Z_{if(0)}Z_{jf'(0)}\Sigma''_{Z(1)} + \frac{1}{M_Z^2}\left(G_{if(0)}G_{jf'(1)} + G_{if(1)}G_{jf'(0)}\right)\right.$$
$$\left. + \frac{iM_Z\Gamma_Z - \Sigma_{\gamma\gamma(1)}}{M_Z^4}G_{if(0)}G_{jf'(0)} + B_{ij(1)}\right]_{s=M_Z^2} + B^S_{\gamma Z,ij(1)}, \tag{198}$$

$$S'^{(0)}_{ij} = -\frac{1}{M_Z^4}G_{if(0)}G_{jf'(0)}, \tag{199}$$

where

$$Z_{Vf(1)} = v_{f(1)}^{\mathrm{Z}} + v_{f(0)}^{\gamma} \frac{\Sigma_{\gamma Z(1)}}{M_{\mathrm{Z}}^2}, \qquad\qquad Z_{Af(1)} = a_{f(1)}^{\mathrm{Z}} + a_{f(0)}^{\gamma} \frac{\Sigma_{\gamma Z(1)}}{M_{\mathrm{Z}}^2}, \qquad (200)$$

$$Z_{Vf(2)} = v_{f(2)}^{\mathrm{Z}} + v_{f(1)}^{\gamma} \frac{\Sigma_{\gamma Z(1)}}{M_{\mathrm{Z}}^2} \qquad\qquad Z_{Af(2)} = a_{f(2)}^{\mathrm{Z}} + a_{f(1)}^{\gamma} \frac{\Sigma_{\gamma Z(1)}}{M_{\mathrm{Z}}^2}$$

$$+ v_{f(0)}^{\gamma} \left(\frac{\Sigma_{\gamma Z(2)}}{M_{\mathrm{Z}}^2} - \frac{\Sigma_{\gamma Z(1)}\Sigma_{\gamma\gamma(1)}}{M_{\mathrm{Z}}^4} \right), \qquad\qquad + a_{f(0)}^{\gamma} \left(\frac{\Sigma_{\gamma Z(2)}}{M_{\mathrm{Z}}^2} - \frac{\Sigma_{\gamma Z(1)}\Sigma_{\gamma\gamma(1)}}{M_{\mathrm{Z}}^4} \right),$$

$$\qquad (201)$$

$$Z'_{Vf(1)} = v_{f(1)}^{\mathrm{Z}'} + v_{f(0)}^{\gamma} \left(\frac{\Sigma'_{\gamma Z(1)}}{M_{\mathrm{Z}}^2} - \frac{\Sigma_{\gamma Z(1)}}{M_{\mathrm{Z}}^4} \right), \qquad Z'_{Af(1)} = a_{f(1)}^{\mathrm{Z}'} + a_{f(0)}^{\gamma} \left(\frac{\Sigma'_{\gamma Z(1)}}{M_{\mathrm{Z}}^2} - \frac{\Sigma_{\gamma Z(1)}}{M_{\mathrm{Z}}^4} \right),$$

$$\qquad (202)$$

$$\Sigma'_{Z(1)} = \Sigma'_{ZZ(1)}, \qquad (203)$$

$$\Sigma'_{Z(2)} = \Sigma'_{ZZ(2)} - \frac{2}{M_{\mathrm{Z}}^2} \Sigma_{\gamma Z(1)} \Sigma'_{\gamma Z(1)} + \frac{(\Sigma_{\gamma Z(1)})^2}{M_{\mathrm{Z}}^4}, \qquad (204)$$

$$\Sigma''_{Z(1)} = \Sigma''_{ZZ(1)}. \qquad (205)$$

The subscripts (n) again indicate the loop order.

4.2.4 The EWPOs defined at the Z-boson resonance

To link the theoretical prediction to experimental data, we reparametrize the EWPOs in terms of form factors defined in Ref. [73] and in terms of the effective weak mixing angle $\sin^2 \theta_{\mathrm{eff}}^f$ defined in Eq.(153). Up to NNLO, along with the power counting $\Gamma_{\mathrm{Z}}/M_{\mathrm{Z}} \sim \alpha$, they read

$$\sin^2 \theta_{\mathrm{eff}}^f = \frac{1}{4|Q_f|} \left[1 - \mathrm{Re}\, \frac{Z_{Vf}}{Z_{Af}} \right]_{s=M_{\mathrm{Z}}^2}, \qquad (206)$$

$$F_A^f = \left[\frac{|Z_{Af}|^2}{1 + \mathrm{Re}\, \Sigma'_Z} - \frac{1}{2} M_{\mathrm{Z}} \Gamma_{\mathrm{Z}} |a_{f(0)}^{\mathrm{Z}}|^2 \, \mathrm{Im}\, \Sigma''_Z \right]_{s=M_{\mathrm{Z}}^2} + \mathcal{O}(\alpha^3), \qquad (207)$$

$$F_V^f = \left[\frac{|Z_{Vf}|^2}{1 + \mathrm{Re}\, \Sigma'_Z} - \frac{1}{2} M_{\mathrm{Z}} \Gamma_{\mathrm{Z}} |v_{f(0)}^{\mathrm{Z}}|^2 \, \mathrm{Im}\, \Sigma''_Z \right]_{s=M_{\mathrm{Z}}^2} + \mathcal{O}(\alpha^3) \qquad (208)$$

$$= F_A^f \left[(1 - 4|Q_f| \sin^2 \theta_{\mathrm{eff}}^f)^2 + \left(\mathrm{Im}\, \frac{Z_{Vf}}{Z_{Af}} \right)^2 \right] \qquad (209)$$

For $f = \nu$ the effective weak mixing angle is ill-defined and irrelevant. Then we reparametrize the Laurent series coefficients by using the form factors and the effective weak mixing angles

64

up to NNLO order as follows:

$$
\begin{aligned}
R_{ij}^{(0+1+2)} = 4I_f^3 I_{f'}^3 \sqrt{F_A^f F_A^{f'}} &\left[\tilde{Q}_i^f \tilde{Q}_j^{f'} \left(1 + i\, r_{AA}^I - \tfrac{1}{2}(r_{AA}^I)^2 + \tfrac{1}{2}\delta\overline{X}_{(2)}\right) \right. \\
&\left. + (\tilde{Q}_i^f I_{j,f'} + \tilde{Q}_j^{f'} I_{i,f})(i - r_{AA}^I) - I_{i,f} I_{j,f'} \right] \\
&+ M_Z \Gamma_Z\, Z_{if(0)} Z'_{jf'(0)}\, x_{ij}^I ,
\end{aligned}
\tag{210}
$$

where

$$
\tilde{Q}_V^f = 1 - 4|Q_f| \sin^2 \theta_{\text{eff}}^f, \qquad\qquad\qquad \tilde{Q}_A^f = 1, \tag{211}
$$

$$
I_{V,f} = \frac{1}{(a_{f(0)}^Z)^2}\left[a_{f(0)}^Z \operatorname{Im} Z_{Vf(1)} - v_{f(0)}^Z \operatorname{Im} Z_{Af(1)} \right], \qquad I_{A,f} = 0, \tag{212}
$$

$$
\delta\overline{X}_{(2)} = -(\operatorname{Im} \Sigma'_{Z(1)})^2 + 2\,\frac{B_{\gamma Z, ij(1)}^R}{R_{ij}^{(0)}}, \tag{213}
$$

$$
r_{AA}^I = \frac{\operatorname{Im} Z_{Af(1)}}{a_{f(0)}^Z} + \frac{\operatorname{Im} Z_{Af'(1)}}{a_{f'(0)}^Z} - \operatorname{Im} \Sigma'_{Z(1)}, \tag{214}
$$

$$
x_{ij}^I = \frac{\operatorname{Im} Z'_{if(1)}}{Z_{if(0)}} + \frac{\operatorname{Im} Z'_{jf'(1)}}{Z_{jf'(0)}} - \frac{1}{2}\operatorname{Im} \Sigma''_{Z(1)}. \tag{215}
$$

Instead of expanding the matrix elements about the complex pole, as in eq. (175), and then squaring them to obtain the differential cross-section, as in eq. (172), one can also perform the pole expansion directly for the square matrix element. Aiming, as before, for NNLO precision of the leading pole term, the result can be written as

$$
\begin{aligned}
\operatorname{Re}\{M_{ij} M_{kl}^*\} =\; & \frac{F_A^f F_A^{f'}\left[\tilde{Q}_i^f \tilde{Q}_j^{f'} \tilde{Q}_k^f \tilde{Q}_l^{f'}\left(1 + \delta\overline{X}_{(2)}\right) + \tilde{U}_{ijkl}\right]}{|s - s_0|^2} - \frac{\frac{\Gamma_Z}{M_Z}\tilde{Y}_{ijkl}^I - \frac{\Gamma_Z^2}{M_Z^2} G_{if(0)} G_{jf'(0)} G_{kf(0)} G_{lf'(0)}}{|s - s_0|^2} \\
&+ \frac{s - M_Z^2}{|s - s_0|^2}\left[\tilde{X}_{ijkl} + M_Z^{-2}\tilde{Y}_{ijkl}^R\right] + \frac{(s - M_Z^2)^2}{|s - s_0|^2} M_Z^{-4}\tilde{V}_{ijkl},
\end{aligned}
\tag{216}
$$

where

$$
\tilde{U}_{ijkl} = \tilde{Q}_i^f \tilde{Q}_k^f I_{j,f'} I_{l,f'} + \tilde{Q}_j^{f'} \tilde{Q}_l^{f'} I_{i,f} I_{k,f} + (\tilde{Q}_i^f I_{k,f} - \tilde{Q}_k^f I_{i,f})(\tilde{Q}_l^{f'} I_{j,f'} - \tilde{Q}_j^{f'} I_{l,f'}), \tag{217}
$$

$$
\begin{aligned}
\tilde{X}_{ijkl} = &\left[Z_{if(0)} Z_{jf'(0)}\left(Z_{kf(0)} \operatorname{Re} Z'_{lf'(1)} + Z_{lf'(0)} \operatorname{Re} Z'_{kf(1)} - \tfrac{1}{2} Z_{kf(0)} Z_{lf'(0)} \operatorname{Re} \Sigma''_{Z(1)}\right)\right] \\
&+ \left[i \leftrightarrow k, j \leftrightarrow l \right],
\end{aligned}
\tag{218}
$$

$$
\tilde{Y}_{ijkl}^R = \operatorname{Re} \tilde{Y}_{ijkl}, \qquad \tilde{Y}_{ijkl}^I = \operatorname{Im} \tilde{Y}_{ijkl}, \tag{219}
$$

$$
\begin{aligned}
\tilde{Y}_{ijkl} = &\left[Z_{if(0)} Z_{jf'(0)} G_{kf(0)} G_{lf'(1)} + Z_{if(0)} Z_{jf'(0)} G_{kf(1)} G_{lf'(0)} + Z_{if(0)} Z_{jf'(1)}^* G_{kf(0)} G_{lf'(0)} \right. \\
&+ Z_{if(1)}^* Z_{jf'(0)} G_{kf(0)} G_{lf'(0)} + Z_{if(0)} Z_{jf'(0)} G_{kf(0)} G_{lf'(0)}\left(1 - \Sigma'^*_{Z(1)} - M_Z^{-2}\Sigma_{\gamma\gamma(1)}\right) \\
&\left. + M_Z^2 Z_{if(0)} Z_{jf'(0)}\left(B_{kl(1)} + B_{\gamma Z, kl(1)}^S\right)\right] + \left[i \leftrightarrow k, j \leftrightarrow l \right],
\end{aligned}
\tag{220}
$$

65

$$\tilde{V}_{ijkl} = \left[G_{if(0)} G_{jf'(0)} \left(\tfrac{1}{2} G_{kf(0)} G_{lf'(0)} - Z_{kf(0)} Z_{lf'(0)} \right) \right] + \left[i \leftrightarrow k, j \leftrightarrow l \right]. \tag{221}$$

Both the matrix element coefficients (210) and (197)–(199), as well as the squared matrix elements (216) are implemented in the GRIFFIN library.

4.3 The structure of the C++ implementation

The theory framework is implemented within a structure of classes in C++. In v1.0, only the SM predictions for EWPOs and polarized matrix elements near the Z-peak up to NNLO along with partial higher orders have been implemented. Yet in principle one can use GRIFFIN to study the observables defined at a certain gauge resonance from a given model, up to arbitrary higher orders. The library has two base classes defined in accordance with input and output shown as in Table. 9. The two base classes are

- class `inval`, which contains user-provided input parameters for a given model (such as the SM or some extension thereof);
- class `psobs`, which returns a numerical prediction for an observable or pseudo-observable, for the input parameters provided by an `inval` object.

In its basic form, `inval` simply has some basic methods for setting and retrieving the values of some input parameters. However, one can define extended classes derived from `inval` to perform computations of input parameters, such as translating between masses in the complex-pole scheme and the running-width scheme, see eq. (176), or computing the W-boson mass from the Fermi constant [65].

The base version of GRIFFIN defines a set of input parameters for SM calculations, listed in Tab. 9. Most of these parameters are defined within the on-shell (OS) renormalization scheme, with the exception of light quark masses and the strong coupling, for which the $\overline{\text{MS}}$ scheme is assumed (at the scale $\mu = M_Z$). Additional input parameters for flavor physics or BSM scenarios can be easily added to these.

The user has the option to choose between input classes that either use $\{\alpha(0), M_W, M_Z\}$ or $\{\alpha(0), G_\mu, M_Z\}$ as inputs to define the electroweak couplings. Here $\alpha(0)$ is the electromagnetic coupling in the Thomson limit, and G_μ is the Fermi constant of muon decay. An additional input is the shift $\Delta\alpha$ between the running electromagnetic couplings at the scales $q^2 = 0$ and $q^2 = M_Z^2$. $\Delta\alpha$ receives contributions from leptons, which has been computed to four-loop order [163], and from quarks or hadrons, which can be extracted from data [165, 166, 209].

A child class decending from `psobs` can in principle encode predictions for any observable or pseudo-observable within any given model. The base version of GRIFFIN includes SM

class inval		class psobs	
input parameters (in the SM)		output observables	
Boson masses and widths	$M_{\mathrm{W,Z,H}}$ $\Gamma_{\mathrm{W,Z}}$	pesudo-observables defined at Z-peak	$F_{V,A}$, $\sin^2\theta^f_{eff}$ $\Gamma_{\mathrm{Z}\to f\bar{f}}$, Δr , etc
Fermion masses	$m^{\mathrm{OS}}_{\mathrm{e},\mu,\tau}$ $m^{\overline{\mathrm{MS}}}_{\mathrm{d,u,s,c}}(M_{\mathrm{Z}})$ $m^{\mathrm{OS}}_{\mathrm{t}}$	amplitude coefficients under pole scheme	R, S, and S'
Couplings	$\alpha(0)$ $\Delta\alpha \equiv 1 - \alpha(0)/\alpha(M_{\mathrm{Z}}^2)$ $\alpha_s^{\overline{\mathrm{MS}}}(M_{\mathrm{Z}}^2)$, G_μ	(polarized) matrix element square near Z-peak	$\mathrm{Re}\, M_{ij}M^*_{kl}$

Table 9: the category of two base classes in the SM.

predictions for form factors, such as $\sin^2\theta^f_{\mathrm{eff}}$ and $F^f_{V,A}$, and for matrix elements for the process $f\bar{f} \to f'\bar{f}'$ near the Z resonance, using the complex pole expansion described in the previous section. GRIFFIN version 1.0 contains the following SM corrections:

- Complete one-loop corrections for $\sin^2\theta^f_{\mathrm{eff}}$ [63, 64] are implemented in the class `SW_SMNLO`. On top of this, electroweak [127, 66, 67, 68, 69, 70], mixed electroweak-QCD [76, 71, 77, 78, 79] two-loop corrections, leading fermionic three-loop corrections of orders $\mathcal{O}(\alpha^3)$ and $\mathcal{O}(\alpha^2\alpha_{\mathrm{s}})$ [8, 210], non-factorizable $\mathcal{O}(\alpha\alpha_{\mathrm{s}})$ $Zb\bar{b}$ vertex contributions [80, 81, 82, 83, 84, 85] are implemented in `SW_SMNNLO`. In addition, partial higher-order corrections are available in the class `SW_SMNNLO`. The latter include corrections in the limit of a large top Yukawa coupling y_{t}, where $\alpha_{\mathrm{t}} \equiv y_{\mathrm{t}}^2/(4\pi)$. These include corrections to the EW ρ parameter defined as the ratio bewteen neutral current and charged current at zero momentum transfer [211]:

$$\rho = \frac{J_{NC}(0)}{J_{CC}(0)}. \tag{222}$$

A correction to ρ will shift $\sin^2 \theta_{\text{eff}}^f$ and F_A^f by

$$\delta \sin^2 \theta_{\text{eff}}^f = \frac{M_W^2}{M_Z^2} \delta \rho \,, \qquad \delta F_A^f = \frac{\alpha \pi (1 - 2c_w^2)}{4 c_w^2 s_w^4} \delta \rho, \tag{223}$$

In practice, the ρ parameter is useful for capturing leading corrections proportional to some power of the top Yukawa coupling.

- Similarly, the classes `FA_SMNLO` and `FV_SMNLO` provide one-loop corrections [64] for the form factors $F_{V,A}^f$, whereas `FA_SMNNLO` and `FV_SMNNLO` contain electroweak [72, 73, 74, 75] and mixed electroweak-QCD [76, 71, 77, 78, 79] two-loop corrections, as well as the partial higher-order corrections and non-factorizable contributions mentioned in the previous bullet point.

- For the process $f\bar{f} \to f'\bar{f}'$ All contributions needed to compute the matrix element coefficient R to NNLO accuracy according to (210), and the coefficients S and S' to NLO and LO, respectively, see eqs. (197)–(199). These are available in the classes `mat_SMNNLO`.

- All contributions required to compute the squared matrix elements to NNLO accuracy according to eq. (216) are implemented in the class `msq_SMNNLO`.

- When using the input parameter set $\{\alpha(0), G_\mu, M_Z\}$, one needs to compute M_W from these quantities according to

$$G_\mu = \frac{\pi \alpha}{\sqrt{2} M_W^2 (1 - M_W^2 / M_Z^2)} (1 + \Delta r). \tag{224}$$

Here Δr accounts for radiative corrections. The class `dr_SMNNLO` contains all higher-order corrections discussed in Ref. [65], plus the leading fermionic three-loop corrections of orders $\mathcal{O}(\alpha^3)$ and $\mathcal{O}(\alpha^2 \alpha_s)$ [8, 210]. These corrections are used in the input classes `invalGmu` and `SMvalGmu`.

Corrections entering through $\delta\rho$:			
	drho2aas	$\mathcal{O}(\alpha_{\mathrm{t}}\alpha_{\mathrm{s}})$	[76, 71]
	drho2a2	$\mathcal{O}(\alpha_{\mathrm{t}}^2)$	[212, 213, 214, 215, 216]
*	drho3aas2	$\mathcal{O}(\alpha_{\mathrm{t}}\alpha_{\mathrm{s}}^2)$	[86, 87]
*	drho3a2as	$\mathcal{O}(\alpha_{\mathrm{t}}^2\alpha_{\mathrm{s}})$	[88, 89]
*	drho3a3	$\mathcal{O}(\alpha_{\mathrm{t}}^3)$	[88, 89]
*	drho3aas3	$\mathcal{O}(\alpha_{\mathrm{t}}\alpha_{\mathrm{s}}^3)$	[90, 91, 92]

Full corrections to F_A^f, $\sin^2\theta_{\mathrm{eff}}^f$:			
*	res2ff	$\mathcal{O}(\alpha_f^2)$	[127, 66, 73]
*	res2fb	$\mathcal{O}(\alpha_f\alpha_b)$	[127, 66, 69, 73]
*	res2bb	$\mathcal{O}(\alpha_b^2)$	[67, 68, 70, 74, 75]
*	res2aas	$\mathcal{O}(\alpha\alpha_{\mathrm{s}})$	[77, 78, 79] (correction to internal gauge-boson self-energies)
*	res2aasnf	$\mathcal{O}(\alpha\alpha_{\mathrm{s}})$	[80, 81, 82, 83, 84, 85] (non-factorizable final-state corrections for $f = q$)
*	res3fff	$\mathcal{O}(\alpha_f^3)$	[8]
*	res3ffa2as	$\mathcal{O}(\alpha_f^2\alpha_{\mathrm{s}})$	[210]

Figure 13: All contributions implemented in classes `FA_SMNNLO`, `FV_SMNNLO`, `SW_SMNNLO`. Note that the meaningful sum of all contributions are indicated by an asterik (*).
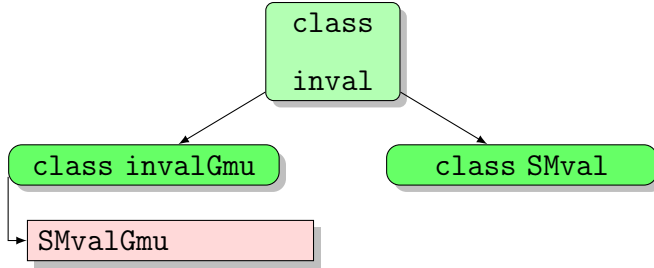
Figure 14: The hierarchy of classes for GRIFFIN's input. The base class `inval` is an abstract class that users need to define input parameters for a certain model (such as the SM or beyond) in its offspring. In GRIFFIN 1.0, we have only implemented the SM for the Z resonance (and muon-decay). Hence the derived classes defines different EW input parameter schemes.
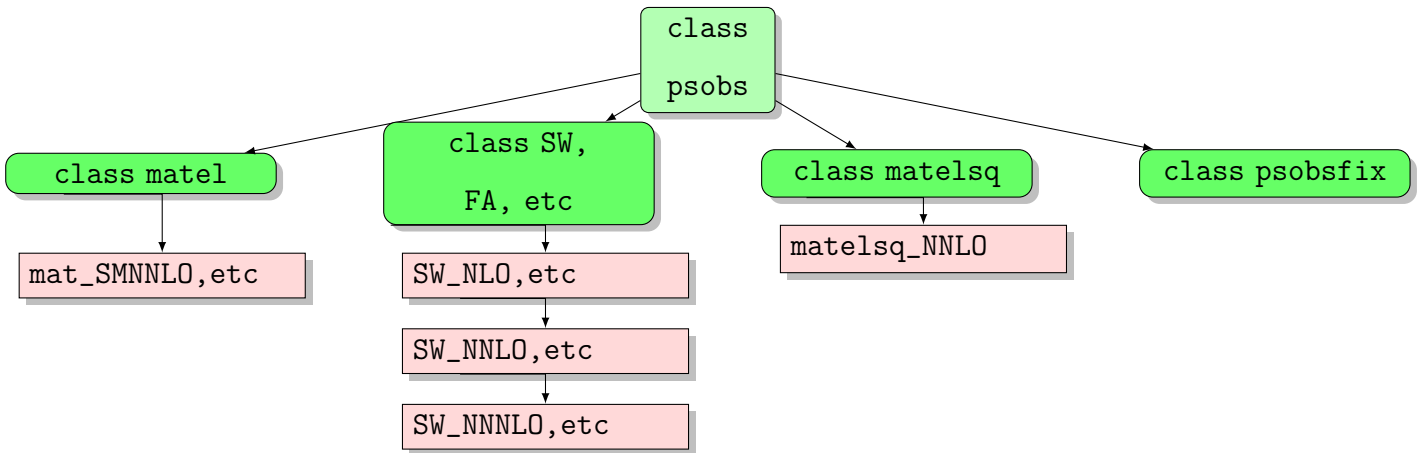

Figure 15: The hierarchy of classes for GRIFFIN's output. The base class `psobs` is an abstract class where several virtual member functions are defined. The user can in principle define new derived classes based off their own purpose. In GRIFFIN 1.0, three types of derived classes, and their sub-derived classes of higher order are defined accordingly.

4.4 Benchmark Tests and comparision

We performed a benchmark test of the EWPOs in comparison with the existing library of EW radiative corrections – DIZET v 6.45 at NNLO.

4.4.1 the comparison of the EWPOs

In DIZET, the form factor is defined as Eq. 2.4.9 and Eq.2.4.10 in Ref. [187].

$$\Gamma_{Z \to f\bar{f}} = \Gamma_0 c_f |\rho_Z^f| (|g_Z^f|^2 R_V^f + R_A^f) + \delta_{\alpha\alpha_s}, \tag{225}$$

where we have set all lepton mass to be zero and

$$\Gamma_0 = \frac{G_\mu M_Z^3}{24\sqrt{2}\pi}. \tag{226}$$

Whereas in GRIFFIN, we define the partial width of Z-boson as

$$\Gamma_{Z \to f\bar{f}} = \frac{N_c^f M_Z}{12\pi} (F_V^f R_V^f + F_A^f R_A). \tag{227}$$

In Eq. 4.4.1, the g_Z^f is defined as a complex-valued variable as

$$g_Z^f = \frac{v_f}{a_f} = 1 - 4|Q_f|(\kappa_Z^f s_w^2 + I_f^2), \tag{228}$$

where κ_Z^f is again, defined as a complex-valued variable. If the effective weak mixing angle $sin^2\theta_{eff}^f$ defined in GRIFFIN is the same as that in DIZET, we would have the following identity:

$$g_Z^f = \frac{Z_{Vf}}{Z_{Af}}, \tag{229}$$

thereby obtaining the relation between rho_Z^f and F_A^f through the partial width:

$$\Gamma_{Zf\bar{f}} = \frac{N_c^f M_Z}{12\pi} F_A^f \left(\frac{F_V^f}{F_A^f} + 1\right) = \frac{N_c^f M_Z}{12\pi} F_A^f (|g_Z^f|^2 + 1) = \Gamma_0 c_f |\rho_Z^f| (|g_Z^f|^2 + 1), \tag{230}$$

where the radiators are turned off from both side of the equation. Given that the color number c_f and N_c^f are the same, It is thus easy to obtain the relation between $|\rho_Z^f|$ and F_A^f

$$|\rho_Z^f| = \frac{2\sqrt{2}F_A^f}{G_\mu M_Z^2} \tag{231}$$

One should notice that the mixed QCD-EW corrections are considered as additive part in Z widths, whereas in GRIFFIN, they are all absorbed in form factors and their radiators $F_{V,A}$ and $R_{V,A}$, respectively, thus causing the numerical discrepancy while transferring the

71

form factors $F_{V,A}$ into ρ_Z^f. Besides, one also has to notice that Eq. 231 is the modulus of ρ_Z^f instead of $\mathrm{Re}\,\rho_Z^f$. Hence to compare this observables, we need to use both $\mathrm{Im}\,\rho_Z^f$ and $\mathrm{Re}\,\rho_Z^f$ output from DIZET to reconstruct $|\rho_Z^f|$. Due to the limited options of EW input schemes offered by subroutine DIZET, we have to set G_μ, M_Z as input and output $M_W, \Gamma_{W,Z}$, which will be adopted by GRIFFIN as inputs, shown as below.

GRIFFIN input parameters	
DIZET input parameters	DIZET output
$\alpha_s(M_Z^2) = 0.118, \quad \alpha = 1/137.035989500$	$\Gamma_Z = 2.495599$ GeV
$\Delta\alpha = 0.0594976, \quad M_Z = 91.1876$ GeV, $\quad G_\mu = 1.16638 \times 10^{-5}$	$M_W = 80.3532$ GeV $\Gamma_W = 2.089580$ GeV
$m_t = 173.0999$ GeV, $\quad m_H = 125.0$ GeV, $\quad m_{\mathrm{e},\mu,\tau,\mathrm{u,d,s,c,b}} = 0$ GeV	

Table 10: the benchmark input values for numerical comparison between Zfitter and Griffin and different EW input schemes used in each program.

Here we compared three sets of precision observables : form factor ρ_Z^f defined in DIZET, $\sin^2\theta_{eff}^f$, and partial Z width Γ_Z.

	DIZET	GRIFFIN
Δr	3.665994×10^{-2}	3.66597×10^{-2}

Table 11: the benchmark values for Δr, including complete $\mathcal{O}(\alpha^2)$ corrections, $\mathcal{O}(\alpha\alpha_s)$ and $\mathcal{O}(\alpha\alpha_s^2)$ QCD corrections, as well as leading three-loop corrections in an expansion in m_t^2 of $\mathcal{O}(\alpha^3)$ and $\mathcal{O}(\alpha^2\alpha_s)$.

In Tab. 12, we have shown the numerical comparison among several EWPOs and form factors. For most predictions given by both programs, numbers agree with each other by at least four decimal points. The discrepancy is mildly larger for the form factor $|\rho_Z^f|$ in

	$\|\rho_Z^f\|$		$\sin^2\theta_{eff}^f$		$\Gamma_{Z\to f\bar{f}}$	
	DIZET 6.45	GRIFFIN	DIZET 6.45	GRIFFIN	DIZET 6.45	GRIFFIN
$\nu\bar{\nu}$	1.00800	1.00808	0.231255	NAN	0.167208	0.167189
$\bar{l}$	1.00510	1.00512	0.231637	0.231647	0.083981	0.0839657
$u\bar{u}$	1.00579	1.00567	0.231530	0.231565	0.299868	0.299868
$d\bar{d}$	1.00676	1.00644	0.231403	0.231459	0.382814	0.382755
$b\bar{b}$	0.99692	0.99420	0.232876	0.232886	0.376785	0.377421

Table 12: The numerical comparison of the EWPOs and form factors ρ between DIZET and GRIFFIN. General agreements are achieved up to the different definition of form factors and the parametric shift due to different input schemes.

$Z \to q\bar{q}$ channel, which reflects the different parametrization of the Z-width adopted by the two programs. In DIZET, the mixed EW-QCD correction is an outcast from form factors, while the same contribution is encapsulated in $F_{A,V}$ in GRIFFIN. And indeed, one can see the partial width $\Gamma_{Z\to q\bar{q}}$ has better agreement after all. The flags used by DIZET V.6.45 are listed as follows:

IHVP=5	IAMT4=8	IQCD=3	IMOMS=1	IMASS=0
ISCRE=0	IALEM=0	IMASK=0	ISCAL=0	IBARB=2
IFTJR=1	IFACR=0	IFACT=0	IHIGS=0	IAFMT=3
IEWLC=0	ICZAK=1	IHIGS=1	IALE2=3	IGFER=2
IDDZZ=1	IAMW2=1	ISFSR=1	IDMWW=0	IDSWW=0

4.5   Discussion and outlook

In this chapter, we report a new package recently developed that provides an extendable framework in the presence of a hierarchy of C++ classes to compute EWPOs and observables within a given model. The prototype of this package provides the SM predictions for EWPOs and (polarized) cross-sections in the vicinity of the Z resonance. In this package, we use the pole scheme to lay out the framework describing the Z-boson resonance, ensuring our amplitudes are manifestly gauge-invariant at arbitrary higher orders. We primarily choose the CEEX scheme for the IR subtraction to incorporate with existing MC programs such as KKMC. Although the external user can, in principle, use their favored schemes to deal with the IR subtraction. We have implemented the radiative corrections of EWPOs and relevant form factors, including $\mathcal{O}(\alpha, \alpha^2, \alpha\alpha_\mathrm{s}, \alpha_t\alpha_\mathrm{s}, \alpha_t\alpha_\mathrm{s}^2, \alpha_t^2\alpha_\mathrm{s}, \alpha_t^3, \alpha_t\alpha_\mathrm{s}^3)$. There is still a part of work left over as implementing the leading fermionic three-loop corrections from chapter 3 into the package, which are expected to be done soon. All the implemented corrections accumulatively can be used to construct NNLO plus partial higher orders of the cross-section of $e^+e^- \to ff'$ near the Z-pole. For one-loop corrections, we use housemade C code to evaluate one-loop scalar Feynman integrals. For corrections beyond the one-loop level, the grid interpolation technique is adopted to compute the numerical results of various multi-loop integrals. In principle, one can also link GRIFFIN to their preferred external loop calculation packages. This package can be treated as a library of EW radiative corrections; thereby, one can perform the precision test of a particular model by interfacing it with MC tools such as KKMC or KORALZ. We have performed the benchmark test for the evaluation of the EWPOs and compared it with DIZET v.6.45. Due to the different frameworks set up in the two programs, the numerics' agreement is not perfect but under control. The ongoing work compares the differential cross sections among ZFITTER, KKMC, which is expected to be done soon. The future projection is fairly straightforward:

- the implementation of theory error estimation for observables and pseudo-observables;
- matrix elements for four-fermion scatterings being far-away from the Z resonance;
- the implementation of Bhabha scattering for the precision of background;
- Drell-Yan process at the (HL-)LHC with both charge and neutral resonance;
- predictions for EWPOs in BSM theories or in terms of effective theory extensions of the SM with higher-dimensional operators ;
- ...

5.0   Conclusion

As stated already in 1.2, the future e^+e^- colliders project a substantially improved experimental accuracy compared with that of the LEP/SLC for all eletroweak measurements. Consequently, such tremendous precision given by any future e^+e^- colliders, such as the FCC-ee, ILC/Giga-Z, CLIC, and CEPC, ursher us into the area of three-loop and leading four-loop electroweak calculations. For the Standard Model calculations of the Z-pole observables introduced in 1.2, the complete two-loop and partial higher-loop corrections are known. The so-called intrinsic theoretical uncertainties due to uncontrolled higher-order terms are estimated to be smaller than the experimental accuracy reached by the LEP, but larger than that of the FCC-ee, CEPC, CLIC, and ILC/Giga-Z (see Table. 2), thus making a new round of calculation indispensable. In this thesis, we highlight our recent calculations of leading fermionic three-loop corrections to the W-boson mass and Z-pole observables at both $\mathcal{O}(\alpha^3)$ and $\mathcal{O}(\alpha^2\alpha_s)$. They are considered as a set of sizable corrections owing to the power of the top mass and flavor number enhancement. However, they turn out to be milder than one would expect due to some accidental cancellations, urging the effort of calculating the remaining three-loop contributions, which requires further developments on technical aspects so that all the contributing Feynman integrals can be efficiently evaluated.

All aforementioned EWPOs that encapsulate the dominant radiative corrections in the SM and that are most sensitive to BSM physics are defined at the Z resonance peak ($\sqrt{s} = M_Z$). Thus fully describing the Z resonance near its pole position, containing hard contributions from $s-$channel photon exchange and box diagrams, initial- and final-state QED and QCD radiation, and acceptance of detector become important, consequently requiring a generic form of $e^+e^- \rightarrow Z \rightarrow f\bar{f}$ that respects unitarity, analyticity, and gauge-invariance. Such requirements can be fulfilled by the 'pole scheme', where the matrix element near the Z-pole is constructed as a Laurent expansion in the complex $s-$plane with a single simple pole as the resonance term and a Taylor series as background. Albeit the tremendous success made by predecessors mentioned in section 4.1 during LEP/SLC era, due to the inextendability or dated programming structures of those software packages, a new program framework that is modularized/object-oriented is needed for the study of future Z-factory. In chapter 4, we reported a developing package GRIFFIN structured in a hierarchy of classes. In this package, we have implemented full two-loop and partial higher-loop corrections to the EWPOs and constructed the NNLO description of cross-sections in the vicinity of the Z-pole. A benchmark comparison of the electroweak form factors and other EWPOs between GRIF-

FIN and DIZET v6.45 has been shown. Although quantities are defined in slightly different ways in two programs, a general numerical agreement can be achieved with discrepancies under controlled. They comparison among GRIFFIN, ZFITTER/DIZET v6.42, and KKM-C/DIZET v6.45 is a non-trivial task where a detailed understanding in all three packages is needed. It is thus left as a part of ongoing work which remains unreported. As future projections, we expect GRIFFIN can be used in studies of any four-fermion scattering/decay processes with arbitrary higher orders.

6.1   Projection operators for amplitudes

6.1.1   Projecting the transverse component of the self-energy

For the gauge-boson self energy one has

$$\Sigma_{\mu\nu}^{ab} = (-g_{\mu\nu} + \frac{p_\mu p_\nu}{p^2})\Sigma_T^{ab} - \frac{p_\mu p_\nu}{p^2}\Sigma_L^{ab}(p^2), \tag{232}$$

where one can project out the transverse part and the longitudinal part by applying

$$\Sigma_T^{ab} = \frac{1}{D-1}(-g^{\mu\nu} + \frac{p^\mu p^\nu}{p^2})\Sigma_{\mu\nu}^{ab}; \quad \Sigma_L^{ab} = -\frac{p^\mu p^\nu}{p^2}\Sigma_{\mu\nu}^{ab}, \tag{233}$$

where p^μ is the external momentum, a, b can be WW, ZZ, and γZ. Especially when $p^2 = 0$, $\Sigma_T^{ab} = \Sigma_L^{ab}$, and

$$\Sigma_T^{ab} = \frac{-1}{D}g^{\mu\nu}\Sigma_{\mu\nu}^{ab} \tag{234}$$

6.1.2   Projecting the vector and axial vector form factor

For a generalized chiral coupling Gff we can write:

$$\hat{\Gamma}_\mu = ig\gamma_\mu(G_V(s) - G_A(s)\gamma^5) \tag{235}$$

One can easily project out the form factors $G_{V,A}$ as

$$G_V(s) = \frac{1}{2(2-D)s}\text{Tr}\left[\gamma^\mu \not{p_1}\hat{\Gamma}_\mu(s)\not{p_2}\right], \tag{236}$$

$$G_A(s) = \frac{1}{2(2-D)s}\text{Tr}\left[\gamma^5\gamma^\mu \not{p_1}\hat{\Gamma}_\mu(s)\not{p_2}\right]. \tag{237}$$

6.1.3   Projection operators for box amplitudes

$$\mathcal{M}_{XY} = -ie^4 N_c Q_f^2 \int \frac{d^4k}{(2\pi)^4} \frac{\left(\bar{v}(p_2)G_{i,XX}^\mu \not{k}G_{i,YY}^\nu u(p_1)\right)\left(v(q_1)G_{f,XX}^\mu(\not{p_1} - \not{k} + \not{q_1})G_{f,YY}^\nu \bar{u}(q_2)\right)}{k^2((k+p_2)^2 - m_X^2)(k+p_2-q_2)^2((k+p_2-q_1-q_2)^2 - m_Y^2)}, \tag{238}$$

where

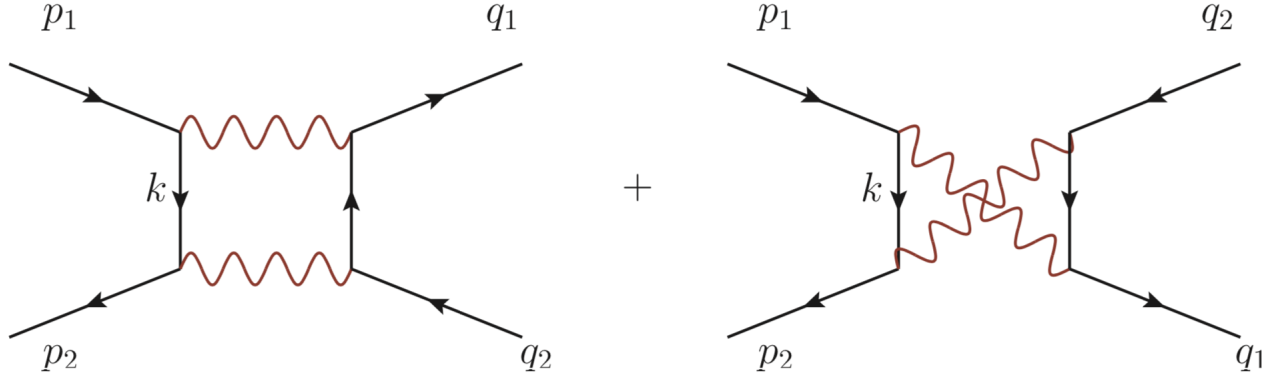$$G_{j,kl}^\mu = g_{ik}^R\gamma^\mu\gamma^6 + g_{jl}^L\gamma^\mu\gamma^7$$

Figure 16: The generic box diagram considered in $e^+e^- \to Z \to ff'$

and

$$\gamma^{6,7} = \frac{1 \pm \gamma^5}{2} \; .$$

Using $\{\gamma^\mu, \gamma^5\} = 0$ in 4-dim, $\gamma^6 \gamma^7 = 0$, $(\gamma^a)^2 = \gamma^a$. X and Y stands for two internal gauge bosons. We tend to work out the numerator projection in 4-dimension thoroughly so no γ^5 issue will come up.

$$\gamma^\tau (\gamma^6 + \gamma^7) \slashed{k} \gamma^\nu (\gamma^6 + \gamma^7) = \gamma^\tau \slashed{k} \gamma^\nu (\gamma^6 + \gamma^7) \tag{239}$$

$$\mathcal{M}_{XY} = -ie^4 N_c Q_f^2 \int \frac{d^4 k}{(2\pi)^4}$$
$$\frac{\left(\bar{v}(p_2) \gamma^\mu \slashed{k} \gamma^\nu (g_{iX}^R g_{iY}^R \gamma^6 + g_{iX}^L g_{iY}^L \gamma^7) u(p_1) \right) \left(v(q_1)(\gamma^\mu (\slashed{p}_1 - \slashed{k} + \slashed{q}_1) \gamma^\nu (g_{fX}^R g_{fY}^R \gamma^6 + g_{iX}^L g_{iY}^L \gamma^7) \bar{u}(q_2) \right)}{k^2((k+p_2)^2 - m_X^2)(k+p_2 - q_2)^2((k+p_2-q_1-q_2)^2 - m_Y^2)} .$$
$$\tag{240}$$

And $\mathcal{M}_{XY}$ can be decomposed into the following

$$\mathcal{M}_{XY} = \sum_{a,b} \mathcal{A}^{ab} \tag{241}$$

where $\{a,b\} = \{L,R\}, \{L,L\}, \{R,R\}, \{R,L\}$, and by defining

$$\Gamma_1 \otimes \Gamma_2 \equiv [\bar{v}(p_2)\Gamma_1 u(p_1)][v(q_1)\Gamma_2 \bar{u}(q_2)], \tag{242}$$

78

the amplitude can be written as a product of two Dirac chain Γ_i as

$$\mathcal{A}_1^{ab} = \gamma^\tau \slashed{k} \gamma^a \otimes \gamma^\tau \slashed{Q} \gamma^\nu \gamma^b \tag{243}$$

where $Q = k + p_2 - q_2$. And we ignore integral notation for the moment. One should always keep in mind that to match up with our framework set-up, we need to eventually project all amplitudes onto $V - A$ basis, with that been said, we need to first project out the coefficients for each $L - R$ basis vector and then convert them to $V - A$ basis. A generic Dirac chain can be decomposed into

$$\Gamma = a_1 1 + b_1 \gamma^\nu + b_2 \gamma^\nu \gamma^5 + a_2 \gamma^5 + c_1 \sigma^{\tau\nu} + c_2 \sigma^{\tau\nu} \gamma^5 \tag{244}$$

Here we dealing with massless fermions, hence the chirality between an initial and final fermion would not reversed through Dirac chain transition. A simple conclusion which can be found is that only vector and axial vector transitions will maintain the chirality of initial and final fermions [?]. Hence we only need to project out the coefficients b_1, b_2. And alternatively, these two basis can combine together to be a left-hand or right-hand basis.

$$\Gamma_a^{i,f} = (a_{i,f} 1 + b_{i,f} \gamma^\nu + c_{i,f} \sigma^{\tau\nu}) \gamma^a \tag{245}$$

We come up with a projector looks like the following

$$\mathcal{F}_{ab} = \mathcal{N}_{ab} [\slashed{p}_2 \gamma^\mu \slashed{p}_1 \Gamma_{XY}^{ia}][\slashed{q}_1 \gamma_\mu \slashed{q}_2 \Gamma_{XY}^{fb}], \tag{246}$$

where $\mathcal{F}$ is the product of coefficients $b_1 b_2$. And the $\mathcal{N}$ is the normalizing factor given at each projector.

To determine the normalizing factor one should use the generic form of Dirac chains for both initial state and final state as given in (245).

$$[\slashed{p}_2 \gamma^\mu \slashed{p}_1 \Gamma_{XY}^{iR(L)}][\slashed{q}_1 \gamma_\mu \slashed{q}_2 \Gamma_{XY}^{fR(L)}] = 4 b_1^i b_2^f u^2 \tag{247}$$

$$[\slashed{p}_2 \gamma^\mu \slashed{p}_1 \Gamma_{XY}^{iR(L)}][\slashed{q}_1 \gamma_\mu \slashed{q}_2 \Gamma_{XY}^{fL(R)}] = 4 b_1^i b_2^f t^2 \tag{248}$$

Hence we get

$$\mathcal{F}_{RR(LL)} = \frac{1}{4u^2} [\slashed{p}_2 \gamma^\mu \slashed{p}_1 \Gamma_{\gamma\gamma}^{iR(L)}][\slashed{q}_1 \gamma_\mu \slashed{q}_2 \Gamma_{\gamma\gamma}^{fR(L)}] \tag{249}$$

$$\mathcal{F}_{RL(LR)} = \frac{1}{4t^2} [\slashed{p}_2 \gamma^\mu \slashed{p}_1 \Gamma_{\gamma\gamma}^{iR(L)}][\slashed{q}_1 \gamma_\mu \slashed{q}_2 \Gamma_{\gamma\gamma}^{fL(R)}] \tag{250}$$

For parallel box

$$\Gamma_{XY}^{p(c),iL} = g_{iX}^L g_{iY}^L \gamma^\tau \slashed{k} \gamma^\nu \gamma^7 \tag{251}$$

$$\Gamma_{XY}^{p(c),iR} = g_{iX}^R g_{iY}^R \gamma^\tau \slashed{k} \gamma^\nu \gamma^6 \tag{252}$$

$$\Gamma_{XY}^{p,fL} = g_{fX}^L g_{fY}^L \gamma^\nu (\slashed{k} + \slashed{p_2} - \slashed{q_2}) \gamma^\tau \gamma^7 \tag{253}$$

$$\Gamma_{XY}^{p,fR} = g_{fX}^R g_{fY}^R \gamma^\nu (\slashed{k} + \slashed{p_2} - \slashed{q_2}) \gamma^\tau \gamma^6 \tag{254}$$

$$\Gamma_{XY}^{c,fL} = g_{fX}^L g_{fY}^L \gamma^\tau (-\slashed{k} - \slashed{p_2} + \slashed{q_1}) \gamma^\nu \gamma^7 \tag{255}$$

$$\Gamma_{XY}^{c,fR} = g_{fX}^R g_{fY}^R \gamma^\tau (-\slashed{k} - \slashed{p_2} + \slashed{q_1}) \gamma^\nu \gamma^6, \tag{256}$$

$$\tag{257}$$

where $g_{X,Y}^{L,R}$ denotes the fermion's Gauge coupling on L-R basis. For instance, for photon boxes, all these gs are Q_e. But for ZZ box, they become

$$g_{Zff}^L = \frac{I_3 - s_w^2 Q_f}{s_w c_w} \quad g_{Zff}^R = \frac{-s_w}{c_w} Q_f \tag{258}$$

Now we can plug (257) in to to carry out the helicity amplitude, with the help of FEYNCALC. One should keep in mind that we can carry out the Dirac trace algebra in 4 dimension with no issues, but we nevertheless need to do loop integral reduction in D-dim fashion. When the reduction is performed in D-dimension, there is still a left-over Levi-Civita symbol as $\epsilon^{p_1 p_2 q_1 q_2}$. Due to momentum conservation of the scattering process, we know those four momenta that show up at the index of ϵ are related to each other hence this Levi-Civita symbol should vanish eventually in our calculation.

Then, after we obtain the helicity amplitude. We can write the $B_{\gamma\gamma}$ as

$$B_{\gamma\gamma} = \mathcal{F}_{RR}\gamma^\mu\gamma^6 \otimes \gamma_\mu\gamma^6 + \mathcal{F}_{RL}\gamma^\mu\gamma^6 \otimes \gamma_\mu\gamma^7 + \mathcal{F}_{LR}\gamma^\mu\gamma^7 \otimes \gamma_\mu\gamma^6 + \mathcal{F}_{LL}\gamma^\mu\gamma^7 \otimes \gamma_\mu\gamma^7 \tag{259}$$

Convert (259) into V-A basis in which we parametrize $B_{\gamma\gamma}$ as

$$B_{\gamma\gamma} = B_{VV,\gamma\gamma}\gamma^\mu \otimes \gamma_\mu + B_{VA,\gamma\gamma}\gamma^\mu \otimes \gamma_\mu\gamma^5 + B_{AV,\gamma\gamma}\gamma^\mu\gamma^5 \otimes \gamma_\mu + B_{AA,\gamma\gamma}\gamma^\mu\gamma^5 \otimes \gamma_\mu\gamma^5 \tag{260}$$

By inspecting the tree level relation between V-A coupling and L-R coupling, we get

$$B_{VV} = \frac{1}{4}(\mathcal{F}_{LL} + \mathcal{F}_{RR} + \mathcal{F}_{RL} + \mathcal{F}_{LR}) \tag{261}$$

$$B_{AA} = \frac{1}{4}(\mathcal{F}_{LL} + \mathcal{F}_{RR} - \mathcal{F}_{RL} - \mathcal{F}_{LR}) \tag{262}$$

$$B_{VA} = \frac{1}{4}(-\mathcal{F}_{RR} + \mathcal{F}_{LL} + \mathcal{F}_{RL} - \mathcal{F}_{LR}) \tag{263}$$

$$B_{AV} = \frac{1}{4}(-\mathcal{F}_{RR} + \mathcal{F}_{LL} - \mathcal{F}_{RL} + \mathcal{F}_{LR}) \tag{264}$$

$$\tag{265}$$

In the end, the $B_{ij,\gamma\gamma}$ in terms of Passarino-Veltmann master integrals are

$$
\begin{aligned}
B_{VV,\gamma\gamma} =\ & \frac{e^4(t-u)\mathrm{B}_0\left(s,m_\gamma^2,m_\gamma^2\right)}{16\pi^2 tu} + \frac{e^4\mathrm{B}_0(u,0,0)}{16\pi^2 t} - \frac{e^4\mathrm{B}_0(t,0,0)}{16\pi^2 u} - \frac{e^4\left(t^4-u^4\right)\mathrm{C}_0\left(0,s,0,0,m_\gamma^2,m_\gamma^2\right)}{16\pi^2 t^2 u^2} \\
& + \frac{e^4 u(t-u)\mathrm{C}_0\left(u,0,0,0,0,m_\gamma^2\right)}{16\pi^2 t^2} + \frac{e^4 t(t-u)\mathrm{C}_0\left(t,0,0,0,0,m_\gamma^2\right)}{16\pi^2 u^2} \\
& + \frac{e^4\left(t^3+3tu^2\right)\mathrm{D}_0\left(t,0,s,0,0,0,0,0,m_\gamma^2,m_\gamma^2\right)}{32\pi^2 u^2} - \frac{e^4\left(3t^2 u+u^3\right)\mathrm{D}_0\left(u,0,s,0,0,0,0,0,m_\gamma^2,m_\gamma^2\right)}{32\pi^2 t^2} \\
B_{AA,\gamma\gamma} =\ & \frac{e^4(t+u)\mathrm{B}_0\left(s,m_\gamma^2,m_\gamma^2\right)}{16\pi^2 tu} - \frac{e^4\mathrm{B}_0(u,0,0)}{16\pi^2 t} - \frac{e^4\mathrm{B}_0(t,0,0)}{16\pi^2 u} - \frac{e^4\left(t^2-u^2\right)^2\mathrm{C}_0\left(0,s,0,0,m_\gamma^2,m_\gamma^2\right)}{16\pi^2 t^2 u^2} \\
& - \frac{e^4 u(t-u)\mathrm{C}_0\left(u,0,0,0,0,m_\gamma^2\right)}{16\pi^2 t^2} + \frac{e^4 t(t-u)\mathrm{C}_0\left(t,0,0,0,0,m_\gamma^2\right)}{16\pi^2 u^2} \\
& + \frac{e^4\left(t^3-tu^2\right)\mathrm{D}_0\left(t,0,s,0,0,0,0,0,m_\gamma^2,m_\gamma^2\right)}{32\pi^2 u^2} + \frac{e^4\left(u^3-t^2 u\right)\mathrm{D}_0\left(u,0,s,0,0,0,0,0,m_\gamma^2,m_\gamma^2\right)}{32\pi^2 t^2} \\
B_{AV,\gamma\gamma} =\ & B_{VA,\gamma\gamma} = 0
\end{aligned}
$$

6.2 Feynman loop integrals

6.2.1 The derivative of one-loop integrals

$$B_0(p^2, m_1^2, m_2^2) = \frac{(2\pi\mu)^{4-D}}{i\pi^2} \int d^D q \frac{1}{(q^2 - m_1^2 + i\epsilon)((q+p_1)^2 - m_2^2 + i\epsilon)} \equiv \mathbf{I}_{1,1} \tag{266}$$

By chain rules:

$$\frac{\partial B_0}{\partial p^2} = \frac{\partial B_0}{\partial p^\mu}\frac{\partial p^\mu}{\partial p^2} \quad \Rightarrow \quad \frac{\partial B_0}{\partial p^\mu} = 2p_\mu \frac{\partial B_0}{\partial p^2}, \tag{267}$$
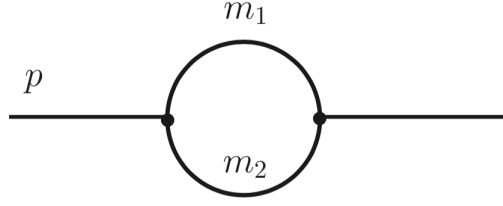
81

Figure 17: scalar one-loop of two-point function

and for $p^2 \neq 0$

$$\frac{\partial B_0}{\partial p^2} = \frac{1}{2p_\mu}\frac{\partial B_0}{\partial p^\mu} = \frac{1}{2p^2}p^\mu\frac{\partial}{\partial p^\mu}\mathbf{I}_{1,1} = \frac{1}{2p^2}(-\mathbf{I}_{1,1} + (p^2 - m_1^2 - m_2^2)\mathbf{I}_{1,2} + \mathbf{I}_{2,0}) \tag{268}$$

$$= \frac{1}{2p^2}\left[B_0(0, m_2^2, m_2^2) - B_0(p^2, m_1^2, m_2^2) + (p^2 - m_1^2 - m_2^2)C_0(0, p^2, p^2, m_2^2, m_2^2, m_1^2)\right] \tag{269}$$

For $p^2 = 0$, one cannot simply apply the same chain rule as Eq. (268). Instead, we can do as follows

$$\frac{\partial^2}{\partial p_\mu \partial p^\mu}B_0(p^2, m_1^2, m_2^2)\Big|_{p^2=0} = \frac{\partial}{\partial p_\mu}\left(2p_\mu\frac{\partial B_0(p^2, m_1^2, m_2^2)}{\partial p^2}\right)_{p^2=0} \tag{270}$$

$$= D\frac{\partial B_0(p^2, m_1^2, m_2^2)}{\partial p^2}\Big|_{p^2\to 0} + 2p_\mu\frac{\partial}{\partial p_\mu}\frac{\partial B_0(p^2, m_1^2, m_2^2)}{\partial p^2}\Big|_{p^2\to 0} \tag{271}$$

Since $\frac{\partial x^\mu}{\partial x^\nu} = \delta_\nu^\mu \Rightarrow \frac{\partial p_\mu}{\partial p_\mu} = D$. And rewriting the second term in Eq. (271) by chain rules:

$$\frac{\partial}{\partial p_\mu}\frac{\partial B_0}{\partial p^2} = \frac{\partial p^2}{\partial p_\mu}\frac{\partial}{\partial p^2}\frac{\partial B_0}{\partial p^2} = 2p^\mu\frac{\partial^2 B_0}{\partial(p^2)^2}\Big|_{p^2\to 0}, \tag{272}$$

we eventually get

$$\frac{\partial^2}{\partial p_\mu \partial p^\mu}B_0 = 2D\frac{\partial B_0}{\partial p^2}\Big|_{p^2\to 0} + \underbrace{4p^2\frac{\partial^2 B_0}{\partial(p^2)^2}\Big|_{p^2\to 0}}_{=0} \tag{273}$$

82

Hence by reverting this equation we get

$$\frac{\partial B_0}{\partial p^2}\Big|_{p^2 \to 0} = \frac{1}{2D}\frac{\partial^2}{\partial p^2}B_0\frac{1}{2D}\frac{\partial}{\partial p^\mu}\frac{\partial}{\partial p_\mu}\mathbf{I}_{1,1} \tag{274}$$

$$= \frac{1}{2D}\frac{\partial}{\partial p^\mu}(-2(q^\mu + p^\mu))\mathbf{I}_{1,2} \tag{275}$$

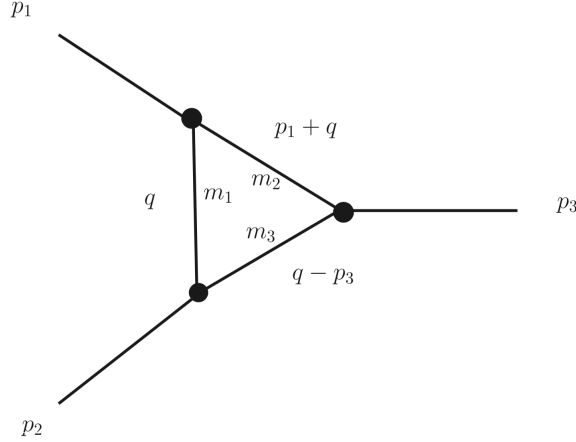$$= \frac{1}{2D}\Big(-2D\mathbf{I}_{1,2} + 8\mathbf{I}_{1,2} + 8m_2^2\mathbf{I}_{1,3}\Big)_{p^2 \to 0} \tag{276}$$

Figure 18: scalar one-loop of three-point function

$$C_0(p_1^2, p_2^2, p_3^2, m_1^2, m_2^2, m_3^2) = \frac{\mu^{4-D}}{i\pi^{D/2}r_\Gamma}\int d^D q \frac{1}{[q^2 - m_1^2][(q+p_1)^2 - m_2^2][(q-p_3)^2 - m_3^2]} \tag{277}$$

$$= \int d^D q \frac{1}{D_1 D_2 D_3} \equiv \mathbf{I}_{1,1,1} \tag{278}$$

and

$$r_\Gamma = \frac{\Gamma^2(1-\epsilon)\Gamma(1+\epsilon)}{\Gamma(1-2\epsilon)} = 1 + \mathcal{O}(\epsilon) \tag{279}$$

We are looking for solving the derivative of C_0 with constraints as

$$\frac{\partial}{\partial p_1^2}C_0(p1^2, 0, 0, m_1^2, m_1^2, m_2^2) \tag{280}$$

$$p_1^2 = s \quad p_2^2 = p_3^2 = 0 \quad m_1 = m_2. \tag{281}$$

Consequently one can also find the following relations

$$p_1 \cdot p_2 = -\frac{s}{2} \quad p_1 \cdot p_3 = -\frac{s}{2} \tag{282}$$

We can define variable p_3 as a function of two independent variables p_1 and p_2. Then by applying the chain rule

$$p_{1\mu} \frac{\partial C_0}{\partial p_{1\mu}} = p_{1\mu} \left(\frac{\partial C_0}{\partial p_1^2} \frac{\partial p_1^2}{\partial p_{1\mu}} + \frac{\partial C_0}{\partial p_3^2} \frac{\partial p_3^2}{\partial p_{1\mu}} \right) \tag{283}$$

$$= \frac{\partial C_0}{\partial p_1^2} 2s + p_{1\mu} \frac{\partial C_0}{\partial p_3^2} \frac{\partial (-p_1 - p_2)^2}{\partial p_{1\mu}} \tag{284}$$

$$= \frac{\partial C_0}{\partial p_1^2} 2s + p_{1\mu} \frac{\partial C_0}{\partial p_3^2} (2p_1^\mu + 2p_2^\mu) \tag{285}$$

$$= \frac{\partial C_0}{\partial p_1^2} 2s + s \frac{\partial C_0}{\partial p_3^2}, \tag{286}$$

where $p_1 \cdot p_2 = -\frac{s}{2}$ is applied.

We shall see that by applying chain rule this way, we can ensure the partial derivative $\frac{\partial C_0}{\partial p_1^2}$ having both p_2^2 and p_3^2 fixed, which is consistent with the constraints given by this problem.

Alternatively, one can write down another equation by dotting $p_{2\mu}$ in front of $\frac{\partial C_0}{\partial p_{1\mu}}$ instead of $p_{1\mu}$:

$$p_{2\mu} \frac{\partial C_0}{\partial p_{1\mu}} = p_{2\mu} \left(\frac{\partial C_0}{\partial p_1^2} \frac{\partial p_1^2}{\partial p_{1\mu}} + \frac{\partial C_0}{\partial p_3^2} \frac{\partial p_3^2}{\partial p_{1\mu}} \right) \tag{287}$$

$$= -\frac{\partial C_0}{\partial p_1^2} s + p_{2\mu} \frac{\partial C_0}{\partial p_3^2} \frac{\partial (-p_1 - p_2)^2}{\partial p_{1\mu}} \tag{288}$$

$$= -\frac{\partial C_0}{\partial p_1^2} s + p_{2\mu} \frac{\partial C_0}{\partial p_3^2} (2p_1^\mu + 2p_2^\mu) \tag{289}$$

$$= -\frac{\partial C_0}{\partial p_1^2} s - s \frac{\partial C_0}{\partial p_3^2}. \tag{290}$$

Then, combing (286),(290) together, we can perform a Guassian elimination of $\frac{\partial C_0}{\partial p_{1\mu}}$:

$$p_{1\mu} \frac{\partial C_0}{\partial p_{1\mu}} = \frac{\partial C_0}{\partial p_1^2} 2s + s \frac{\partial C_0}{\partial p_3^2} \tag{291}$$

$$p_{2\mu} \frac{\partial C_0}{\partial p_{1\mu}} = -\frac{\partial C_0}{\partial p_1^2} s - s \frac{\partial C_0}{\partial p_3^2}, \tag{292}$$

$$\tag{293}$$

and

$$\frac{\partial C_0}{\partial p_1^2} = \frac{1}{s}(p_{1\mu}\frac{\partial C_0}{\partial p_{1\mu}} + p_{2\mu}\frac{\partial C_0}{\partial p_{1\mu}}), \tag{294}$$

where

$$\frac{\partial C_0}{\partial p_1} = -2(p_1^\mu + p_2^\mu + q^\mu)\mathbf{I}_{1,1,2} - 2(p_1^\mu + q^\mu)\mathbf{I}_{1,2,1} \tag{295}$$

Hence by plugging (295) back into(294), we get

$$\frac{\partial C_0}{\partial p_1^2} = \frac{1}{s}(-(\mathbf{3}^- - \mathbf{1}^- + m_2^2 - m_1^2)(\mathbf{I}_{1,1,2} + \mathbf{I}_{1,2,1}) - s\mathbf{I}_{1,2,1}) \tag{296}$$

$$= \frac{1}{s}(-\mathbf{I}_{1,1,1} + \mathbf{I}_{0,1,2} - (m_2^2 - m_1^2)(\mathbf{I}_{1,1,2} + \mathbf{I}_{1,2,1}) - s\mathbf{I}_{1,2,0} + \mathbf{I}_{0,2,1}) \tag{297}$$

Then by further applying the IBP identities, one can reduce it down to a linear combination of A_0, B_0, and C_0 functions.

6.2.2 Derivative of two-loop self-energy MIs

With the help of chain rules, we obtain

$$\begin{aligned}
\frac{\partial}{\partial p^2}I(...;p^2 = 0) &= \frac{1}{2d}\frac{\partial^2}{\partial p_\mu \partial p^\mu}I(...;p^2)\Big|_{p^2=0} \\
&= \frac{2}{d}\Big[\Big(1 + a_2 + a_5 - \frac{d}{2}\Big)(a_2\mathbf{2}^+ + a_5\mathbf{5}^+) \\
&\quad + m_2^2 a_2(a_2 + 1)\mathbf{2}^{++} + m_5^2 a_5(a_5 + 1)\mathbf{5}^{++} \\
&\quad + a_2 a_5((m_2^2 - m_3^2 + m_5^2)\mathbf{2}^+\mathbf{5}^+ - \mathbf{2}^+\mathbf{3}^-\mathbf{5}^+)I\Big]_{p^2=0},
\end{aligned} \tag{298}$$

whereas for $p^2 \neq 0$, one obtains

$$\begin{aligned}
\frac{\partial}{\partial p^2}I(...;p^2 \neq 0) &= -\frac{1}{2p^2}p^\mu\frac{\partial}{\partial p^\mu}I(...;p^2) \\
&= -\frac{1}{2p^2}\Big[(a_2 + a_5) - a_2\mathbf{1}^-\mathbf{2}^+ - a_5\mathbf{4}^-\mathbf{5}^+ \\
&\quad + a_2(m_2^2 - m_1^2 + p^2)\mathbf{2}^+ + a_5(m_5^2 - m_4^2 + p^2)\mathbf{5}^+\Big]I,
\end{aligned} \tag{299}$$

where I is defined as the most generic two-loop self-energy master integral

$$\begin{aligned}
&I(a_1, a_2, ..., m_1, m_2, ..., ; p^2) \\
&\equiv \int \frac{d^d q_1 \, d^d q_2}{(q_1^2 - m_1^2)^{a_1}((q_1 + p)^2 - m_2^2)^{a_2}((q_2 - q_1)^2 - m_3^2)^{a_3}(q_2^2 - m_4^2)((q_2 + p)^2 - m_5^2)^{a_5}}
\end{aligned} \tag{300}$$

85

and the standard lowering/raising operators are defined as

$$\mathbf{4^-5^+}I = I(a_4 - 1, a_5 + 1). \tag{301}$$

Then one can apply IBP identities again to further reduce the raised/lowered MI integrals $I(...; p^2)$ down to the chosen MI basis such as Fig. 10.

Bibliography

[1] K. G. Chetyrkin and F. V. Tkachov. Integration by Parts: The Algorithm to Calculate beta Functions in 4 Loops. *Nucl. Phys. B*, 192:159–204, 1981.

[2] CEPC Study Group, J. Guimarã_es da Costa, Y. Gao, S. Jin, J. Qian, C. Tully, C. Young, L. Wang, M. Ruan, H. Zhu, Q. Ouyang et al. CEPC Conceptual Design Report: Volume 2 - Physics & Detector. 2018.

[3] A. Abada et al. FCC-ee: The Lepton Collider: Future Circular Collider Conceptual Design Report Volume 2. *Eur. Phys. J. ST*, 228(2):261–623, 2019.

[4] Keisuke Fujii et al. Tests of the Standard Model at the International Linear Collider. 8 2019.

[5] Graham W. Wilson. Updated Study of a Precision Measurement of the W Mass from a Threshold Scan Using Polarized e$^-$ and e$^+$ at ILC. In *International Workshop on Future Linear Colliders*, 3 2016.

[6] Zhenyu Zhao, Siqi Yang, Manqi Ruan, Minghui Liu, and Liang Han. Measurement of the effective weak mixing angle at the CEPC. 4 2022.

[7] M. Tanabashi et al. Review of Particle Physics. *Phys. Rev. D*, 98(3):030001, 2018.

[8] Lisong Chen and Ayres Freitas. Leading fermionic three-loop corrections to electroweak precision observables. *JHEP*, 07:210, 2020.

[9] Stefan Bauberger, Ayres Freitas, and Daniel Wiegand. TVID 2: Evaluation of planar-type three-loop self-energy integrals with arbitrary masses. *JHEP*, 01:024, 2020.

[10] H. Fritzsch, Murray Gell-Mann, and H. Leutwyler. Advantages of the Color Octet Gluon Picture. *Phys. Lett.*, 47B:365–368, 1973.

[11] D. J. Gross and Frank Wilczek. Asymptotically Free Gauge Theories I. *Phys. Rev.*, D8:3633–3652, 1973.

[12] D. J. Gross and Frank Wilczek. Asymptotically Free Gauge Theories II. *Phys. Rev.*, D9:980–993, 1974.

[13] H. David Politzer. Reliable Perturbative Results for Strong Interactions? *Phys. Rev. Lett.*, 30:1346–1349, 1973.

[14] S. L. Glashow. Partial Symmetries of Weak Interactions. *Nucl. Phys.*, 22:579–588, 1961.

[15] Steven Weinberg. A Model of Leptons. *Phys. Rev. Lett.*, 19:1264–1266, 1967.

[16] Abdus Salam. Weak and Electromagnetic Interactions. In N. Svartholm, editor, *Elementary Particle Theory, Almqvist and Wiksell, Stockholm*, volume C680519, pages 367–377, 1968.

[17] F. Englert and R. Brout. Broken Symmetry and the Mass of Gauge Vector Mesons. *Phys. Rev. Lett.*, 13:321–323, 1964.

[18] Peter W. Higgs. Broken Symmetries and the Masses of Gauge Bosons. *Phys. Rev. Lett.*, 13:508–509, 1964.

[19] Peter W. Higgs. Broken symmetries, massless particles and gauge fields. *Phys. Lett.*, 12:132–133, 1964.

[20] G. S. Guralnik, C. R. Hagen, and T. W. B. Kibble. Global Conservation Laws and Massless Particles. *Phys. Rev. Lett.*, 13:585–587, 1964.

[21] Peter W. Higgs. Spontaneous Symmetry Breakdown without Massless Bosons. *Phys. Rev.*, 145:1156–1163, 1966.

[22] Nicola Cabibbo. Unitary Symmetry and Leptonic Decays. *Phys. Rev. Lett.*, 10:531–533, 1963.

[23] Makoto Kobayashi and Toshihide Maskawa. CP Violation in the Renormalizable Theory of Weak Interaction. *Prog. Theor. Phys.*, 49:652–657, 1973.

[24] Gerard 't Hooft. Renormalization of Massless Yang-Mills Fields. *Nucl. Phys.*, B33:173–199, 1971.

[25] Gerard 't Hooft. Renormalizable Lagrangians for Massive Yang-Mills Fields. *Nucl. Phys.*, B35:167–188, 1971.

[26] Gerard 't Hooft and M. J. G. Veltman. Regularization and Renormalization of Gauge Fields. *Nucl. Phys. B*, 44:189–213, 1972.

[27] B. W. Lee and Jean Zinn-Justin. Spontaneously Broken Gauge Symmetries Part 1: Preliminaries. *Phys. Rev.*, D5:3121–3137, 1972.

[28] B. W. Lee and Jean Zinn-Justin. Spontaneously Broken Gauge Symmetries Part 4: General Gauge Formulation. *Phys. Rev.*, D7:1049–1056, 1973.

[29] B. W. Lee. Transformation properties of proper vertices in gauge theories. *Phys. Lett.*, 46B:214–216, 1973.

[30] Benjamin W. Lee. Renormalization of gauge theories: unbroken and broken. *Phys. Rev.*, D9:933–946, 1974.

[31] B. W. Lee and Jean Zinn-Justin. Spontaneously Broken Gauge Symmetries Part 2: Perturbation Theory and Renormalization. *Phys. Rev.*, D5:3137–3155, 1972. [Erratum: Phys. Rev. D8 (1973) 4654].

[32] L. D. Faddeev and V. N. Popov. Feynman Diagrams for the Yang-Mills Field. *Phys. Lett. B*, 25:29–30, 1967.

[33] C. Becchi, A. Rouet, and R. Stora. Renormalization of the Abelian Higgs-Kibble Model. *Commun. Math. Phys.*, 42:127–162, 1975.

[34] Jihn E. Kim, Paul Langacker, M. Levine, and H. H. Williams. A Theoretical and Experimental Review of the Weak Neutral Current: A Determination of Its Structure and Limits on Deviations from the Minimal SU(2)-L x U(1) Electroweak Theory. *Rev. Mod. Phys.*, 53:211, 1981.

[35] Ugo Amaldi, Albrecht Bohm, L. S. Durkin, Paul Langacker, Alfred K. Mann, William J. Marciano, Alberto Sirlin, and H. H. Williams. A Comprehensive Analysis of Data Pertaining to the Weak Neutral Current and the Intermediate Vector Boson Masses. *Phys. Rev. D*, 36:1385, 1987.

[36] G. Costa, John R. Ellis, Gian Luigi Fogli, Dimitri V. Nanopoulos, and F. Zwirner. Neutral Currents Within and Beyond the Standard Model. *Nucl. Phys. B*, 297:244–286, 1988.

[37] G. Arnison et al. Experimental Observation of Isolated Large Transverse Energy Electrons with Associated Missing Energy at $\sqrt{s} = 540$ GeV. *Phys. Lett. B*, 122:103–116, 1983.

[38] G. Arnison et al. Experimental Observation of Lepton Pairs of Invariant Mass Around 95-GeV/c**2 at the CERN SPS Collider. *Phys. Lett. B*, 126:398–410, 1983.

[39] P. Bagnaia et al. Evidence for $Z^0 \to e^+ e^-$ at the CERN $\bar{p}p$ Collider. *Phys. Lett. B*, 129:130–140, 1983.

[40] M. Banner et al. Observation of Single Isolated Electrons of High Transverse Momentum in Events with Missing Transverse Energy at the CERN anti-p p Collider. *Phys. Lett. B*, 122:476–485, 1983.

[41] S. Schael et al. Precision electroweak measurements on the Z resonance. *Phys. Rept.*, 427:257–454, 2006.

[42] D. C. Kennedy and Paul Langacker. Precision electroweak experiments and heavy physics: A Global analysis. *Phys. Rev. Lett.*, 65:2967–2970, 1990. [Erratum: Phys.Rev.Lett. 66, 395 (1991)].

[43] Paul Langacker and Ming-xing Luo. Implications of precision electroweak experiments for M_t, ρ_0, $\sin^2 \theta_W$ and grand unification. *Phys. Rev. D*, 44:817–822, 1991.

[44] Jens Erler and Paul Langacker. Implications of high precision experiments and the CDF top quark candidates. *Phys. Rev. D*, 52:441–450, 1995.

[45] F. Abe et al. Observation of top quark production in $\bar{p}p$ collisions. *Phys. Rev. Lett.*, 74:2626–2631, 1995.

[46] S. Abachi et al. Observation of the top quark. *Phys. Rev. Lett.*, 74:2632–2637, 1995.

[47] S. Schael et al. Electroweak Measurements in Electron-Positron Collisions at W-Boson-Pair Energies at LEP. *Phys. Rept.*, 532:119–244, 2013.

[48] Jens Erler. The Mass of the Higgs Boson in the Standard Electroweak Model. *Phys. Rev. D*, 81:051301, 2010.

[49] M. Baak, M. Goebel, J. Haller, A. Hoecker, D. Ludwig, K. Moenig, M. Schott, and J. Stelzer. Updated Status of the Global Electroweak Fit and Constraints on New Physics. *Eur. Phys. J. C*, 72:2003, 2012.

[50] Jens Erler. Weighing in on the Higgs. 1 2012.

[51] Georges Aad et al. Observation of a new particle in the search for the Standard Model Higgs boson with the ATLAS detector at the LHC. *Phys. Lett. B*, 716:1–29, 2012.

[52] Serguei Chatrchyan et al. Observation of a New Boson at a Mass of 125 GeV with the CMS Experiment at the LHC. *Phys. Lett. B*, 716:30–61, 2012.

[53] Ayres Freitas. Precision Tests of the Standard Model. *PoS*, TASI2020:005, 2021.

[54] Timo van Ritbergen and Robin G. Stuart. On the precise determination of the Fermi coupling constant from the muon lifetime. *Nucl. Phys. B*, 564:343–390, 2000.

[55] M. Steinhauser and T. Seidensticker. Second order corrections to the muon lifetime and the semileptonic B decay. *Phys. Lett. B*, 467:271–278, 1999.

[56] Alexey Pak and Andrzej Czarnecki. Mass effects in muon and semileptonic b —> c decays. *Phys. Rev. Lett.*, 100:241807, 2008.

[57] Victor Mukhamedovich Abazov et al. Measurement of the W Boson Mass with the D0 Detector. *Phys. Rev. Lett.*, 108:151804, 2012.

[58] T. Aaltonen et al. Precise measurement of the W-boson mass with the CDF II detector. *Phys. Rev. Lett.*, 108:151803, 2012.

[59] Morad Aaboud et al. Measurement of the W-boson mass in pp collisions at $\sqrt{s} = 7$ TeV with the ATLAS detector. *Eur. Phys. J. C*, 78(2):110, 2018. [Erratum: Eur.Phys.J.C 78, 898 (2018)].

[60] Roel Aaij et al. Measurement of the W boson mass. *JHEP*, 01:036, 2022.

[61] T. Aaltonen et al. High-precision measurement of the W boson mass with the CDF II detector. *Science*, 376(6589):170–176, 2022.

[62] Jens Erler and Matthias Schott. Electroweak Precision Tests of the Standard Model after the Discovery of the Higgs Boson. *Prog. Part. Nucl. Phys.*, 106:68–119, 2019.

[63] W. J. Marciano and A. Sirlin. Radiative corrections to neutrino induced neutral current phenomena in the $SU(2)_L$ x U(1) theory. *Phys. Rev.*, D22:2695, 1980. Erratum: Phys. Rev. D31 (1985) 213.

[64] A. A. Akhundov, D. Yu. Bardin, and T. Riemann. Electroweak One Loop Corrections to the Decay of the Neutral Vector Boson. *Nucl. Phys. B*, 276:1–13, 1986.

[65] M. Awramik, M. Czakon, A. Freitas, and G. Weiglein. Precise prediction for the W boson mass in the standard model. *Phys. Rev. D*, 69:053006, 2004.

[66] W. Hollik, U. Meier, and S. Uccirati. The Effective electroweak mixing angle sin**2 theta(eff) with two-loop fermionic contributions. *Nucl. Phys. B*, 731:213–224, 2005.

[67] M. Awramik, M. Czakon, and A. Freitas. Bosonic corrections to the effective weak mixing angle at O(alpha**2). *Phys. Lett. B*, 642:563–566, 2006.

[68] W. Hollik, U. Meier, and S. Uccirati. The effective electroweak mixing angle $\sin^2\theta^{\text{eff}}$ with two-loop bosonic contributions. *Nucl. Phys.*, B765:154–165, 2007.

[69] M. Awramik, M. Czakon, A. Freitas, and B.A. Kniehl. Two-loop electroweak fermionic corrections to $\sin^2\theta_{\text{eff}}^{\text{b}\bar{\text{b}}}$. *Nucl. Phys.*, B813:174–187, 2009.

[70] Ievgen Dubovyk, Ayres Freitas, Janusz Gluza, Tord Riemann, and Johann Usovitsch. The two-loop electroweak bosonic corrections to $\sin^2\theta_{\text{eff}}^{\text{b}}$. *Phys. Lett.*, B762:184–189, 2016.

[71] A. Djouadi. $O(\alpha\alpha_s)$ vacuum polarization functions of the standard model gauge bosons. *Nuovo Cim.*, A100:357, 1988.

[72] Ayres Freitas. Two-loop fermionic electroweak corrections to the Z-boson width and production rate. *Phys. Lett. B*, 730:50–52, 2014.

[73] Ayres Freitas. Higher-order electroweak corrections to the partial widths and branching ratios of the Z boson. *JHEP*, 04:070, 2014.

[74] Ievgen Dubovyk, Ayres Freitas, Janusz Gluza, Tord Riemann, and Johann Usovitsch. Complete electroweak two-loop corrections to Z boson production and decay. *Phys. Lett.*, B783:86–94, 2018.

[75] Ievgen Dubovyk, Ayres Freitas, Janusz Gluza, Tord Riemann, and Johann Usovitsch. Electroweak pseudo-observables and Z-boson form factors at two-loop accuracy. *JHEP*, 08:113, 2019.

[76] A. Djouadi and C. Verzegnassi. Virtual very heavy top effects in LEP/SLC precision measurements. *Phys. Lett.*, B195:265–271, 1987.

[77] Bernd A. Kniehl. Two loop corrections to the vacuum polarizations in perturbative QCD. *Nucl. Phys.*, B347:86–104, 1990.

[78] Bernd A. Kniehl and Alberto Sirlin. Dispersion relations for vacuum polarization functions in electroweak physics. *Nucl. Phys.*, B371:141–148, 1992.

[79] A. Djouadi and P. Gambino. Electroweak gauge boson selfenergies: Complete QCD corrections. *Phys. Rev.*, D49:3499–3511, 1994. Erratum: Phys. Rev. D53 (1996) 4111.

[80] Andrzej Czarnecki and Johann H. Kuhn. Nonfactorizable QCD and electroweak corrections to the hadronic Z boson decay rate. *Phys. Rev. Lett.*, 77:3955–3958, 1996.

[81] R. Harlander, T. Seidensticker, and M. Steinhauser. Complete corrections of order $\alpha\alpha_s$ to the decay of the Z boson into bottom quarks. *Phys. Lett.*, B426:125–132, 1998.

[82] J. Fleischer, O. Tarasov, F. Jegerlehner, and P. Raczka. Two loop $O(\alpha_s G_\mu m_t^2)$ corrections to the partial decay width of the Z^0 into $b\bar{b}$ final states in the large top mass limit. *Phys. Lett.*, B293:437–444, 1992.

[83] Gerhard Buchalla and Andrzej J. Buras. QCD corrections to the $\bar{s}dZ$ vertex for arbitrary top quark mass. *Nucl. Phys.*, B398:285–300, 1993.

[84] Giuseppe Degrassi. Current algebra approach to heavy top effects in $Z \to b + \bar{b}$. *Nucl. Phys.*, B407:271–289, 1993.

[85] K. Chetyrkin, A. Kwiatkowski, and M. Steinhauser. Leading top mass corrections of order $O(\alpha\alpha_s m_t^2/m_W^2)$ to partial decay rate $\Gamma(Z \to b\bar{b})$. *Mod. Phys. Lett.*, A8:2785–2792, 1993.

[86] L. Avdeev, J. Fleischer, S. Mikhailov, and O. Tarasov. $0(\alpha\alpha_s^2)$ correction to the electroweak ρ parameter. *Phys. Lett.*, B336:560–566, 1994. Erratum: Phys. Lett. B349 (1995) 597.

[87] K.G. Chetyrkin, Johann H. Kühn, and M. Steinhauser. Corrections of order $O(G_F M_t^2 \alpha_s^2)$ to the ρ parameter. *Phys. Lett.*, B351:331–338, doi:10.1016/0370–2693(95)00380–4, 1995.

[88] J. J. van der Bij, K. G. Chetyrkin, M. Faisst, G. Jikia, and T. Seidensticker. Three loop leading top mass contributions to the ρ parameter. *Phys. Lett.*, B498:156–162, 2001.

[89] M. Faisst, Johann H. Kühn, T. Seidensticker, and O. Veretin. Three loop top quark contributions to the ρ parameter. *Nucl. Phys.*, B665:649–662, 2003.

[90] Y. Schröder and M. Steinhauser. Four-loop singlet contribution to the ρ parameter. *Phys. Lett.*, B622:124–130, 2005.

[91] K. G. Chetyrkin, M. Faisst, Johann H. Kühn, P. Maierhöfer, and Christian Sturm. Four-loop QCD corrections to the ρ parameter. *Phys. Rev. Lett.*, 97:102003, 2006.

[92] R. Boughezal and M. Czakon. Single scale tadpoles and $O(G_F m_t^2 \alpha_s^3)$ corrections to the ρ parameter. *Nucl. Phys.*, B755:221–238, 2006.

[93] A. Abada et al. FCC-ee: The Lepton Collider: Future Circular Collider Conceptual Design Report Volume 2. *Eur. Phys. J. ST*, 228(2):261–623, 2019.

[94] Howard Baer, Tim Barklow, Keisuke Fujii, Yuanning Gao, Andre Hoang, Shinya Kanemura, Jenny List, Heather E. Logan, Andrei Nomerotski, Maxim Perelstein, et al. The International Linear Collider Technical Design Report - Volume 2: Physics, . 2013.

[95] Philip Bambade et al. The International Linear Collider: A Global Project, . 3 2019.

[96] Physics and Detectors at CLIC: CLIC Conceptual Design Report. 2 2012.

[97] T.K. Charles et al. The Compact Linear Collider (CLIC) - 2018 Summary Report. 2/2018, 12 2018.

[98] Ansgar Denner and Stefan Dittmaier. Electroweak Radiative Corrections for Collider Physics. *Phys. Rept.*, 864:1–163, 2020.

[99] M. Bohm, H. Spiesberger, and W. Hollik. On the One Loop Renormalization of the Electroweak Standard Model and Its Application to Leptonic Processes. *Fortsch. Phys.*, 34:687–751, 1986.

[100] A. Sirlin. Radiative Corrections in the SU(2)-L x U(1) Theory: A Simple Renormalization Framework. *Phys. Rev. D*, 22:971–981, 1980.

[101] V. A. Smirnov. *Feynman integral calculus*. 2006.

[102] Ayres Freitas. Numerical multi-loop integrals and applications. *Prog. Part. Nucl. Phys.*, 90:201–240, 2016.

[103] A. V. Smirnov and A. V. Petukhov. The Number of Master Integrals is Finite. *Lett. Math. Phys.*, 97:37–44, 2011.

[104] T. Gehrmann and E. Remiddi. Differential equations for two loop four point functions. *Nucl. Phys. B*, 580:485–518, 2000.

[105] S. G. Gorishnii, S. A. Larin, L. R. Surguladze, and F. V. Tkachov. Mincer: Program for Multiloop Calculations in Quantum Field Theory for the Schoonschip System. *Comput. Phys. Commun.*, 55:381–408, 1989.

[106] A. V. Smirnov. Algorithm FIRE – Feynman Integral REduction. *JHEP*, 10:107, 2008.

[107] C. Studerus. Reduze-Feynman Integral Reduction in C++. *Comput. Phys. Commun.*, 181:1293–1300, 2010.

[108] Roman N. Lee. LiteRed 1.4: a powerful tool for reduction of multiloop integrals. *J. Phys. Conf. Ser.*, 523:012059, 2014.

[109] Charalampos Anastasiou and Achilleas Lazopoulos. Automatic integral reduction for higher order perturbative calculations. *JHEP*, 07:046, 2004.

[110] Gerard 't Hooft and M. J. G. Veltman. Scalar One Loop Integrals. *Nucl. Phys. B*, 153:365–401, 1979.

[111] Richard J. Gonsalves. DIMENSIONALLY REGULARIZED TWO LOOP ON-SHELL QUARK FORM-FACTOR. *Phys. Rev. D*, 28:1542, 1983.

[112] G. Kramer and B. Lampe. Integrals for Two Loop Calculations in Massless QCD. *J. Math. Phys.*, 28:945, 1987.

[113] W. L. van Neerven. Dimensional Regularization of Mass and Infrared Singularities in Two Loop On-shell Vertex Functions. *Nucl. Phys. B*, 268:453–488, 1986.

[114] M. Beneke, A. Signer, and Vladimir A. Smirnov. Two loop correction to the leptonic decay of quarkonium. *Phys. Rev. Lett.*, 80:2535–2538, 1998.

[115] Andrzej Czarnecki and Kirill Melnikov. Expansion of bound state energies in powers of m / M. *Phys. Rev. Lett.*, 87:013001, 2001.

[116] K. G. Chetyrkin and M. Steinhauser. The Relation between the MS-bar and the on-shell quark mass at order alpha(s)**3. *Nucl. Phys. B*, 573:617–651, 2000.

[117] A. Ghinculov and J. J. van der Bij. Massive two loop diagrams: The Higgs propagator. *Nucl. Phys. B*, 436:30–48, 1995.

[118] Adrian Ghinculov. Two loop heavy Higgs correction to Higgs decay into vector bosons. *Nucl. Phys. B*, 455:21–38, 1995.

[119] Adrian Ghinculov and York-Peng Yao. Exact nonfactorizable O(alpha(s)g**2) two loop contribution to Z —> b anti-b. *Mod. Phys. Lett. A*, 15:1967–1976, 2000.

[120] Adrian Ghinculov and York-Peng Yao. Exact O(g**2 alpha(s)) top decay width from general massive two loop integrals. *Mod. Phys. Lett. A*, 15:925–930, 2000.

[121] A. Ghinculov, T. Hurth, G. Isidori, and Y. P. Yao. The Rare decay $B \to X_s l^+ l^-$ to NNLL precision for arbitrary dilepton invariant mass. *Nucl. Phys. B*, 685:351–392, 2004.

[122] M. Awramik, M. Czakon, and A. Freitas. Electroweak two-loop corrections to the effective weak mixing angle. *JHEP*, 11:048, 2006.

[123] A. Freitas, W. Hollik, W. Walter, and G. Weiglein. Complete fermionic two loop results for the M(W) - M(Z) interdependence. *Phys. Lett. B*, 495:338–346, 2000. [Erratum: Phys.Lett.B 570, 265 (2003)].

[124] M. Awramik and M. Czakon. Complete two loop bosonic contributions to the muon lifetime in the standard model. *Phys. Rev. Lett.*, 89:241801, 2002.

[125] M. Awramik and M. Czakon. Complete two loop electroweak contributions to the muon lifetime in the standard model. *Phys. Lett. B*, 568:48–54, 2003.

[126] Ayres Freitas, W. Hollik, W. Walter, and Georg Weiglein. Electroweak two loop corrections to the $M_W - M_Z$ mass correlation in the standard model. *Nucl. Phys. B*, 632:189–218, 2002. [Erratum: Nucl.Phys.B 666, 305–307 (2003)].

[127] M. Awramik, M. Czakon, A. Freitas, and G. Weiglein. Complete two-loop electroweak fermionic corrections to $\sin^2 \theta_{\text{eff}}^{\text{lept}}$ and indirect determination of the Higgs boson mass. *Phys. Rev. Lett.*, 93:201805, 2004.

[128] Stefano Actis, Michal Czakon, Janusz Gluza, and Tord Riemann. Virtual hadronic and leptonic contributions to Bhabha scattering. *Phys. Rev. Lett.*, 100:131602, 2008.

[129] Stefano Actis, Michal Czakon, Janusz Gluza, and Tord Riemann. Virtual Hadronic and Heavy-Fermion O(alpha**2) Corrections to Bhabha Scattering. *Phys. Rev. D*, 78:085019, 2008.

[130] Qian Song and Ayres Freitas. On the evaluation of two-loop electroweak box diagrams for $e^+ e^- \to HZ$ production. *JHEP*, 04:179, 2021.

[131] S. Bauberger, Frits A. Berends, M. Bohm, and M. Buza. Analytical and numerical methods for massive two loop selfenergy diagrams. *Nucl. Phys. B*, 434:383–407, 1995.

[132] S. Bauberger and M. Bohm. Simple one-dimensional integral representations for two loop selfenergies: The Master diagram. *Nucl. Phys. B*, 445:25–48, 1995.

[133] Stefan Bauberger and Ayres Freitas. TVID: Three-loop Vacuum Integrals from Dispersion relations. 2 2017.

[134] Paolo Gambino and Pietro Antonio Grassi. The Nielsen identities of the SM and the definition of mass. *Phys. Rev. D*, 62:076002, 2000.

[135] Robin G. Stuart. General renormalization of the gauge invariant perturbation expansion near the Z0 resonance. *Phys. Lett. B*, 272:353–358, 1991.

[136] Scott Willenbrock. Mass and width of an unstable particle. 3 2022.

[137] Arno R. Bohm and Yoshihiro Sato. Relativistic resonances: Their masses, widths, lifetimes, superposition, and causal evolution. *Phys. Rev. D*, 71:085018, 2005.

[138] Yong Zhou. Gauge dependence of on-shell and pole mass renormalization prescriptions. *Commun. Theor. Phys.*, 49:1249–1260, 2008.

[139] Yong Zhou. Gauge dependence of fermion mass renormalization schemes. 10 2005.

[140] Yong Zhou. A New wave-function renormalization prescription for unstable particle. 10 2005.

[141] S. Willenbrock and G. Valencia. On the definition of the Z boson mass. *Phys. Lett. B*, 259:373–376, 1991.

[142] A. Sirlin. Theoretical considerations concerning the Z0 mass. *Phys. Rev. Lett.*, 67:2127–2130, 1991.

[143] Robin G. Stuart. Gauge invariance, analyticity and physical observables at the Z0 resonance. *Phys. Lett. B*, 262:113–119, 1991.

[144] Helene G. J. Veltman. Mass and width of unstable gauge bosons. *Z. Phys. C*, 62:35–52, 1994.

[145] Andre Aeppli, Geert Jan van Oldenborgh, and Daniel Wyler. Unstable particles in one loop calculations. *Nucl. Phys. B*, 428:126–146, 1994.

[146] Doreen Wackeroth and Wolfgang Hollik. Electroweak radiative corrections to resonant charged gauge boson production. *Phys. Rev. D*, 55:6788–6818, 1997.

[147] Stefan Dittmaier and Michael Krämer. Electroweak radiative corrections to W boson production at hadron colliders. *Phys. Rev. D*, 65:073007, 2002.

[148] Reports of the working group on precision calculations for the Z resonance. In *Workshop Group on Precision Calculations for the Z Resonance (2nd meeting held Mar 31, 3rd meeting held Jun 13)*, CERN Yellow Reports: Monographs, 3 1995.

[149] R. Frederix, S. Frixione, V. Hirschi, D. Pagani, H. S. Shao, and M. Zaro. The automation of next-to-leading order electroweak calculations. *JHEP*, 07:185, 2018. [Erratum: JHEP 11, 085 (2021)].

[150] Mudit Rai, Lisong Chen, and Daniel Boyanovsky. Infrared dressing in real time: emergence of anomalous dimensions. *Phys. Rev. D*, 104:085021, 2021.

[151] Daniel Boyanovsky, Mudit Rai, and Lisong Chen. Ultralight dark matter or dark radiation cosmologically produced from infrared dressing. *Phys. Rev. D*, 104(12):123552, 2021.

[152] Daniel Boyanovsky. Threshold and infrared singularities: Time evolution, asymptotic state, and entanglement entropy. *Phys. Rev. D*, 105(5):056012, 2022.

[153] Wim Beenakker, Geert Jan van Oldenborgh, Ansgar Denner, Stefan Dittmaier, Jiri Hoogland, Ronald Kleiss, Costas G. Papadopoulos, and Giampiero Passarino. The Fermion loop scheme for finite width effects in e^+e^- annihilation into four fermions. *Nucl. Phys. B*, 500:255–298, 1997.

[154] Giampiero Passarino. Single W production and fermion loop scheme: Numerical results. *Nucl. Phys. B*, 578:3–26, 2000.

[155] Ernestos N. Argyres, Wim Beenakker, Geert Jan van Oldenborgh, Ansgar Denner, Stefan Dittmaier, Jiri Hoogland, Ronald Kleiss, Costas G. Papadopoulos, and Giampiero Passarino. Stable calculations for unstable particles: Restoring gauge invariance. *Phys. Lett. B*, 358:339–346, 1995.

[156] M. Beneke, A. P. Chapovsky, A. Signer, and G. Zanderighi. Effective theory approach to unstable particle production. *Phys. Rev. Lett.*, 93:011602, 2004.

[157] M. Beneke, A. P. Chapovsky, A. Signer, and G. Zanderighi. Effective theory calculation of resonant high-energy scattering. *Nucl. Phys. B*, 686:205–247, 2004.

[158] Andre H. Hoang and Christoph J. Reisser. Electroweak absorptive parts in NRQCD matching conditions. *Phys. Rev. D*, 71:074022, 2005.

[159] Martin Beneke, Pietro Falgari, Christian Schwinn, Adrian Signer, and Giulia Zanderighi. Four-fermion production near the W pair production threshold. *Nucl. Phys. B*, 792:89–135, 2008.

[160] S. Actis, M. Beneke, P. Falgari, and C. Schwinn. Dominant NNLO corrections to four-fermion production near the W-pair production threshold. *Nucl. Phys. B*, 807:1–32, 2009.

[161] P. Gambino, P. A. Grassi, and F. Madricardo. Fermion mixing renormalization and gauge invariance. *Phys. Lett. B*, 454:98–104, 1999.

[162] M. Steinhauser. Leptonic contribution to the effective electromagnetic coupling constant up to three loops. *Phys. Lett. B*, 429:158–161, 1998.

[163] Christian Sturm. Leptonic contributions to the effective electromagnetic coupling at four-loop order in QED. *Nucl. Phys. B*, 874:698–719, 2013.

[164] A. Blondel, J. Gluza, S. Jadach, P. Janot, and T. Riemann, editors. *Theory for the FCC-ee: Report on the 11th FCC-ee Workshop Theory and Experiments*, volume 3/2020 of *CERN Yellow Reports: Monographs*, Geneva, 5 2019. CERN.

[165] M. Davier, A. Hoecker, B. Malaescu, and Z. Zhang. A new evaluation of the hadronic vacuum polarisation contributions to the muon anomalous magnetic moment and to $\boldsymbol{\alpha(m_Z^2)}$. *Eur. Phys. J. C*, 80(3):241, 2020. [Erratum: Eur.Phys.J.C 80, 410 (2020)].

[166] Alexander Keshavarzi, Daisuke Nomura, and Thomas Teubner. $g-2$ of charged leptons, $\alpha(M_Z^2)$, and the hyperfine splitting of muonium. *Phys. Rev. D*, 101(1):014029, 2020.

[167] Florian Burger, Karl Jansen, Marcus Petschlies, and Grit Pientka. Leading hadronic contributions to the running of the electroweak coupling constants from lattice QCD. *JHEP*, 11:215, 2015.

[168] Marco Cè, Teseo San José, Antoine Gérardin, Harvey B. Meyer, Kohtaroh Miura, Konstantin Ottnad, Andreas Risch, Jonas Wilhelm, and Hartmut Wittig. The hadronic contribution to the running of the electromagnetic coupling and the electroweak mixing angle. *PoS*, LATTICE2019:010, 2019.

[169] Marco Cè, Antoine Gérardin, Georg von Hippel, Harvey B. Meyer, Kohtaroh Miura, Konstantin Ottnad, Andreas Risch, Teseo San José, Jonas Wilhelm, and Hartmut Wittig. The hadronic running of the electromagnetic coupling and the electroweak mixing angle from lattice QCD. 3 2022.

[170] G. Abbiendi et al. Measurement of the running of the QED coupling in small-angle Bhabha scattering at LEP. *Eur. Phys. J. C*, 45:1–21, 2006.

[171] P. Achard et al. Measurement of the running of the electromagnetic coupling at large momentum-transfer at LEP. *Phys. Lett. B*, 623:26–36, 2005.

[172] A. Anastasi et al. Measurement of the running of the fine structure constant below 1 GeV with the KLOE Detector. *Phys. Lett. B*, 767:485–492, 2017.

[173] R. Tarrach. The Pole Mass in Perturbative QCD. *Nucl. Phys. B*, 183:384–396, 1981.

[174] N. Gray, David J. Broadhurst, W. Grafe, and K. Schilcher. Three Loop Relation of Quark (Modified) Ms and Pole Masses. *Z. Phys. C*, 48:673–680, 1990.

[175] Matteo Fael, Fabian Lange, Kay Schönwald, and Matthias Steinhauser. A semi-analytic method to compute Feynman integrals applied to four-loop corrections to the $\overline{\text{MS}}$-pole quark mass relation. *JHEP*, 09:152, 2021.

[176] Andy Buckley et al. General-purpose event generators for LHC physics. *Phys. Rept.*, 504:145–233, 2011.

[177] V. Tishchenko et al. Detailed Report of the MuLan Measurement of the Positive Muon Lifetime and Determination of the Fermi Constant. *Phys. Rev. D*, 87(5):052003, 2013.

[178] Thomas Hahn. Generating Feynman diagrams and amplitudes with FeynArts 3. *Comput. Phys. Commun.*, 140:418–431, 2001.

[179] Vladyslav Shtabovenko, Rolf Mertig, and Frederik Orellana. New Developments in FeynCalc 9.0. *Comput. Phys. Commun.*, 207:432–444, 2016.

[180] A. V. Smirnov and F. S. Chuharev. FIRE6: Feynman Integral REduction with Modular Arithmetic. *Comput. Phys. Commun.*, 247:106877, 2020.

[181] G. Weiglein, R. Scharf, and M. Bohm. Reduction of general two loop selfenergies to standard scalar integrals. *Nucl. Phys. B*, 416:606–644, 1994.

[182] U. Nierste, D. Muller, and M. Bohm. Two loop relevant parts of D-dimensional massive scalar one loop integrals. *Z. Phys. C*, 57:605–614, 1993.

[183] A. Freitas et al. Theoretical uncertainties for electroweak and Higgs-boson precision measurements at FCC-ee. 6 2019.

[184] A. Blondel et al. Standard model theory for the FCC-ee Tera-Z stage. In *Mini Workshop on Precision EW and QCD Calculations for the FCC Studies : Methods and Techniques*, volume 3/2019 of *CERN Yellow Reports: Monographs*, Geneva, 9 2018. CERN.

[185] D. Yu. Bardin, Mikhail S. Bilenky, T. Riemann, M. Sachwitz, and H. Vogt. Dizet: A Program Package for the Calculation of Electroweak One Loop Corrections for the Process e+ e- —> f+ f- Around the Z0 Peak. *Comput. Phys. Commun.*, 59:303–312, 1990.

[186] Guido Montagna, Oreste Nicrosini, Fulvio Piccinini, and Giampiero Passarino. TOPAZ0 4.0: A New version of a computer program for evaluation of deconvoluted and realistic observables at LEP-1 and LEP-2. *Comput. Phys. Commun.*, 117:278–289, 1999.

[187] Dmitri Yu. Bardin, P. Christova, M. Jack, L. Kalinovskaya, A. Olchevski, S. Riemann, and T. Riemann. ZFITTER v.6.21: A Semianalytical program for fermion pair production in e^+e^- annihilation. *Comput. Phys. Commun.*, 133:229–395, 2001.

[188] A. B. Arbuzov, M. Awramik, M. Czakon, A. Freitas, M. W. Grunewald, Klaus Monig, S. Riemann, and T. Riemann. ZFITTER: A Semi-analytical program for fermion pair production in e+ e- annihilation, from version 6.21 to version 6.42. *Comput. Phys. Commun.*, 174:728–758, 2006.

[189] Dmitri Yu. Bardin, L. Kalinovskaya, and G. Nanava. An Electroweak library for the calculation of EWRC to e+ e- —> f anti-f within the topfit project. 12 2000.

[190] U. Baur, O. Brein, W. Hollik, C. Schappacher, and D. Wackeroth. Electroweak radiative corrections to neutral current Drell-Yan processes at hadron colliders. *Phys. Rev. D*, 65:033007, 2002.

[191] Stefan Dittmaier, Timo Schmidt, and Jan Schwarz. Mixed NNLO QCD×electroweak corrections of $\mathcal{O}(N_f\alpha_s\alpha)$ to single-W/Z production at the LHC. *JHEP*, 12:201, 2020.

[192] J. Gluza, A. Lorca, and T. Riemann. Automated use of DIANA for two-fermion production at colliders. *Nucl. Instrum. Meth. A*, 534:289–292, 2004.

[193] C. M. Carloni Calame, G. Montagna, O. Nicrosini, and A. Vicini. Precision electroweak calculation of the charged current Drell-Yan process. *JHEP*, 12:016, 2006.

[194] C. M. Carloni Calame, G. Montagna, O. Nicrosini, and A. Vicini. Precision electroweak calculation of the production of a high transverse-momentum lepton pair at hadron colliders. *JHEP*, 10:109, 2007.

[195] A. Arbuzov, D. Bardin, S. Bondarenko, P. Christova, L. Kalinovskaya, G. Nanava, and R. Sadykov. One-loop corrections to the Drell–Yan process in SANC. (II). The Neutral current case. *Eur. Phys. J. C*, 54:451–460, 2008.

[196] D. Yu. Bardin et al. Precision Description of Processes at Colliders in the SANC System. *Phys. Part. Nucl.*, 50(4):395–432, 2019.

[197] W. Płaczek, S. Jadach, and M. W. Krasny. Drell-Yan processes with WINHAC. *Acta Phys. Polon. B*, 44(11):2171–2178, 2013.

[198] Luca Barze, Guido Montagna, Paolo Nason, Oreste Nicrosini, Fulvio Piccinini, and Alessandro Vicini. Neutral current Drell-Yan with combined QCD and electroweak corrections in the POWHEG BOX. *Eur. Phys. J. C*, 73(6):2474, 2013.

[199] S. Jadach, B. F. L. Ward, and Z. Was. The Monte Carlo program KORALZ, for the lepton or quark pair production at LEP / SLC energies: From version 4.0 to version 4.04. *Comput. Phys. Commun.*, 124:233–237, 2000.

[200] A. Arbuzov, S. Jadach, Z. Wąs, B. F. L. Ward, and S. A. Yost. The Monte Carlo Program KKMC , for the Lepton or Quark Pair Production at LEP/SLC Energies—Updates of electroweak calculations. *Comput. Phys. Commun.*, 260:107734, 2021.

[201] S. Jadach, B. F. L. Ward, and Z. Was. Coherent exclusive exponentiation CEEX: The Case of the resonant e+ e- collision. *Phys. Lett. B*, 449:97–108, 1999.

[202] K. G. Chetyrkin, Johann H. Kuhn, and A. Kwiatkowski. QCD corrections to the e^+e^- cross-section and the Z boson decay rate. *Phys. Rept.*, 277:189–281, 1996.

[203] R. Harlander, T. Seidensticker, and M. Steinhauser. Complete corrections of Order alpha alpha-s to the decay of the Z boson into bottom quarks. *Phys. Lett. B*, 426:125–132, 1998.

[204] W. Beenakker, A. P. Chapovsky, and Frits A. Berends. Nonfactorizable corrections to W pair production. *Phys. Lett. B*, 411:203–210, 1997.

[205] W. Beenakker, A. P. Chapovsky, and Frits A. Berends. Nonfactorizable corrections to W pair production: Methods and analytic results. *Nucl. Phys. B*, 508:17–63, 1997.

[206] S. Jadach, B. F. L. Ward, and Z. Was. Coherent exclusive exponentiation for precision Monte Carlo calculations. *Phys. Rev. D*, 63:113009, 2001.

[207] Mario Greco, G. Pancheri-Srivastava, and Y. Srivastava. Radiative Corrections to e+ e- —> mu+ mu- Around the Z0. *Nucl. Phys. B*, 171:118, 1980. [Erratum: Nucl.Phys.B 197, 543 (1982)].

[208] Stanislaw Jadach and Z. Was. Suppression of QED Interference Contributions to the Charge Asymmetry at the Z^0 Resonance. *Phys. Lett. B*, 219:103–106, 1989.

[209] F. Jegerlehner. $\alpha_{QED,eff}$(s) for precision physics at the FCC-ee/ILC. In A. Blondel, J. Gluza, S. Jadach, P. Janot, and T. Riemann, editors, *Theory for the FCC-ee: Report on the 11th FCC-ee Workshop Theory and Experiments*, volume 3/2020 of *CERN Yellow Reports: Monographs*, pages 9–37, 2020.

[210] Lisong Chen and Ayres Freitas. Mixed EW-QCD leading fermionic three-loop corrections at $\mathcal{O}(\alpha_s\alpha^2)$ to electroweak precision observables. *JHEP*, 03:215, 2021.

[211] M. J. G. Veltman. Limit on Mass Differences in the Weinberg Model. *Nucl. Phys. B*, 123:89–99, 1977.

[212] J. J. van der Bij and F. Hoogeveen. Two Loop Correction to Weak Interaction Parameters Due to a Heavy Fermion Doublet. *Nucl. Phys. B*, 283:477–492, 1987.

[213] Riccardo Barbieri, Matteo Beccaria, Paolo Ciafaloni, Giuseppe Curci, and Andrea Vicere. Radiative correction effects of a very heavy top. *Phys. Lett. B*, 288:95–98, 1992. [Erratum: Phys.Lett.B 312, 511–511 (1993)].

[214] Riccardo Barbieri, Matteo Beccaria, Paolo Ciafaloni, Giuseppe Curci, and Andrea Vicere. Two loop heavy top effects in the Standard Model. *Nucl. Phys. B*, 409:105–127, 1993.

[215] J. Fleischer, O. V. Tarasov, and F. Jegerlehner. Two loop heavy top corrections to the rho parameter: A Simple formula valid for arbitrary Higgs mass. *Phys. Lett. B*, 319:249–256, 1993.

[216] J. Fleischer, O. V. Tarasov, and F. Jegerlehner. Two loop large top mass corrections to electroweak parameters: Analytic results valid for arbitrary Higgs mass. *Phys. Rev. D*, 51:3820–3837, 1995.